

Nanoengineered Carbon-Based Interfaces for Advanced Energy and Photonics Applications: A Recent Progress and Innovations

Igor Levchenko,* Oleg Baranov, Claudia Riccardi, H. Eduardo Roman, Uroš Cvelbar, Elena P. Ivanova, Mandhakini Mohandas, Patrik Ščajev, Tadas Malinauskas, Shuyan Xu, and Kateryna Bazaka

As famed quantum physicist W. Pauli once said, “The surface was invented by the devil”. The nonequilibrium state of particles forming the surface, and the presence of dangling bonds transform the surfaces into a 2D reactor with high physical and chemical reactivity. When two such active surfaces are matched, their interface becomes even more reactive, giving rise to novel properties or enhanced performance. For this reason, much effort is applied to design nanoengineered interfacial systems for applications spanning all facets of human life. This review article discusses recent, mostly within two years, progress in the design of complex, sophisticated carbon-based interfacial material systems for energy and photonics applications, with the aim to emphasize some of the most interesting and important examples of such systems. Differences in the processes that take place on flat and 3D (curved) surfaces are discussed, with the view of guiding the design and construction of complex functional interfaces, focusing on several points that are of particular importance to the ongoing development of advanced interfacial material systems.

1. Introduction

“Often, it may be said that the interface is the device”.^[1] Although at the time referring to the specific case of semiconductor heterojunction devices, and the revolutionary impact these have had on the field of microelectronics, Prof. Herbert Kroemer’s words can be readily applied to any field transformed by the use of nanoscale materials and their systems, from medicine to chemical engineering, with the particular importance of the devices for the photonic and energy storage applications. Indeed, as the devices reduce in size, the relative contribution of interface properties and processes to device performance increases, while those of the material bulk become less important. As


I. Levchenko, S. Xu
Plasma Sources and Application Centre
NIE

Nanyang Technological University
Singapore 637616, Singapore
E-mail: levchenko.igor@nie.edu.sg

O. Baranov
Department of Theoretical Mechanics, Engineering
and Robomechanical Systems
National Aerospace University
Kharkiv 61070, Ukraine

O. Baranov, U. Cvelbar
Department of Gaseous Electronics
Jožef Stefan Institute
Ljubljana 1000, Slovenia

C. Riccardi, H. E. Roman
Dipartimento di Fisica “Giuseppe Occhialini”
Università degli Studi di Milano-Bicocca
Piazza della Scienza 3, Milan I20126, Italy

 The ORCID identification number(s) for the author(s) of this article can be found under <https://doi.org/10.1002/admi.202201739>.

© 2022 The Authors. Advanced Materials Interfaces published by Wiley-VCH GmbH. This is an open access article under the terms of the Creative Commons Attribution License, which permits use, distribution and reproduction in any medium, provided the original work is properly cited.

DOI: 10.1002/admi.202201739

E. P. Ivanova
School of Science
RMIT University
PO Box 2476, Melbourne, VIC 3001, Australia

M. Mohandas
Center for Nanoscience and Technology
Anna University
Chennai 600 025, India

P. Ščajev, T. Malinauskas
Institute of Photonics and Nanotechnology
Faculty of Physics
Vilnius University
Saulėtekio av. 3, Vilnius 10257, Lithuania

K. Bazaka
School of Engineering
The Australian National University
Canberra, ACT 2601, Australia

K. Bazaka
Faculty of Engineering
Queensland University of Technology
Brisbane, QLD 4000, Australia

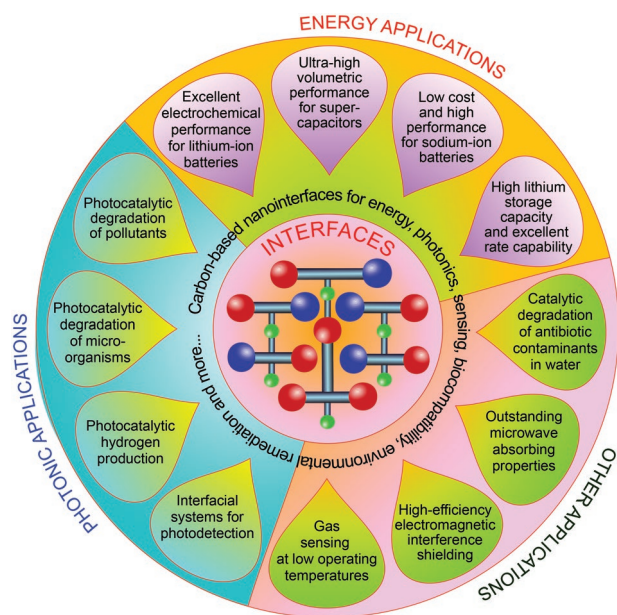


Figure 1. A spectrum of applications that rely on sophisticatedly designed nanointerfaces, with the energy and photonics applications shown as separate groups of key importance for many advanced applications. From energy and sensing to biomedical and environmental applications—and even to superconductivity that can be realized by appropriately interfacing graphene layers in the assembly.

a result, more than ever, attention is drawn to engineering of the interface, as it allows for the realization of properties that may be difficult, if not impossible, to obtain otherwise. Not surprisingly, much effort has been devoted to the development of material systems with a complex architecture and multicomponent composition,^[2–6] where the existence of specific interfaces (between components within a material system, and between the system and its ambient environment) enhances desirable material characteristics and/or addresses the shortcomings that hinder the use of simpler, single-component material platforms made of the same bulk materials. Examples of their use in wearable energy harvesting systems,^[7–9] photocatalysis^[10]

and chemical catalysis,^[11–14] hydrogen energy,^[15,16] protecting coatings,^[17] biosensors^[18] and sensors,^[19–22] nanomedicine,^[23–26] water purification^[27,28] and splitting,^[29,30] biotechnology,^[31–35] and space exploration^[36–40] abound (**Figure 1**).

The performance of device for energy generation, storage, and conversion is intimately linked to the ability of materials to form complex heterogenous interfaces.^[41–44] This holds true for both the efficiency with which the device, e.g., captures photonic energy and forms electron–hole pairs, or produces reactive species in the photocatalytic process, and its mechanical and chemical stability over time. In addition to inorganic functional nanocomposites and nanomaterials, e.g. those derived from silica,^[45,46] carbon-based materials, and metal oxide nanoparticles derived from organic feedstocks, including waste^[47–49] and biomass feedstocks^[50,51] have been gaining popularity, for they promise to deliver advanced performance at a minimal cost to the environment. It is worth noting that while synthesis of functional nanomaterials from minimally processed precursors is attractive,^[52,53] in some cases, their production may be difficult to scale up without the loss of their intricate structure or quality,^[54,55] with an immediate impact on the quality of the engineered interface.

One of the most important phenomena related to energy application is superconductivity, which has been recently discovered in the interfacial graphene systems, specifically in the twisted bilayer, trilayer, and quadrilayer graphenes.^[59–61] When two layers of graphene are twisted with respect to each other at an angle of $\approx 1^\circ$, interesting strong-correlation physics and even superconductivity could be achieved due to the creation of distinct minibands in moiré superlattices (**Figure 2**).^[62] This prominent demonstration of the unusual capabilities of interfacial material systems promises more breakthrough discoveries in the nearest future.

- ✓ Engineered interfaces of functional material systems with a complex, multicomponent architecture are challenging to design and develop, yet they offer significantly greater potential for the advancement of many critical applications, from energy to environmental remediation and health, when compared to solid materials.

In this review article, we will consider recent progress in the development of complex material systems for energy and

SUPERCONDUCTIVITY IN INTERFACING TWISTED BILAYER, TRILAYER AND QUADRILAYER GRAPHENES

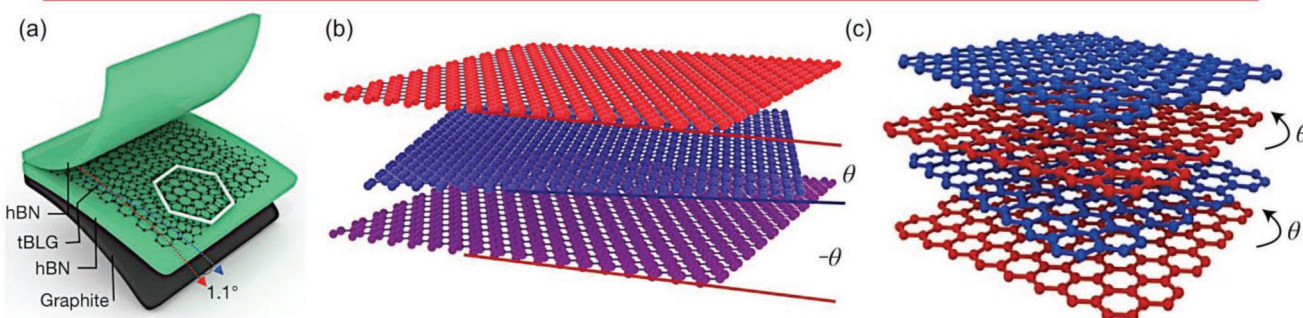


Figure 2. Sophisticatedly engineered interfacial systems can bring unique properties, including superconductivity demonstrated in interfacial twisted a) bilayer, b) trilayer, and c) quadrilayer graphenes. In the system shown in (a), about 1° of an angle is quite sufficient to create the Moiré superlattice minibands that feature an ultrafast optical response together with the ultrahigh carrier mobility, resulting in the superconductivity. (a) Reproduced with permission.^[56] Copyright 2019, Springer Nature. (b) Reproduced with permission.^[57] Copyright 2021, Springer Nature. (c) Reproduced with permission.^[58] Copyright 2022, Springer Nature.

photonics applications, with a focus on the important interfacial properties that have been realized in these systems, and their impact on the device performance.

2. Engineered Nanoscale Interfaces Based on Flat and 3D Carbons: The Difference

Engineered nanomaterials can be viewed as a virtually infinite matrix of material systems and architectures that can be created by controlling the properties of individual building blocks/components and how these are assembled. Each system would be unique in terms of its properties and performance, being a result of synergistic and antagonistic interactions between the individual constituents that can vary in their shape, internal crystallinity, and external surface chemistry. The shapes of the 3D nanoscale component can take are multitudinous and extremely diverse, from relatively simple spheres, cubes, and triangles to more complex tubes, branches, and needles, and play an important role in defining not only wettability of the surface but also the manner in which the material would interact with biomolecules and cells. The internal crystallinity of the nanoscale component will define the photonic and electronic properties of the building block, as well as its transport, sorption, and catalytic activity irrespective to their 2D or 3D shape. These properties are critical for photonics, optoelectronics, and energy harvesting and storage applications. The surface properties of the components will determine the type of chemical and biochemical reactions that could take place, where on the particle this would take place, and whether the reaction or interaction, e.g. binding, would be selective. The amphiphilic and amphoteric behavior of the component in response to changes in pH or temperature would also be defined by the surface properties, and so would the cell–surface and protein–surface interactions, and antimicrobial activity of the material. As such, surface chemistry, as well as porosity, crystallinity, homogeneity, and roughness, are all critical in determining the potential of these materials for sensing, photocatalysis, environmental and biomedical applications.

Enhanced or novel properties may also arise as different components are assembled, with the distribution, alignment, and orientation of components with respect to each other playing a decisive role in defining the bulk properties of the entire material system. The possibility of such interactions increases at the number and variety of interfacing elements grow, and their assembly evolves. While it opens up more opportunities for novel applications, the increasing complexity also makes it more challenging to understand, predict, and optimize the structure–property relationship of the resulting microscopic or macroscopic material, and its performance in a given application. **Figure 3a,b** captures some of the facets of this complexity, comparing and contrasting a “flat” 2D material system with a far more elaborate 3D architecture. It should be noted that the processing environments required for the fabrication of more sophisticated multicomponent engineered systems are often more complex, featuring additional means for the control of movement of fluxes of particles and energy to different points across the material surface.

Curvature and complexity of surfaces influence many, if not all, key physical processes that are involved in the formation of complex interfaces. Processes on a flat substrate are in general

simpler to understand and model, due to the absence of strong localized electric fields and nonuniform diffusional fluxes. Processes on 3D, nonflat surfaces are much more complex, with a strong influence of localized electric fields at the sharp edges and conical surfaces, and nonuniform assembly of building blocks on nonflat features. In turn, surface curvature and localized electric fields influence some key activation energies, such as surface diffusion activation energy, adsorption and desorption energies, and others. For example, the particle diffusing on the surface with curvature r will be subject to decreasing evaporation activation energy according to $\varepsilon_v(r) = \varepsilon_a - \varepsilon_s \frac{\lambda}{r}$, where ε_a is the evaporation energy for the flat surface, ε_s is the specific surface energy, and λ is the lattice constant.^[63,64] Other activation energies, e.g., diffusion activation energy will be affected in a similar way. Electric fields could also influence activation energies of particles on the surface via several effects, such as, e.g., a decrease in surface diffusion activation energy via adatom interactions with the electric field. Adatoms that feature polarizability or have the dipole moment in the electric field E will acquire the total dipole moment $\tilde{P} = \tilde{p} + \alpha E$, where \tilde{p} is the dipole moment of the adatom, and α is the polarizability. In this case, diffusion activation energy becomes

$$\varepsilon_{de} = \varepsilon_d + \frac{\partial E}{\partial r} \frac{\lambda}{e} (\tilde{p} + \alpha E(r)) \quad (1)$$

Local heating due to ion bombardment to 3D nanostructures also changes the particle behavior, e.g., the ratio ν_τ of surface diffusion time at some temperature T to the surface diffusion time occurring at some elevated nanoparticle temperature could be estimated as

$$\nu_\tau = \exp \left[\frac{e\varepsilon_d}{kT} \left(\frac{1}{kTn/e\varepsilon_i + 1} \right) \right] \quad (2)$$

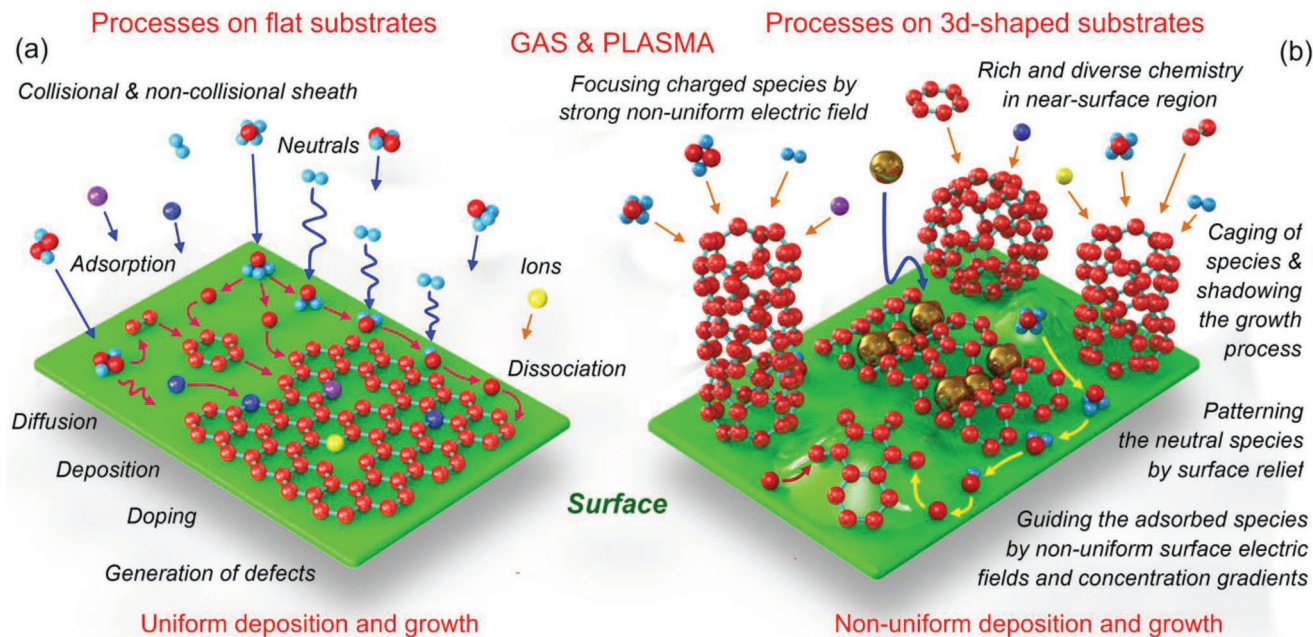
where ε_d is the diffusion activation energy, ε_i is the ion energy, k is the Boltzmann constant, and e is the electron charge.^[65]

These and other effects on surfaces with a complex shape result in the formation of more elaborate, well-developed interfacial systems. **Figure 3c** shows an example of complex growth of core–shell SiC–C nanoparticles, which results in the formation of different structures (carbon core and Si under-shell or SiC under-shell) depending on the process conditions. **Figure 3d** shows the 3D visualization of the nanodot pattern and the adatom density profile on the silicon surface, illustrating very strong variations in adatom density due to the presence of 3D structures.

It is worth noting that for real technological processes and complex materials, the classification of real surfaces into flat and 3D is a simplification. Ideal flat interfaces simply do not exist, and most real interfacial systems feature more or less developed 3D characteristics. However, as many systems are being built on rather flat carbonous structures (often graphenes, though other carbon allotropes are also used), we subdivided the entire spectrum of carbon-based interfaces into flat and 3D for convenience, to facilitate the discussion of several recent examples of promising interfacial systems, focusing on photonic and energy applications where interfacial systems have thus far played an exceptionally important role.

PROCESSES DURING INTERFACE FORMATION ON FLAT AND 3D-SHAPED SURFACES

PROCESSES AT FLAT AND CURVED SURFACES: WHAT ARE THE DIFFERENCES?



HOW THE SURFACE CURVATURE “WORKS”

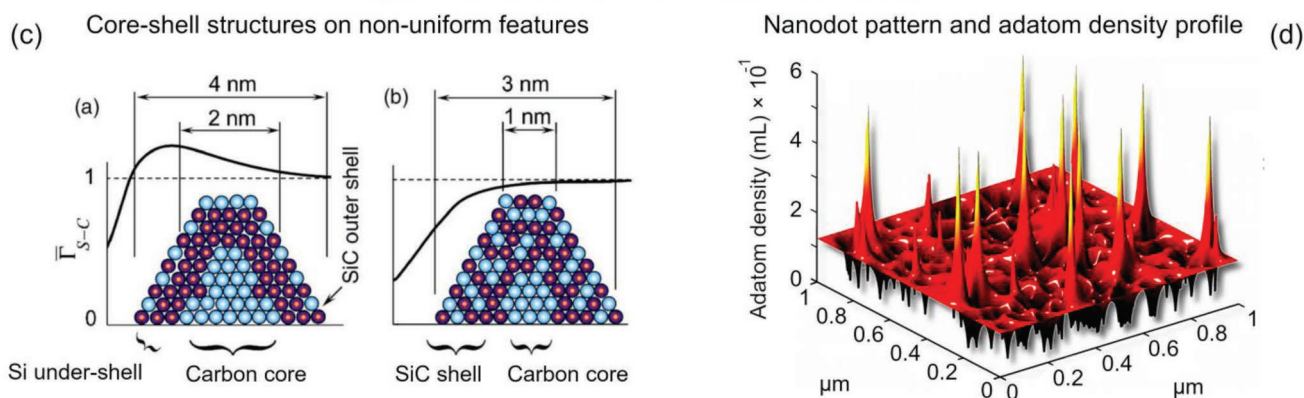


Figure 3. Processes during interface formation on flat and 3D shaped surfaces: a comparison. Curvature and complexity of surfaces influence many, if not all, key processes that are involved in the formation of complex interfaces. a) Processes on flat substrate are in general simpler, without strong localized electric field and nonuniform diffusional fluxes. b) Processes on 3D, nonflat surfaces are much more complex, with a strong influence of localized electric fields at sharp edges and conical surfaces, and nonuniform deposition on well-developed nonflat features. In turn, surface curvature and localized electric fields influence some key activation energies such as surface diffusion activation energy, adsorption and desorption energies, and others. c) Formation, e.g., core–shell structures under different conditions results in their different internal structures. Reproduced with permission.^[66] Copyright 2007, AIP. d) 3D visualization of the nanodot pattern and adatom density profile on the silicon surface, showing very strong variations in adatom density due to the presence of 3D structures on the surface of the substrate. Reproduced with permission.^[67] Copyright 2013, ACS.

✓ Hence, for the purposes of this discussion, a surface composed of horizontal graphene flakes would be considered “flat”, whereas a surface made up of the similar flakes oriented horizontally to the substrate (as in the case of vertically oriented graphene walls) would be considered 3D. A similar notional distinction would be made for a “flat” polymer surface versus that, e.g., etched to show a pattern of tall peaks,^[3] or thermally treated to form 3D hierarchical wrinkles.^[68]

We should however stress that the idea of 2D versus 3D should not be associated with purely geometrical characteristics of structures that make up said surface, but also with the processes that can be impacted by the interfaces having specific properties. In line with this concept, a geometrically flat interface that produces a change in the pattern of distribution of material and energy fluxes to this surface, and as such results in the generation of 3D structures can in principle be considered a 3D interface. For example, if a flat interface is doped, i.e.,

a quantity of doping sites are introduced across the surface of the substrate, what once were a uniform distribution of diffusion and adsorption flows is now changed in 3D scale, with the specific change corresponding to the nature and distribution of doping species. Similarly, in a case when 2D interface changes its shape because of wrinkling, rolling, tubing, stacking, sandwiching etc.—the fluxes also change according to the specific effect associated with the distortion. The effect of geometrical features of the surface has been captured in Figure 2, where a number of the geometry-associated effects are shown to illustrate the main constituents that can be used to make 3D interface by changing only the geometrical descriptors of the surface. In Figure 3, we show several examples of how physical and chemical patterns can be combined to create more complex 3D interfaces. Thus, a change of a substrate curvature (from flat to 3D) changes the pattern of diffusion flows, which can in turn change the pattern of a deposit formed from the species adsorbed onto the flat interface. In turn, wrinkling of a deposit allows changing the adsorption pattern from the species delivered from gas phase. A similar effect can be achieved when species are embedded directly into the crystalline structure of 2D interface, thus changing the chemical potential across the interface. Sharp edges of 1D and 2D structures can be quite useful in controlling the motion of charged species from the 3D environment toward the surface, and the ability of some materials (e.g., carbon) to create different 3D shapes (tubes, sheets, cages) under the action of various driving forces allows using them with respect to all the described effects. A combination of different structures can expand greatly the reaction area, and combinations of chemically activated solid 3D matrices with embedded 0D or 1D nanostructures, solid 1D nanostructures grown on 2D structures, as well as gel or sol of 0D structures caged in 2D nanostructures can also be used for the purpose of creating 3D interfaces.

Unfortunately, the multitude of possible effects, such as a change in chemical properties arising from the introduction of various nanoparticles and reagents, ability to create ion–electron pairs, change the directionality of the chemical bonds, etc., cannot be easily integrated into Figure 3b to cover the entire spectrum of possibilities for interface engineering. For this reason, Figure 3 should be considered as a simplified illustration of just the geometry-associated effects, while other effects are illustrated with appropriate schematics and diagrams in the subsequent sections of the paper.

In the following sections, we will examine a number of carefully selected examples that highlight recent progress in interface engineering on flat and 3D carbons, focusing in particular on fabrication methods that are affordable, simple, and fast, and use widely available and low cost feedstocks.

3. Nanoengineered Interfaces Based on Flat Carbons

While complex, engineered interfaces of various geometries, including those based on mostly flat and mostly well-developed 3D morphologies are important^[69] for various applications including energy,^[70,71] sensors and detectors,^[72,73] memory devices,^[74] supercapacitors,^[75] water treatment,^[76] degradation

of antibiotics,^[77] and many others we will address in this section the recent results obtained for mostly flat or near-flat geometries.

3.1. Carbon-Based Interfaces for Photonic Energy-Driven Applications

Interface engineering, especially at nano- and sub-nanoscales, has been one of the primary drivers of the recent progress in devices that convert photonic energy to other forms of energy, e.g., electrical or chemical.^[11,78] Of particular importance are technologies that use photocatalysis for environmental remediation,^[79] including degradation of recalcitrant pollutants, such as hydrocarbons, pesticides, synthetic dyes, and drugs that pose significant risk for human health and the environment.^[80,81]

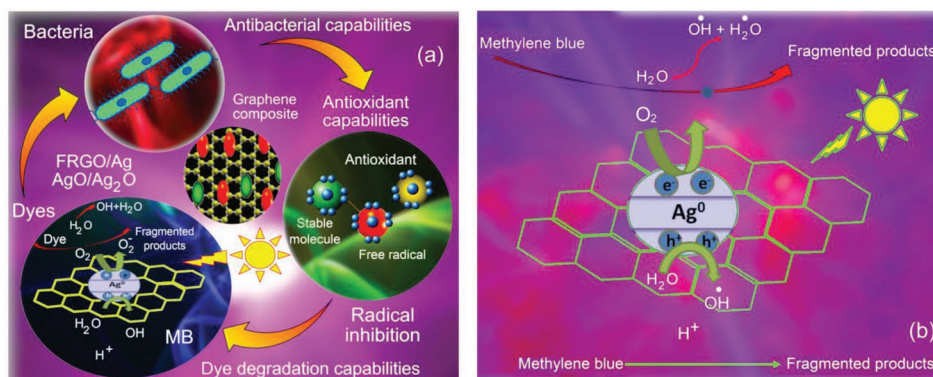
Of particular interest are material interfaces produced as a result of green synthesis, from safe, nontoxic input materials, and in the absence of harmful process reagents. This is because the use of potentially harmful input materials or reagents in the synthesis may produce materials that are contaminated with traces of these substances, preventing their subsequent use in applications where such contaminants would pose threat to humans or animals, e.g., in the purification of waste and drinking water, and in applications related to human or animal health. Where early on, there were concerns about the use of mixed-source input materials such as biomass and organic waste, advances in the understanding of process–property relationships have enabled the synthesis of high-quality materials with excellent control over their bulk and interface properties. Even materials with complex architectures have been produced from biomass using relatively simple synthesis processes.

Lekshmi et al. have recently reported the production of nanocomposites comprising flakes of reduced graphene oxide (rGO) decorated with silver and silver oxide particles. The flakes were synthesized using a facile method of open-air (flame) combustion from the readily available sunflower cooking oil, although other oils, both pristine and used, could be employed in its place. In turn, the production of nanoparticles of Ag, AgO, Ag₂O also involved the use of a natural product, in this case the flavonoid-rich extract from *Coleus aromaticus*, which acted as reducing and capping agent in the phytochemical reduction of AgNO₃, the latter being the most affordable silver precursor. The resulting composite showed a desirable combination of strong photocatalytic activity against chemical dyes, and antioxidant and antibacterial properties, which makes it a promising candidate for drinking and wastewater purification.^[82] This activity was significantly enhanced through the use of a more complex interface structure of the nanocomposite when compared to the pure reduced graphene oxide flakes alone.

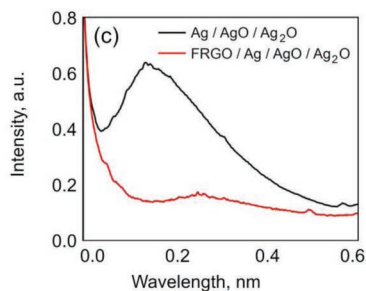
Figure 4a illustrates the spectrum of applications for the multifunctional reduced graphene oxide–silver nanocomposites that includes photocatalysis and antibacterial properties, and Figure 4b illustrates the dye degradation mechanism. For the visible light photocatalysis to be successful, the surfaces of nanoparticles should be designed in a way that supports efficient light absorption in the visible portion of the electromagnetic spectrum and the generation of electron–hole pairs,

COMPLEX INTERFACES ON FLAT CARBONS FOR PHOTONIC APPLICATIONS

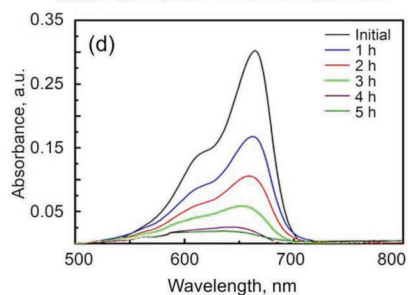
REDUCED GRAPHENE OXIDE – SILVER OXIDE COMPOSITES WITH PHOTOCATALYTIC ACTIVITY



Photoluminescent spectra of graphene oxide - nanocomposites



Photodegradation of MB using graphene oxide - nanocomposites



GRAPHENE-BASED NANOCOMPOSITES FOR PHOTOCATALYTIC DEGRADATION OF MG DYE

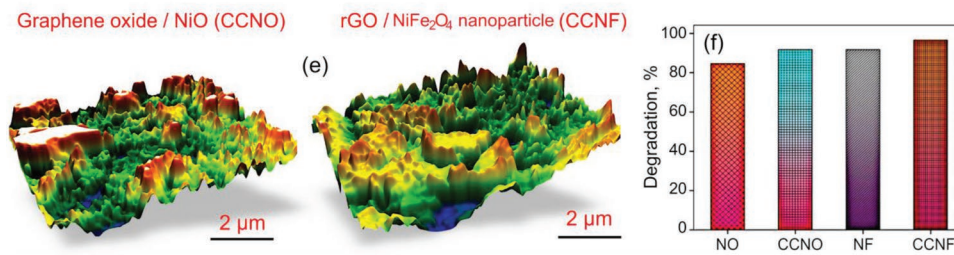


Figure 4. Reduced graphene oxide–silver nanocomposite interfaces for photocatalysis. a) Spectrum of applications for the multifunctional reduced graphene oxide–silver nanocomposites includes photocatalytic degradation of recalcitrant pollutants and pathogenic microorganisms in aqueous media. b) Reactive oxygen species, and in particular hydroxyl radicals, are produced as a result of interactions between photogenerated electrons on the surfaces of silver nanoparticles and water molecules in the solution. The reduced graphene oxide acts as the electron capturing agent. c) Photoluminescent emission spectra for various graphene oxide–silver nanocomposites. d) Effect of contact time on photodegradation of MB dye using reduced graphene oxide–silver nanocomposites. Reproduced with permission.^[82] Copyright 2022, Elsevier. Graphene-based nanocomposite interfaces for photocatalysis. e) Reconstruction of the complex surface topography of graphene oxide–NiO and reduced graphene oxide–NiFe₂O₄ nanocomposites, and f) photodegradation activity toward MG dye for various nanocomposites. Reproduced with permission.^[83] Copyright 2022, Elsevier.

utilizing them efficiently before they are recombined. For the nanocomposite containing a mixture of rGO and Ag/Ag_xO, the addition of the nanoparticles allows one to take advantage of the surface plasmon effects, with the possibility of tuning the latter to interact with light of the specific wavelength range by controlling the dimensions and size of these nanoparticles. In turn, the presence of the reduced graphene oxide flakes enables efficient transfer of the electrons from the silver particles, effectively reducing the rate of recombination of electron–hole pairs. Indeed, in this composite system, reduced graphene oxide largely takes on the responsibility for the efficient generation

of the electron–hole pairs, whereas the role of silver particles is primarily to receive and capture the photons. The mechanism by which anionic graphene oxide and cationic Ag nanoparticles interact is facilitated by the electrostatic forces, and hence is strongly interface-based.

Electrons that accumulate at the surface of silver nanoparticles as a result of their interactions with light can engage in chemical interactions with surrounding molecules; in the case of aqueous environments, the interactions between thus-generated electrons with water leads to the production of highly biochemically reactive hydroxyl radicals. These radicals and their

derivatives play a critical role in the degradation of dyes, as well as inducing oxidative stress in pathogen microorganisms, leading to their inactivation and death. Figure 4c shows the photoluminescent emission spectra of graphene oxide–silver nanocomposites, and Figure 4d demonstrates the efficiency of graphene oxide–silver nanocomposites for the photodegradation of methylene blue (MB). In general, the graphene oxide–silver nanocomposites exhibit better activity than graphene oxide, due to strong reactions at the interfaces.

Tamilselvi et al. have demonstrated the efficient photodegradation of malachite green (MG) dye by the interfacial system of $\text{NiFe}_2\text{O}_4/\text{rGO}$ nanocomposites.^[83] Similarly to the previous example, the rGO flakes were produced from a low-value mixed-chemistry input source that is a by-product of coconut industry, using a low-cost, simple method of hydrothermal synthesis. The final properties of the material were realized by decorating the surfaces of these rGO flakes with NiO and NiFe_2O_4 nanoparticles, thereby improving the chemical reactivity and enhancing the complexity of the resulting 3D composite architecture, and subsequently realizing the visible light driven photocatalytic degradation activity of nearly 97%. Figure 4e shows the representative 3D morphology of the graphene-based nanocomposites produced by the soft bubble assembly approach, and Figure 4e illustrates the photodegradation activity of these composites toward MG dye.

✓ Importantly, these material platforms are multifunctional. In this case the multiple functions are made possible by the strong interfacial interaction between the surfaces of reduced graphene flakes and the NiO and NiFe_2O_4 nanoparticles that decorate them, where the significant surface area of nanoflakes provided a greater number of channels for the diffusion of ions and electrons, leading to enhanced electrochemical performance. Furthermore, the decreased size of the crystallite in the composite increased the contact area between the flakes and the NiO and NiFe_2O_4 nanoparticles, enabling greater adsorption of MG via strong π - π interactions, and efficient scavenging of photoexcited electrons from metal oxide by the carbon sheets.

Figure 5a–e illustrates the preparation, structure, and application of graphene-based interfacial systems consisting of a graphene film and a PbS nanorod array, demonstrating pronounced photodetection properties. Among materials that hold promise for infrared photodetector applications, low-dimensional heterostructures based on PbS are most attractive due to the multiple exciton effects that can be realized in these materials. One of the primary challenges in using PbS-based heterostructures lies in the challenges of growing nanorod arrays with a high degree of control over their nucleation across the substrate surface, and the dimensions and shape of the resulting nanorods. In addition to spatial distribution and morphology, the orientation of these building blocks with respect to the surfaces and other components also plays a role in defining the photodetection performance of the resulting heterostructure.

Yang et al. demonstrated the feasibility of preparing PbS nanorods array-graphene heterostructures with high level of control over ordering, dimensionality, and lattice parameters of PbS components using electrochemical atomic layer epitaxial growth.^[85] Chemical vapor deposition was used to deposit

graphene monolayers on copper. Once the monolayers were lifted off the copper substrate and transferred using a wet transfer method, PbS nanorods were grown on graphene, growing selectively long along (200) orientation. By controlling the underpotential deposition of Pb and S on graphene, nanorods with different size and orientation could be attained.

The interfacial processes played a key role in this system. Specifically, the presence of discontinuous Au nanoparticles on the surface of graphene was a critical factor in enhancing the polarization effect and promoting the adsorption of S^{2-} ions through the preferential formation of Au–S, and subsequently formation of rods with a tetragonal crystal structure (unlike irregular and large crystals that form in the absence of Au under similar conditions).

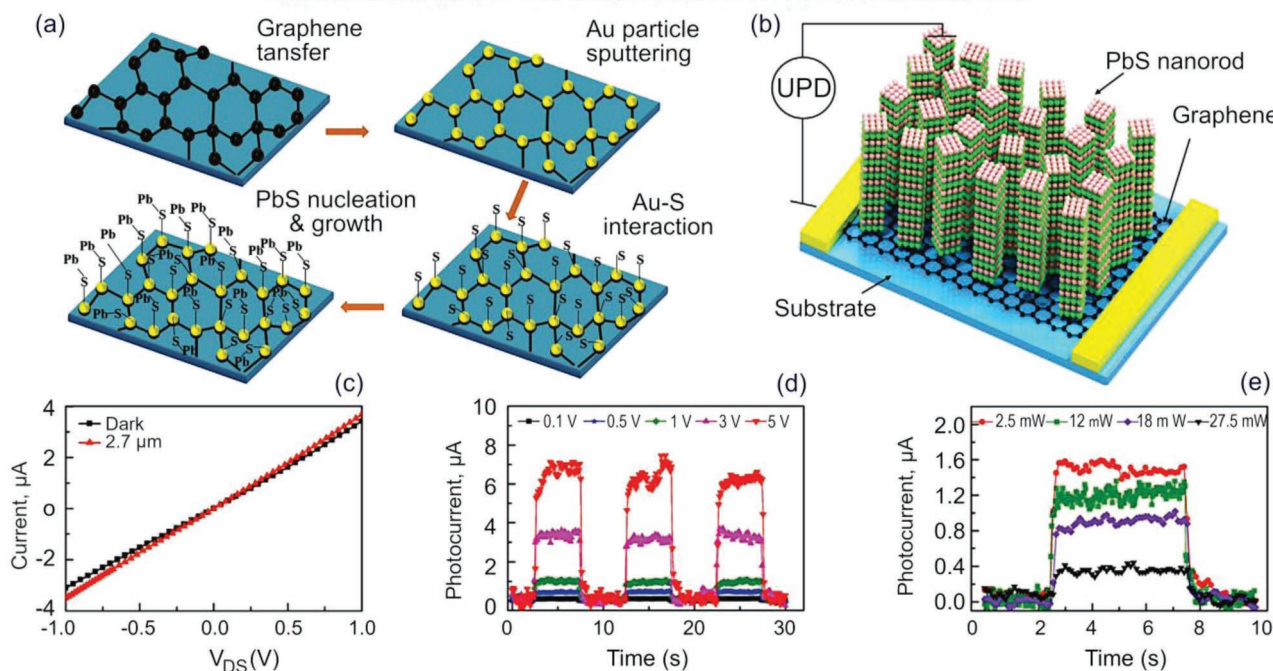
The photodetectors were then constructed using a combination of electron beam lithography, and electron beam and thermal evaporation, with the devices showing outstanding photoresponsivity in excess of 10.4 A W^{-1} (for $2.7 \mu\text{m}$ laser radiation at ambient temperature). The response time for the PbS nanorods–graphene heterostructure was low, attributed to the directional movement of electrons within the 1D structure. This technology provides a possible path for the synthesis of complex material architectures made of hierarchically-organized components of different properties and dimensions for a wide range of applications.

Figure 5f–h shows one more example of designing efficient photocatalytic interfaces based on reduced graphene oxide and fixed bismuth oxybromide iodide solid solution ($\text{BiOBr}_{0.75}\text{I}_{0.25}$ SS).^[86] Among photocatalysts that are able to capture light in the visible range of the electromagnetic spectrum, bismuth oxyhalides offer desirable photocatalytic performance that is attributed to the unique layered structure of this material. In addition to performance, the inexpensive nature of this material makes it promising for larger-scale applications. The fixed $\text{BiOBr}_{0.75}\text{I}_{0.25}$ solid solution has been prepared via single-step solar-driven fixation (Figure 5f). The photocatalytic reactor used to study the photocatalytic activity of the fixed solid solution toward the rhodamine B dye is shown in Figure 5h, and Figure 5g shows the results of the dye degradation tests. In the absence of radical scavengers, an outstanding efficiency of 92% was demonstrated.

Interestingly, synergic interfacial effects caused the superior efficiency of For $\text{BiOBr}_{0.75}\text{I}_{0.25}$ SS. Indeed, the superior efficiency arose as a result of synergy between the solid solution and oxygen vacancies, where the former is related to enhanced visible-light harvesting and the efficiency with which photogenerated charge carriers are separated, in addition to imparting greater oxidation capacity onto photoinduced holes. The latter is responsible for inducing an intermediate level near the Fermi level, which reduces the width of the bandgap and hinders the recombination of e^- and h^+ , increasing their lifetime and hence the photocatalytic activity of the process. Uniform fixation of $\text{BiOBr}_{0.75}\text{I}_{0.25}$ SS on rGO took advantage of such properties of rGO as very high surface area, alignment of energy bands with $\text{BiOBr}_{0.75}\text{I}_{0.25}$ SS, outstanding electrical conductivity and charge carrier mobility, also resulting in a substantial enhancement of optical characteristics of the heterojunction, which is a critical determinant of performance in visible-light driven photocatalysis.

GRAPHENE-BASED INTERFACIAL PHOTOCATALYSIS AND PHOTODETECTION

NANORODS ARRAY ON GRAPHENE FOR PHOTODETECTION



GRAPHENE OXIDE INTERFACES FOR PHOTOCATALYTIC SYSTEMS

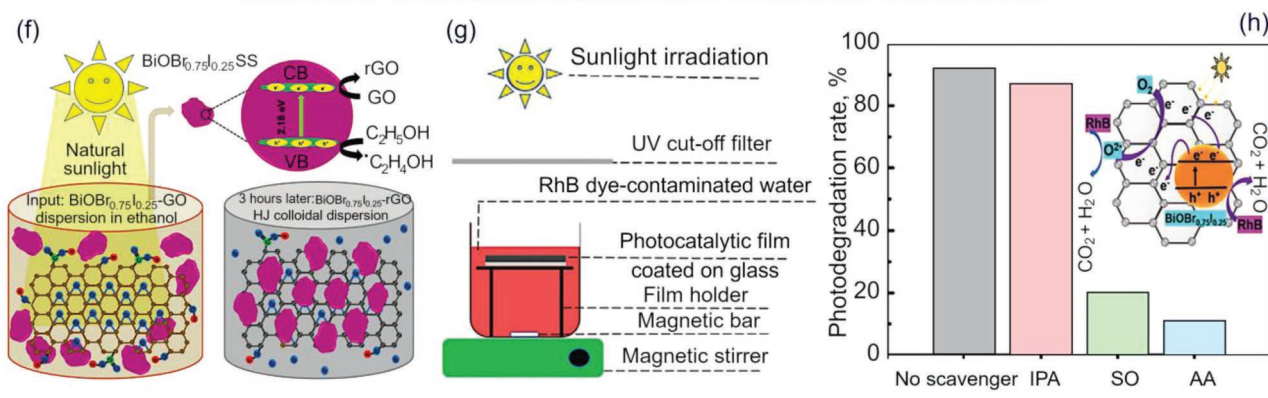


Figure 5. Graphene oxide nanocomposite interfaces for photocatalysis and photodetection. a) Electrochemical growth of PbS nanorods array on graphene, with steps including graphene transfer, deposition of Au nanoparticles onto graphene, formation of Au–S interconnections and finally nucleation and growth of PbS nanorods on flat graphene. b) Schematic of the structural element comprising the heterostructure of PbS nanorod array on graphene. c) Current–voltage dependencies in dark and under 2.7 μm laser illumination. d) Photocurrent for various source and drain voltages. e) Photoswitching characteristics for the device under 2.7 μm laser illumination. Reproduced with permission.^[85] Copyright 2021, Wiley-VCH. Graphene oxide-based interfaces for photocatalysis. f) Preparation of $\text{BiOBr}_{0.75}\text{I}_{0.25}\text{-rGO}$ heterojunction (HJ). g) Photocatalytic reactor used to assess the photocatalytic performance of the $\text{BiOBr}_{0.75}\text{I}_{0.25}\text{-rGO}$ heterojunction for degradation of rhodamine B dye. h) Photodegradation rate is directly affected when scavengers capable of removing photogenerated reactive oxygen species are added into the solution. Reproduced with permission.^[86] Copyright 2021, Wiley-VCH.

Addition of scavengers, in this case that of $\cdot\text{O}_2^-$ and $\cdot\text{OH}$ radicals, revealed that $\cdot\text{O}_2^-$ radicals are the main active species to facilitate the degradation of rhodamine B dye under sunlight irradiation with the wavelength exceeding 420 nm. Addition of ascorbic acid, which is a scavenger of $\cdot\text{O}_2^-$ radicals, dropped the efficiency from 92% to only 11%, thus demonstrating the leading role of the $\cdot\text{O}_2^-$ radicals in the interfacial processes of rhodamine B degradation.^[84] Moreover, $\text{BiOBr}_{0.75}\text{I}_{0.25}\text{-rGO}$ heterojunction films have demonstrated very high durability,

maintaining the high photodegradation rate for rhodamine B for ten consecutively process samples.

In all above examined examples, the sophisticatedly engineered interfaces play a key role in ensuring the targeted material properties. As a characteristic example, in the work by Lekshmi et al. the realization of an increase in chemical activity with respect to photocatalysis of carbon-based nanostructure upon their modification with nanoparticles was demonstrated, where there is a clear relationship between the macroscopic

activity and the ability of the material to create electron–hole pairs more efficiently, while its dispersed or distorted form (from 2D graphene to 3D nanoflakes or wrinkling the surface to increase the surface-to-volume ratio of a 2D interface) allows enhancing greatly the reaction rate due to the increase of the reaction area. Importantly, the work by Yang et al.^[85] demonstrates that, with respect to the 3D interfaces, the main effect is attributed to the chemical activity of the heterostructures enhanced by the physically developed reaction surface after growing the arrays of active 1D nanostructures on a flat interface (graphene substrate with adsorption sites). In particular, peculiarities of graphene crystallinity (200) orientation were used to serve as the nucleation sites for PbS nanorods in the described example.

- ✓ Engineered interfaces with controlled distribution, orientation, and dimensionality of constituent elements may hold the key to maximizing the efficiency with which photonic energy is harvested and converted into chemical energy for degradation of recalcitrant pollutants in aqueous media.

3.2. Graphene-Based Interfaces for Energy Applications: Batteries

Designing sophisticated interfacial carbon-based systems can significantly enhance the efficiency of energy harvesting and storage devices, such as batteries and supercapacitors, bringing with them several valuable advantages such as, e.g., flexibility^[87,88] and ability to generate triboelectric energy.^[89] Recently, many important results in constructing highly efficient interfacial systems for advanced batteries have been achieved,^[90,91] some of the most important of which are reported in this section.^[92–95]

A complex interface in the material based on carbon and in situ generated Mn-deficient nanoarchitectures has been recently designed and tested for rechargeable aqueous zinc-ion batteries.^[96] Cathodes based on Mn have recently been attracting increased attention because of the relative affordability of Mn input material, and the wide spectrum of characteristics that can be attained by varying the structure, phases and stoichiometries in MnO. In this example, a facile process of solvent drying and subsequent calcination at 650 °C in Ar atmosphere was used to produce carbon enfolded ZnO–MnO. X-ray diffraction analyses showed excellent reproducibility of this synthesis method, with the composite having in its structure cubic MnO crystals and hexagonal ZnO crystals constructed from Mn–O₆ octahedral and ZnO₄ tetrahedral units, respectively. High resolution imaging of thus-formed ZnO–MnO nanocomposite showed the presence of porous spherical-shaped particles, with the carbon shell wrapping ZnO. The carbon linkage in the sufficiently graphitized carbon shell plays a key role in facilitating the conduction of ions, thereby positively contributing to the electrochemical performance of the composite. The presence of the Mn vacancy as well as the carbon shell at the interface results in the material showing metallic behavior, as compared to more semiconductor-like defect-free ZnMn₂O₄. Cells built using thus-formed material showed a discharge capacity of ≈220 mAh g⁻¹ (at 100 mA g⁻¹). The cyclic stability was excellent, with 2000 cycles resulting in the decrease in the discharge

capacity to ≈100 mAh g⁻¹, with 100% Coulombic efficiency at 3000 mA g⁻¹. Importantly, the capacity retention was also high, at >85% after 12 months of storage followed by 150 cycles at 100 mA g⁻¹ current density.

A comparative first principle investigation to understand the mechanism by which conductivity is improved in these Mn-deficient nanocomposite electrodes as opposed to related ZnMn₂O₄ and ZnMn₂O₄–MnO structures suggests the possibility of combined intercalation–conversion–deposition reaction mechanism in this interfacial system, although further investigations are required to confirm this hypothesis. **Figure 6a–d** illustrates the schematics and characteristics of Mn deficient ZnMn₂O₄@C nanocomposite, including its in situ formation (**Figure 6a**), and the reaction mechanism of the rechargeable battery built using the material (**Figure 6b**), with the electrochemical characteristics of this electrode, as shown in **Figure 6c,d**. It is evident that the interfacial processes in such a system are quite complex and require deep insight in order to drive material and device optimization. Yet, it is clear that the sophisticatedly designed carbon-based interfacial systems are able to produce record-breaking numbers, such as the very high specific energy density of 296 Wh kg⁻¹ reported in the aforementioned study.

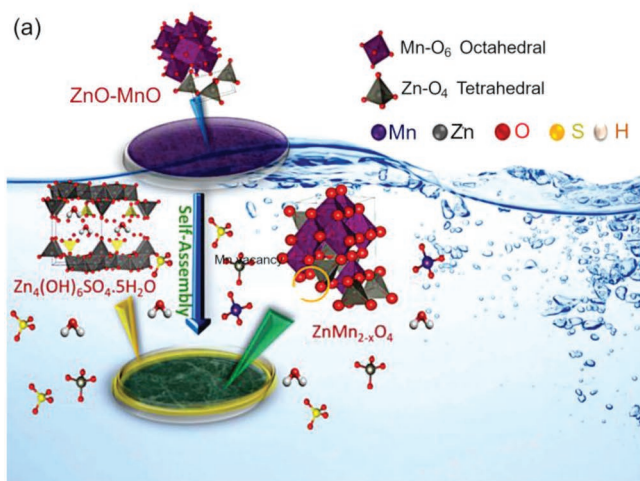
Ma et al. have reported the fabrication of heterostructures of 2D molybdenum dichalcogenide on 2D nitrogen-doped carbon for enhancement of efficiency in potassium-ion batteries.^[97] In their work, the authors have chosen dichalcogenides for their high theoretical capacity, which makes these materials suitable to be used as anodes in potassium-ion batteries. However, suboptimal kinetics of K⁺ insertion, including the collapse of the electrode structure in response to greater levels of K⁺ insertion, limits practical use of dichalcogenide-based electrodes. By assembling MoS₂ and MoSe₂ onto the 2D nitrogen-doped carbon platform, the potassium storage performance of the resulting heterostructure is significantly improved owing to the presence of built-in heterointerfaces that enable efficient K⁺ diffusion. The mechanical properties of the heterostructure, and specifically its ability to withstand volumetric expansion due to high ion diffusion, are substantially improved by the presence of chemical bonds between carbon and S, Se, and Mo. The latter also positively contribute to the stabilization of the discharging product, preventing the dissolution of S and Se and thereby improving the cyclic stability of these electrodes. Moreover, the diffusion of electron is significantly enhanced in this case by the presence of vast interconnected paths within the nitrogen-doped carbon nanostructure, which notably reduces the electron diffusion path. Jointly, these improvements lead to a substantially longer cycle life that is observed in both the MoS₂-on-NC and the MoSe₂-on-NC composites. **Figure 6e–g** illustrates the structure and paths of electron conduction within the heterointerface between the MoSe₂ and N-carbon framework, the charge and discharge characteristics at various current density, and the long-cycle performance of potassium-ion batteries based on this novel material.

A very interesting approach for the coupling of the topological insulator SnSb₂Te₄ nanodots with highly doped graphene was demonstrated to boost the performance of lithium-ion batteries (**Figure 6h–k**).^[98] Topological insulators, i.e., materials that can support the flow of electrons across their surface due to the presence of stable conducting states on their surface,

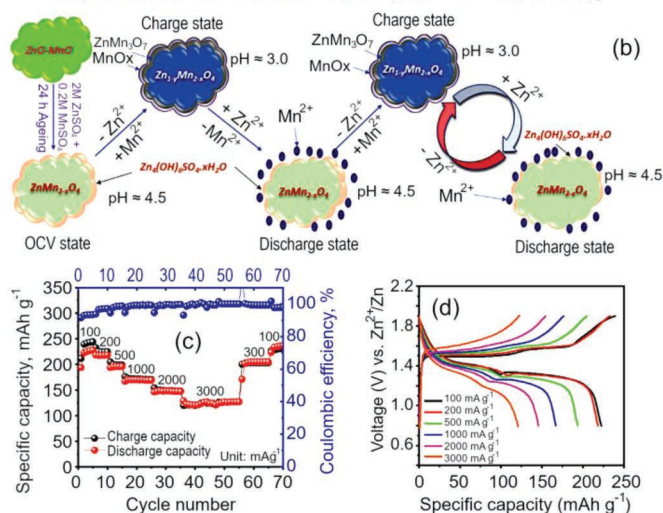
COMPLEX INTERFACES ON FLAT CARBONS FOR ENERGY: BATTERIES

CARBON ENFOLDED NANOCOMPOSITE MATERIAL FOR ZINC-ION BATTERIES

Formation of Mn deficient structure @C

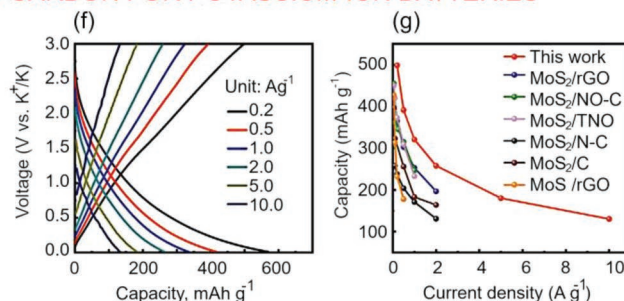
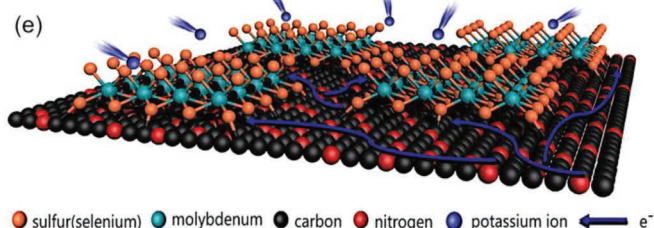


Schematics of reaction mechanism of the battery



HETEROSTRUCTURES ON NITROGEN-DOPED CARBON FOR POTASSIUM-ION BATTERIES

Paths of electron conduction



TOPOLOGICAL INSULATOR NANODOTS ON GRAPHENE FOR LI-ION BATTERIES

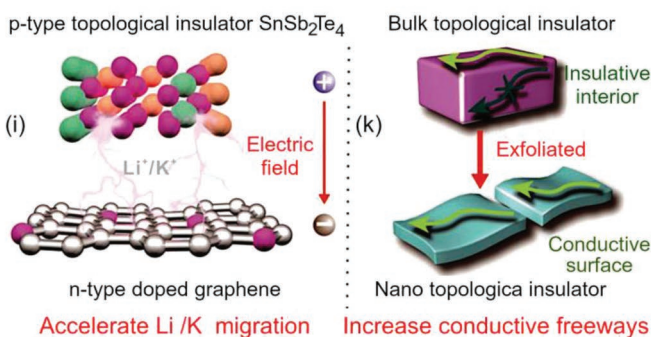
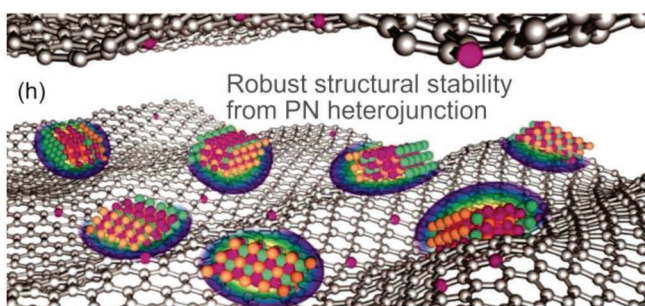


Figure 6. Complex interfaces formed on carbons for Zn-ion batteries. a) Key processes in the in situ assembly of Mn deficient ZnMn₂O₄@C composite architectures. b) Mechanism of reaction for batteries built using Zn/Mn-d-ZMO@C. c, d) Electrochemical characteristics of the electrode composed of ZnO-MnO@C, expressed in terms of its rate capability at different current rate. Reproduced under the terms of the CC-BY license.^[96] Copyright 2021, The Authors, published by Wiley-VCH. Complex interfaces formed on carbons for potassium-ion batteries. e) Graphical representation of possible pathways for electron conduction and K⁺ diffusion at the interface between MoSe₂ and the nitrogen-doped carbon matrix. f) Charge/discharge characteristics for MoSe₂-on-NC as a function of current density, g) comparative performance of potassium-ion batteries comprising MoSe₂-on-NC or MoSe₂ tested under long-cycle conditions. Reproduced with permission.^[97] Copyright 2020, Wiley-VCH. Topological insulator nanodots on graphene for lithium-ion batteries. h) Formation of PN heterojunctions at the interface between topologically insulating SnSb₂Te₄ nanodots and the highly conducting few-layered graphene. i) The mechanism that underpins enhanced movement of Li⁺/K⁺ in the SnSb₂Te₄/G composite material. (j) Reducing the size of SnSb₂Te₄ using ball milling increases the ratio between the conductive surfaces and insulating interior. Reproduced with permission.^[98] Copyright 2020, Wiley-VCH.

have been attracting significant attention for applications in spintronic devices, dissipationless transistors, and magneto- and optoelectronic devices. Yet, their use in devices for electrochemical energy storage has thus far been limited, most probably due to the challenges in realizing devices with high-rate capability and long-term cycling stability. SnSb_2Te_4 is a highly conductive p-type topological insulator abundant in native conductive surface states. In this study, the flakes of SnSb_2Te_4 were produced by means of ball milling and unzipping with graphite, a technique that is both simple and easy to scale up. The PN heterojunctions that formed between thin SnSb_2Te_4 nanodots and the single-atom doped graphene during their coupling are responsible for the accelerated ion transport, as well as superior lifespan, high-rate capability, and durable cycling performance of both Li-ion and K-ion pseudocapacitors, at 373 mAh g^{-1} even at 10 A g^{-1} for the Li-ion devices.

Shen et al. have demonstrated the dual strategy of nano-engineering and cation doping to prepare Fe/Mn-based layered oxide cathodes for sodium-ion batteries,^[102] which are a good candidate for grid-scale energy storage.^[99] Figure 7a illustrates the scheme of a battery that comprises the $\text{P2-Na}_{0.76}\text{Cu}_{0.22}\text{Fe}_{0.30}\text{Mn}_{0.48}\text{O}_2$ cathode interfacing the hard carbon anode. Due to their relative abundance and desirable theoretical specific capacity, transition metal oxides, such as iron and manganese, and their layered assemblies have emerged as promising cathode materials for sodium-ion batteries. However, rapid capacity loss still limits their use in rechargeable batteries. To overcome this challenge, the authors have taken advantage of a novel $\text{P2-Na}_{0.76}\text{Cu}_{0.22}\text{Fe}_{0.30}\text{Mn}_{0.48}\text{O}_2$ cathode, which they have manufactured to have a hierarchical architecture resembling a pearl necklace. The addition of the Cu dopant to the cathode further boosted the Na-storage performance of the battery, where a well matching anode made of the chemically presodiated hard carbon was also used. Presodiation using a sodiation reagent such as sodium biphenyl helps overcome the low initial Coulombic efficiency and compensate for the irreversible capacity loss of hard carbon anodes, thereby allowing for this material to be used for low-cost and high-energy density sodium-ion batteries.

Figure 7b demonstrates the cycling performance of the soft-packed Na ion full battery at 0.1 C within the voltage range of 1.6–3.8 V, with a promising energy density of 177.4 Wh kg^{-1} . It can be seen that even after 100 cycles, the discharge capacity remains at ≈ 95 mA h g^{-1} , which corresponds to a desirable capacity retention of over 80%. Presodiation of the anode allowed for the reversible capacity of ≈ 210 mA h g^{-1} with an operating potential of ≈ 0.13 V versus Na^+/Na to be maintained. These results demonstrate that $\text{P2-Na}_{0.76}\text{Cu}_{0.22}\text{Fe}_{0.30}\text{Mn}_{0.48}\text{O}_2$ with nanonecklace-like architecture is a promising new path toward the practical realization of sodium-ion batteries based on high-performance Fe/Mn-based layered oxide cathodes.

In another recent example, a complex nanoarchitecture comprising a graphene heteronetwork doped with MoS_2 , N, and S uniformly decorated with small $\text{CoS}_x@Cu_2\text{MoS}_4$ core@shell structures was demonstrated by Nguyen et al.^[103] This interfacial system demonstrated ability to sustain reactions related to the reduction and evolution of oxygen,^[100,101] and for the evolution of hydrogen when used in the alkaline medium. Figure 7c illustrates the schematic of the $\text{CoS}_x@Cu_2\text{MoS}_4\text{-MoS}_2/\text{N,S}$ -codoped

graphene interfacial assembly. The long-term stability of an electrolyzer developed using this material was superior to that for a device of $\text{Pt/C} + \text{RuO}_2/\text{C}$, with a cell voltage of 1.60 V. Similarly, when the material was used as cathodic catalyst, the performance was superior to that of based on Pt/C catalyst, delivering a high cell voltage of nearly 1.45 V and a power density of 40 mW cm^{-2} at 58 mA cm^{-2} . In both cases, the increased performance is inherently related to the processes that take place at the active centers that form at the interface between the highly active core@shell $\text{CoS}_x@Cu_2\text{MoS}_4$ particles and the $\text{MoS}_2/\text{N,S}$ -codoped graphene, the latter offering a large area and high level of porosity. Figure 6c illustrates the comparison of power density achieved in the newly designed Zn–air battery with previously reported examples. Collectively, the results of this study strongly support $\text{CoS}_x@Cu_2\text{MoS}_4\text{-MoS}_2/\text{N,S}$ -codoped graphene as a promising material for multielectrocatalysis applications in both metal–air batteries as well as for hydrogen production.

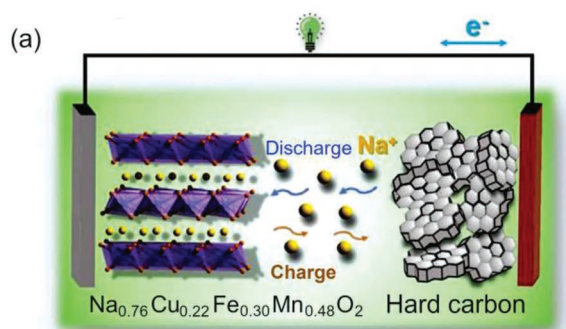
Another promising approach to enhance the properties of Zn–air batteries has been demonstrated by Xiao et al.^[104] Zn–air batteries feature high energy density and low cost that make them suitable candidates for many applications.^[105,106] However, high overpotential is one of the drawbacks of the Zn–air batteries. In the proposed technology, the FeN_4 edge sites were engineering on graphitic nanosheets (Figure 7e,f), as they tend to show a greater level of oxygen catalytic activity compared to single-atom FeN_4 counterpart sites on the graphitic plane. Typically, it is challenging to preferentially introduce defect sites with high degree of precision using a general high-temperature pyrolysis process alone. For this reason, authors have chosen to use a self-sacrificed template to introduce FeN_4 sites specifically along the edges of the highly graphitic nanosheet structure. The controlled graphitic carbon growth was driven by Fe clusters that were formed in situ, and facilitated the formation of the structure with well resolved porosity. These clusters also played the key role in driving the preferential anchoring of FeN_4 . The newly designed material showed promising performance as a cathode in a rechargeable Zn–air battery, being characterized by a low charge–discharge voltage gap of 0.78 V. Importantly, the cyclability of this battery was also very high, showing superior performance to that based on noble metals over 240 cycles (Figure 7g).

Among other important and very useful interfacial processes discussed above, we can stress here the caging of 0D material with 2D carbons, demonstrated by Islam et al.^[96] This example illustrates the possibility of realization of caging 0D material with 2D carbon material and creation of 3D interface by introduction of a large number of such structures into the reaction volume. Also important is the technology reported by Ma et al. on the fabrication of 2D molybdenum dichalcogenide on 2D nitrogen-doped carbon.^[97] This study highlights the benefits of stacking differing 2D materials into a single assembly as a feasible pathway to address the limitations of these materials when they are used alone. Application of topological insulators via anchoring of SnSb_2Te_4 nanodots onto graphene sheets few layers in thickness has been shown to produce a material with sufficient stability to be used as an anode in high-rate Li ion and K-ion batteries, as one more example of complex and very beneficial interfacial processes.^[98] And we should stress again

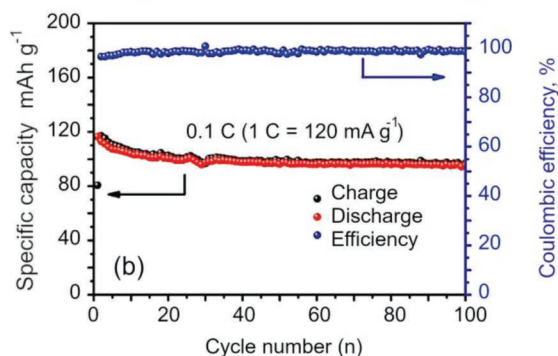
COMPLEX INTERFACES ON FLAT CARBONS FOR ENERGY: BATTERIES

LAYERED OXIDE CATHODES FOR SODIUM-ION BATTERIES

Scheme of full battery

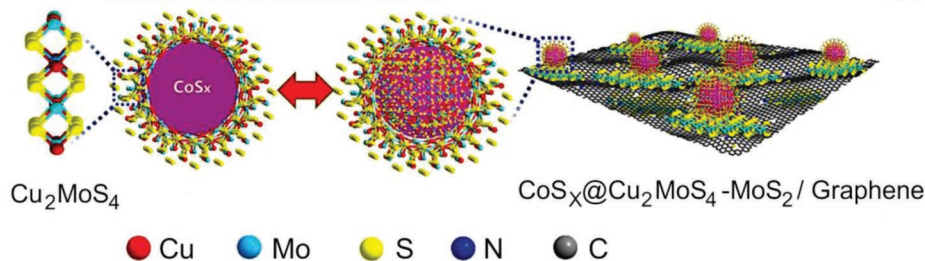


Cycling performance of the full battery

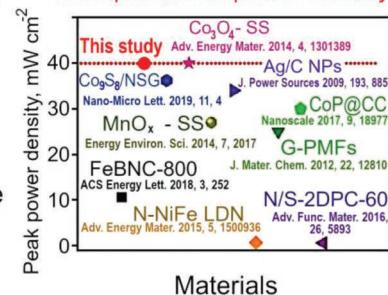


N,S-CODOPED GRAPHENE FOR WATER SPLITTING ZN-AIR BATTERY

Scheme of the facial structure

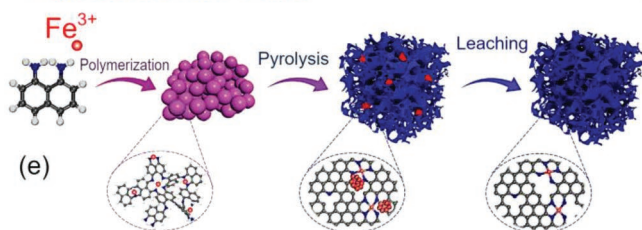


Comparison of power density

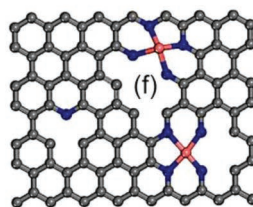


ENGINEERED GRAPHITIC NANOSHEETS FOR RECHARGEABLE ZN-AIR BATTERIES

Preparation of Fe/N-G-SAC



Schematic of Fe/N-G-SAC



Power density curves

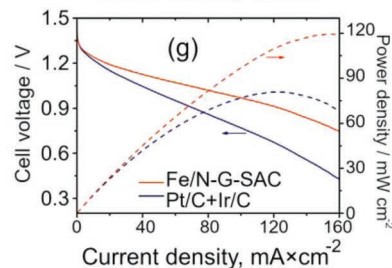


Figure 7. Complex interfaces formed on carbons for energy applications. a) Schematic and b) cycling performance of the battery that uses a chemically presodiated hard carbon anode and a $\text{P}_2\text{-Na}_{0.76}\text{Cu}_{0.22}\text{Fe}_{0.30}\text{Mn}_{0.48}\text{O}_2$ cathode. Performance assessed at the rate of 0.1 C within the $1.6\text{--}3.8 \text{ V}$ voltage range. A reversible capacity of $\approx 210 \text{ mA h g}^{-1}$ is delivered by the presodiated hard carbon anode (at an operating potential of $\approx 0.13 \text{ V}$ vs Na^+/Na). Reproduced under the terms of the CC-BY license.^[102] Copyright 2020, The Authors, published by Wiley-VCH. Codoped graphene interfacial structure for Zn-Air batteries. c) Scheme of the $\text{CoS}_x@ \text{Cu}_2\text{MoS}_4 - \text{MoS}_2 / \text{N,S-codoped graphene}$ interfacial structure, and d) comparison of power density achieved in the newly designed Zn-air battery with previously reported examples. The interface with codoped graphene heteronetwork produces unique properties due to synergistic effects that arise from the use of these building blocks, and at their interface. Reproduced with permission.^[103] Copyright 2020, Wiley-VCH. Engineered graphitic nanosheets for Zn-air batteries. e) Engineered graphitic nanosheets for rechargeable Zn-air batteries. f) Structure of FeN_4 edge sites engineering on graphitic nanosheets. g) Power density curves of the liquid Zn-air battery using various catalysts. The rechargeable Zn-air battery based on the newly designed cathode material shows a low charge-discharge voltage gap and excellent cyclability over 240 cycles. Reproduced with permission.^[104] Copyright 2020, Wiley-VCH.

the importance and advantages of hierarchical interfacial structures, e.g., above-discussed study by Shen et al.,^[102] which have manufactured a novel cathode with a hierarchical architecture resembling a pearl necklace.

✓ The examples examined in this section confirm the importance of engineered carbon interfaces for advancing the performance and long-term stability of low-cost batteries. The following section will further examine their potential for advanced supercapacitors.

3.3. Graphene-Based Interfaces for Energy Applications: Supercapacitors

Along with their application in batteries, materials with complex engineered interfaces can significantly enhance the efficiency of supercapacitors.^[107,108] This section will discuss some of the most important recent examples of the development and use of carbon-based interfaces in supercapacitor technology. Graphenes are a particular promising base for the design of efficient interfacial systems for supercapacitors, allowing for the production of novel efficient electrode materials,^[109,110] application of additive techniques for supercapacitors,^[111] design of double layer capacitance in the graphene-based supercapacitors,^[112] dual-function supercapacitors,^[113] and other graphene-enabled technologies.^[114,115]

Plasma-enabled synthesis of graphene nanosheet/metal oxide architectures and their use to boost the properties of supercapacitors has recently been demonstrated by Huang et al.^[116] The graphene/MnO₂/WO₃ structures were synthesized using a novel one-pot, low-temperature, fast process based on cathodic plasma. The advantages of this process are that it enables graphene, MnO₂, and WO₃ nanostructures to be synthesized sequentially, with the surface area of each building block being available for the charge carrier diffusion in the electrochemical process. Two hours was sufficient to first deposit 0.01–1 μm leaf-like sheets of graphene, onto which MnO₂ nanowires resembling thin and tall petioles ($l = 0.1\text{--}0.3\ \mu\text{m}$, $d = 10\ \text{nm}$) were grown; these in turn were decorated WO₃ petal-like structures with the dimensions of 0.20–2.0 μm (Figure 8a). The resulting graphene/MnO₂/WO₃ nanocomposite had very high surface area of nearly 300 m² g⁻¹, primarily attributed to the presence of graphene nanosheets.

Having a large surface area is desirable as it facilitates faster charge carrier transport during the charge/discharge cycles. The specific capacitance of the graphene/MnO₂/WO₃ electrode was very high, at 620 F g⁻¹ at a current density of 0.5 A g⁻¹, with excellent capacitance retention of 90% after 5000 cycles at 1 A g⁻¹ (Figure 8b). These results highlight the potential of this and similar high surface area heterojunction architectures as high-performance electrodes for energy storage and other advanced applications that require efficient transfer of charge carriers.

In another example, the interfacial system of NiFe₂O₄/reduced graphene nanocomposites prepared using a simple hydrothermal technique showed favorable specific capacitance of nearly 600 F g⁻¹ at a current density of 1 A g⁻¹. Similar to other examples that have already been discussed in this paper, the authors have chosen an affordable and abundant feedstock, namely, the waste product of coconut industry, to fabricate high quality reduced graphene oxide, onto which functional NiO and NiFe₂O₄ nanoparticles were immobilized. The resulting nanocomposites had a hierarchical architecture, with large surface area, and excellent cyclic stability and the columbic efficiency, with an ability to endure up to 2000 charge/discharge cycles.^[83] At higher current density ($\approx 5\ \text{A g}^{-1}$), only 2–4 s were required to complete the charging/discharging cycle, with the specific capacitance of the NiFe₂O₄/reduced graphene electrode being directly proportional to the discharge time. Figure 8c illustrates the 3D morphology of thus-prepared graphene-based interfacial

systems, and Figure 8d shows the graphs of voltage drop for reduced graphene oxide/NiO and reduced graphene oxide/NiFe₂O₄ composites.

Another novel technology based on the use of porous graphene inks for the production of efficient flexible supercapacitors by stamping was recently reported.^[117] One of the main obstacles in the translation of lab scale fabrication based on photolithography to commercial scale is the complexity of applying layers of photoresists, masks, and etchants that may be both expensive and toxic to human health. To overcome this challenge, and reduce the complexity and cost of the preparation of graphene-based planar flexible micro-supercapacitors, the authors used a combination of stamps to apply highly conductive graphene inks onto the surface, being able to quickly assemble complex micro-supercapacitors on a variety of substrate types with a high degree of control over their final structure. Importantly, this was achieved in the absence of metal current collectors, additives, or binders (Figure 8e,f).

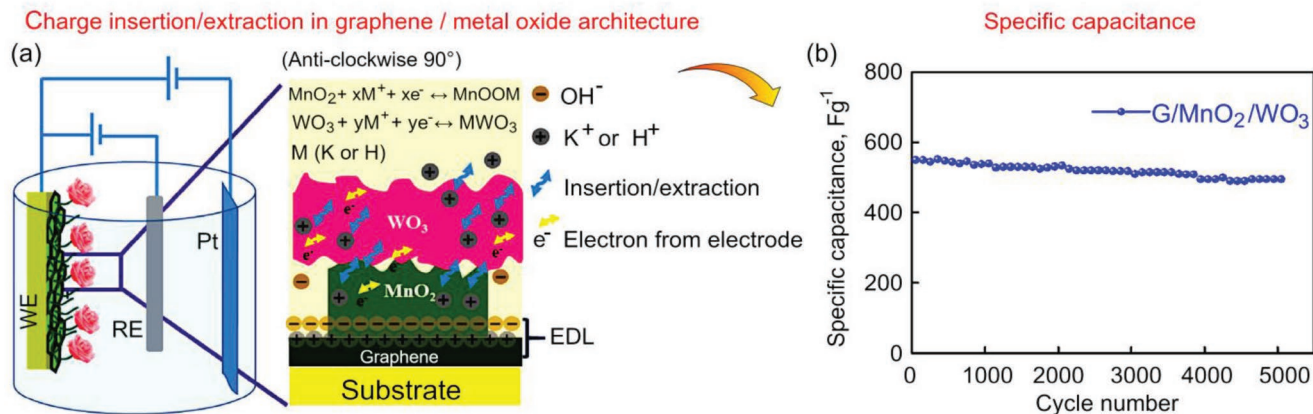
Thus, a complex interfacial system was formed in this example. The porous graphene sheets comprising the inks were in the form of crystalline hexagonal flakes of $\approx 1\ \mu\text{m}$ in size and 3 nm in thickness (≈ 8 sheets), with rough surface, an ultrahigh Brunauer–Emmett–Teller surface area, a mesoporous architecture (pore size of 3–20 nm), and a high density of defects. Collectively, these features enable an abundance of active sites and efficient transport pathways for charge carriers, excellent interfacing with electrolyte, and, as a consequence, enhanced ion transfer for the charging–discharging cycle.

Thus-fabricated devices had high areal capacitance of $\approx 21.7\ \text{mF cm}^{-2}$ at a current of 0.5 mA, couple with a high power density of 6 mW cm⁻² at an energy density of 5 μWh cm². The performance of micro-supercapacitors was maintained over 10 000 charge/discharge cycles, which is a remarkable performance. Importantly, the devices retained their excellent flexibility for over 300 bending cycles. Considering the relative ease, simplicity and flexibility of the fabrication process, and outstanding long-term performance, these micro-supercapacitors are strong candidates for wearable and portable applications (Figure 8g).

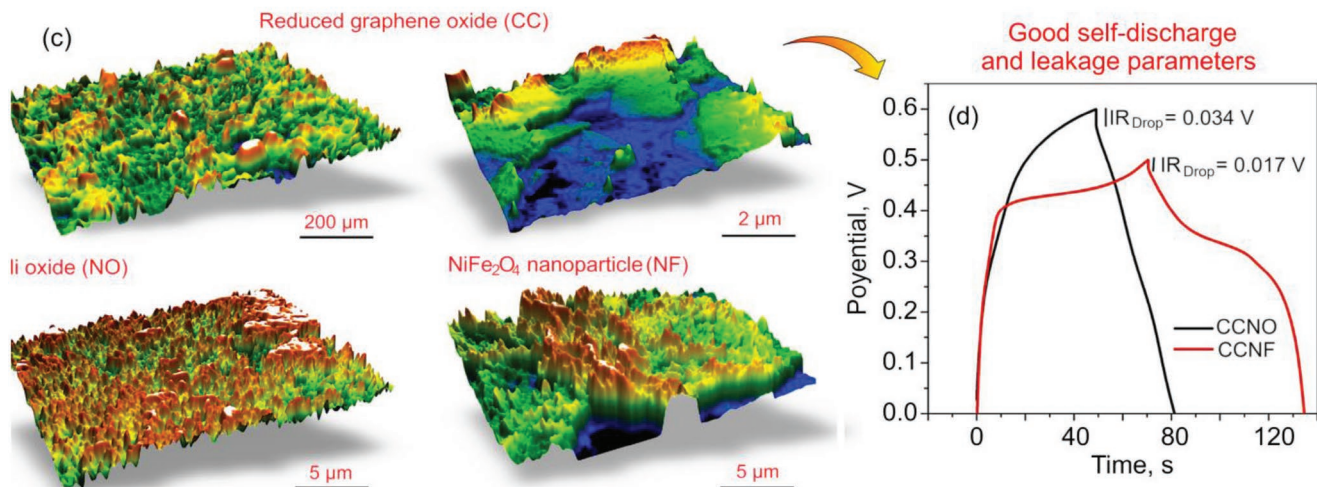
Metal–organic frameworks (MOFs)^[118] are a novel family of advanced materials with a set of unique properties that make them promising for numerous applications, including energy storage and generation.^[119,120] MOFs feature a very high specific surface area and a controllable internal structure. Combining MOFs and graphene into a single interfacial system is promising for the supercapacitor applications, yet requires the use of advanced nanoengineering. Jayaramulu et al. have recently reported^[124] successful construction of a covalent graphene–MOF hybrid architecture for high-performance asymmetric supercapacitors.^[121] A favorable combination of large surface area, multiple levels of porosity and high degree of interconnectivity of the composite structure resulted in excellent electrochemical performance, with a capacitance of up to 651 F g⁻¹. Directly linked to capacitance and cycling stability, the superior charge transport in these structures is attributed to the presence of a π -conjugated structure, the latter being in turn related to the presence of amide linkage. A power cell fabricated using the graphene–MOF hybrid, as well as Ti₃C₂T_x MXene as the opposing electrode in the asymmetric supercapacitor structure

COMPLEX INTERFACES ON FLAT GRAPHENE FOR ENERGY: SUPERCAPACITORS

GRAPHENE NANOSHEET – METAL OXIDE INTERFACES FOR SUPERCAPACITORS



REDUCED GRAPHENE NANOSHEET – NiFe₂O₄ INTERFACES FOR SUPERCAPACITORS



STAMPING STRATEGY FOR PREPARATION OF GRAPHENE-BASED PLANAR MICRO-SUPERCAPACITORS

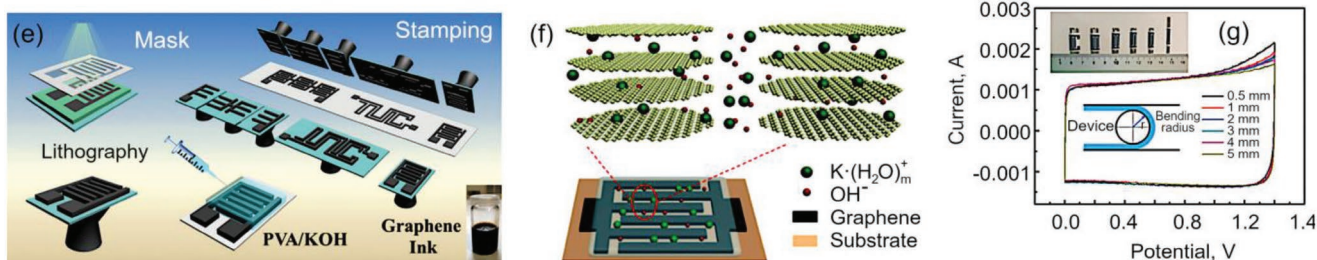


Figure 8. Complex interfaces formed on flat graphene for supercapacitor applications. a) Movement of charge carriers at the surface of graphene/MnO₂/WO₃ composites, when measurement is performed using a three-electrode cell. b) The evolution of specific capacitance of graphene/MnO₂/WO₃ architecture with charge/discharge cycling, at a current density of 1 A g⁻¹. Reproduced with permission.^[116] Copyright 2020, Elsevier. Reduced graphene nanosheets for supercapacitors. c) 3D reconstruction of the surface topography of various graphene-based structures produced from an organic waste feedstock. Complex structures such as reduced graphene oxide/NiO show a more complex surface topography, which may, at least in part, account for the enhanced catalytic activity in the composite materials. d) Voltage drop for reduced graphene oxide/NiO (CCNO) and reduced graphene oxide/NiFe₂O₄ (CCNF) composites. Reproduced with permission.^[83] Copyright 2022, Elsevier. Stamping strategy for preparation of graphene-based planar micro-supercapacitors. e) Stamping technology for flexible graphene-based micro-supercapacitors. f) Proposed charge storage mechanism for the graphene-based micro-supercapacitors. g) Current-voltage dependencies for various bending radii for the flexible graphene-based micro-supercapacitors. Reproduced under the terms of the CC-BY License.^[117] Copyright 2020, The Authors, published by Wiley-VCH.

showed excellent power density of up to 16 kW kg⁻¹ and an energy density of up to 73 Wh kg⁻¹. These performance characteristics are on par with several commercially available Ni/MH and Pb-acid batteries. When moderately loaded and subjected to 10 000 cycles, the supercapacitors maintained ~90% of their initial capacitance value. **Figure 9a,b** illustrates the schematic of the covalent assembly of the graphene acid and amine functionalized metal–organic framework into covalent graphene–metal–organic frameworks under solvothermal conditions via amide bonds. The dependence of specific capacitance of the constructed device on current density is illustrated in **Figure 9c**. **Figure 9d** shows the schematic representation of the synthesis of graphene acid from graphene nitrile and fluorographene, and the corresponding FT-IR spectra. **Figure 8e** presents the CD curves for an asymmetric supercapacitor recorded at various current densities.

Vermisoglou et al. have used a chemical approach to uniformly attach arginine molecules across both sides of the graphene, using guanidine functionality of the arginine for linking.^[125] It should be noted that direct covalent functionalization of graphene is problematic,^[122,123] and it is for this reason that the authors have used fluorographene to resolve this problem. The desired architecture, porosity, and level of functionalization were achieved by adjusting the reaction conditions, particularly the level of pore-forming agent. The resulting capacitance of 390 F g⁻¹ at a current density of 0.25 A g⁻¹ was directly related to the tripling of the specific surface area in the processed material. Thus-functionalized graphene also showed good retention of capacitance, at ~82% after 30 000 charge/discharge cycles. **Figure 9f** illustrates the results of molecular dynamics modeling of the structure. Hydrogen bonds form readily between arginine molecules, with an average of seven hydrogen bonds establishing for every ten surface chemical groups. **Figure 9g** shows the final fluorographene/arginine product, where carbon is shown in gray, fluorine in green, nitrogen in blue, and oxygen in red. **Figure 9h** illustrates the galvanostatic charge/discharge curves for fluorographene/arginine at current densities ranging from 0.25 to 5 A g⁻¹. These results show that material platforms comprising amino acids grafted onto graphene have a promising future in advancing energy storage devices with notably enhanced capacitance and stability.

Figure 9i illustrates the structure of a flexible solid-state supercapacitor designed using flexible graphene oxide and N-doped graphene paper, and **Figure 9j** shows the technology for assembling the flexible graphene oxide (GO) and N-doped graphene (NDG) paper.^[126] The authors used an efficient method of GO–ethanol dispersion filtration to fabricate free-standing flexible GO and NDG paper sheets of a large size reaching to 700 cm² in the case of GO. It was possible to vary the color and writable characteristics of thus-fabricated sheets. NDG paper was prepared using the reduction process, resulting in a material with enhanced electric conductivity, good porosity, and foldability, as well as abundant reactive sites available for ionic insertion. When tested as a material for the supercapacitor electrode, the electrochemical characteristics of the NDG paper was high, with a capacitance of 480 F g⁻¹, and a charge/discharge capacitance of 312.5 F g⁻¹ when used as part of a flexible device. This very important result promises

a wider application of various graphene-based flexible wearable devices fabricated on the base of graphene papers, prepared at the industrial scale using affordable technologies.

- ✓ The described examples demonstrated several interesting engineering solutions, where flat carbon nanostructure-based interfacial systems played a vital role in enabling the realization of desirable characteristics in a new material.

Moreover, when developing interfaces for photonic applications, carbon-based nanostructure can be modified by use of nanoparticles to increase the chemical activity with respect to photocatalysis, when the activity depends on the ability of the material to create electron–hole pairs, while its dispersed or distorted form allows enhancing greatly the reaction rate due to the increase of the reaction area. Moreover, excellent conductivity of carbon nanostructures is applied to remove the charges (electrons) from the charge-producing agent, thus increasing the recombination time, and to deliver them to the charge-consuming agent. It should be noted that the photocatalytic activity of the nanocomposites depends as much on the productivity of active media (metal or metal oxide nanostructures), as it does on the number density of the nanostructures on a surface of the carbon structure or in the volume of the charge-consuming material (e.g., pollutants or pathogenic microorganisms).

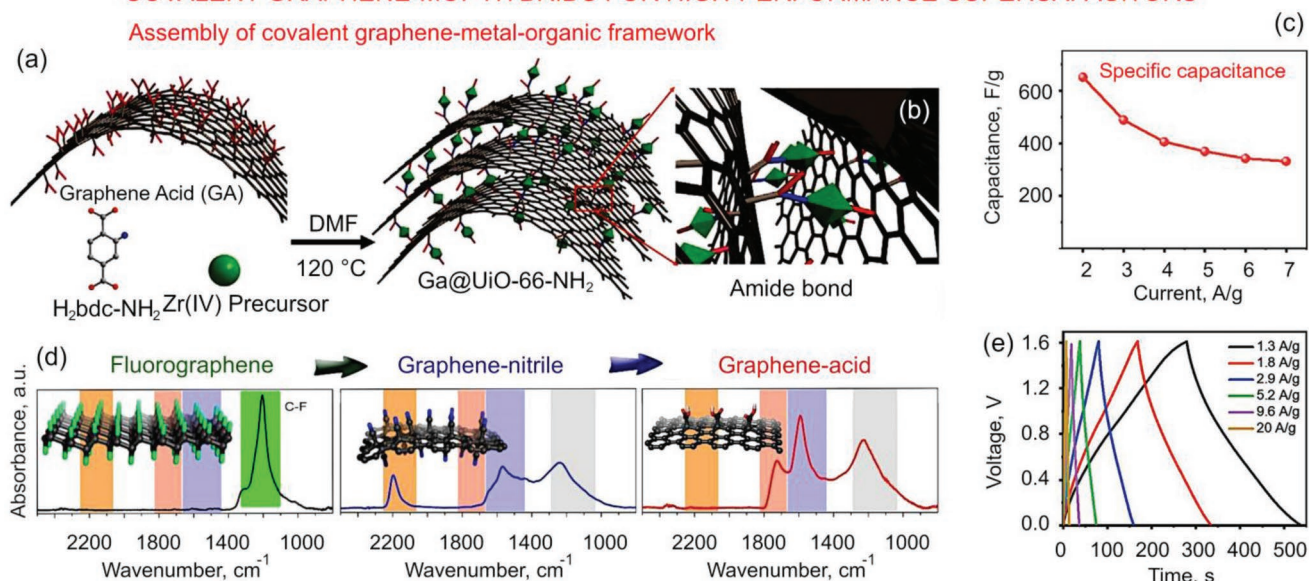
The simple solutions like that proposed by Lekshmi et al. provides a good example of a rather simple process of synthesis of rGO flakes with Ag/AgO/Ag₂O nanoparticles, and a similar approach was used by Tamilselvi et al. who engaged NiFe₂O₄ nanoparticles, while a more sophisticated process proposed by Yang et al. involved the epitaxial growth of PbS nanorods and used peculiarities of graphene crystallinity ((200) orientation) to serve as the nucleation sites. Definitely, this technique provides more possibilities in increasing the productivity by use of the crystallinity control and increasing the number of “elementary charge reactors”. At the same time, the implementation of bismuth oxyhalides with excellent photocatalytic performance like was used by Alansi et al. allows enhancing the power of a single elementary reactor.

Facility of the process proposed by Islam et al. with solvent drying and calcination to produce ZnO–MnO nanoparticles enfolded in a carbon layer to provide the conductivity of ions (unlike the previously considered case of electron conductivity in rGO) looks promising for application in production of batteries. This simple caging of 0D material with 2D carbon material and introduction of a large number of such structures into the reaction volume helps obtain a significant increase in electrochemical performance; however, the stacking of 2D sheets into an effective assembly proposed by Ma et al. 2D molybdenum dichalcogenide on 2D nitrogen-doped carbon looks more effective in increasing the device capacitance. At the same time, not only security of a certain conduction area for the ion transport should be provided, but also the possibility of acceleration of the ion transport as was made by Wu et al. who coupled SnSb₂Te₄ nanodots with highly doped graphene to create effective PN heterojunctions for the purpose. In addition, interesting patterning along the edges of graphitic nanostructure proposed by Xiao et al. looks promising in production of Zn–air batteries. Definitely, cost effectiveness of the future technologies will be considered among the main factors, and

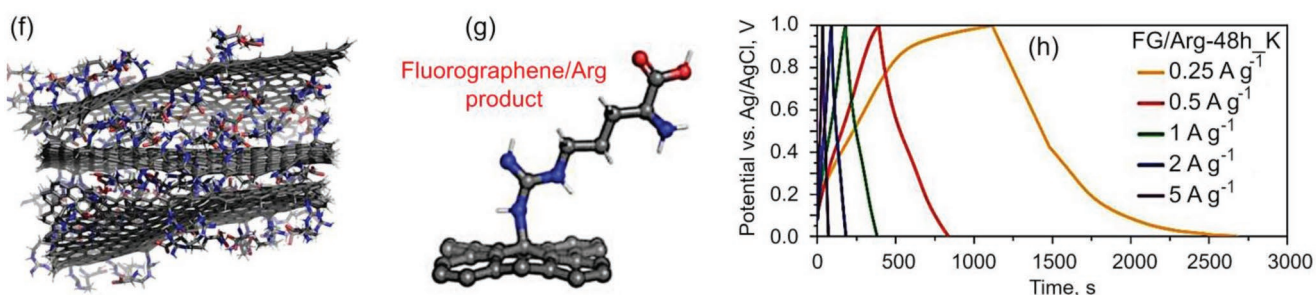
COMPLEX INTERFACES ON FLAT GRAPHENE FOR ENERGY: SUPERCAPACITORS

COVALENT GRAPHENE-MOF HYBRIDS FOR HIGH-PERFORMANCE SUPERCAPACITORS

Assembly of covalent graphene-metal-organic framework



GRAPHENE WITH COVALENTLY GRAFTED AMINO ACID FOR SUSTAINABLE SUPERCAPACITORS



FLEXIBLE N-DOPED GRAPHENE PAPER FOR SUPERCAPACITORS

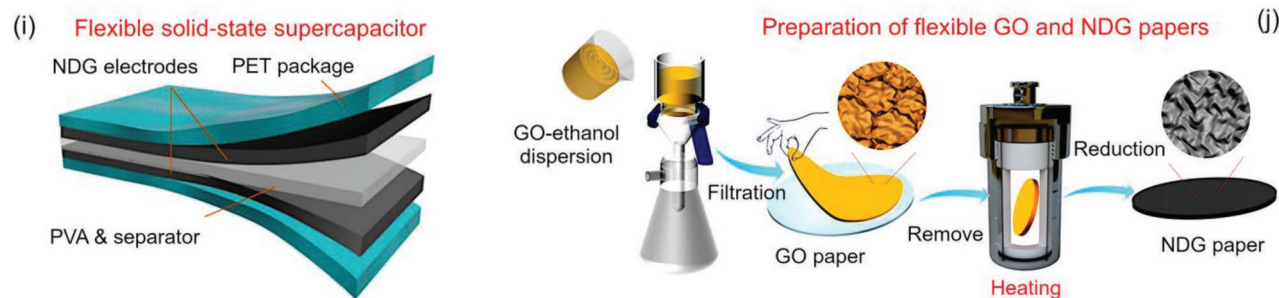


Figure 9. Complex interfaces formed on flat graphene for supercapacitor applications. a) Schematic of the covalent assembly of graphene acid and an amine functionalized metal–organic framework into covalent graphene–metal–organic frameworks under solvothermal conditions, with the linking taking place at the b) amide bond. Blue, red, and gray balls denote N, O, and C atoms, whereas UiO-66-NH₂ nanocrystals are shown as green octahedrons. c) Changes in specific capacitance with current density. d) Schematic representation of the synthesis of graphene acid from graphene nitrile and fluorographene and the corresponding FT-IR spectra. e) CD curves for an asymmetric supercapacitor recorded at various current densities. Reproduced with permission.^[124] Copyright 2021, Wiley-VCH. Graphene with covalently grafted amino acid as a route for sustainable supercapacitors. f) Molecular dynamics simulation reveals fluorographene sheets functionalized with arginine on both sides. Hydrogen bonds form readily between arginine molecules. g) The final fluorographene/Arg product. Color codes are: carbon is gray, fluorine is green, nitrogen is blue, and oxygen is red. h) The galvanostatic charge/discharge curves for fluorographene/Arg at current densities from 0.25 to 5 A g⁻¹. Reproduced with permission under the terms of the CC-BY-NC license.^[125] Copyright 2021, The Authors, published by Wiley-VCH. Flexible N-doping graphene paper for supercapacitors. i) Schematics of the flexible solid-state supercapacitor. j) Schematic of the preparation of flexible graphene oxide (GO) and N-doped graphene (NDG) papers. Reproduced with permission.^[126] Copyright 2020, Wiley-VCH.

with respect to the applied materials, Fe/Mn-based cathodes for batteries proposed by Shen et al., as well as doped graphene decorated with $\text{CoS}_x@ \text{Cu}_2\text{MoS}_4$ core@shell investigated by Nguyen et al. should be noted.

Application of carbon nanostructures in the production of supercapacitors is quite natural by considering the necessity to provide a massive surface-to-volume ratio. Thus, the surface area, effectiveness of its utilization with respect to the electrochemical performance, and flexibility can all be considered as the main factors to consider when selecting proposed solutions. The approach proposed by Huang et al. and Tamilselvi et al. is remarkably simple with respect to providing the surface-to-volume ratio, while the work by Li et al. and Zhang et al. developed the technologies to ensure the necessary flexibility; at the same time Jayaramulu et al. proposed a unique structure with excellent electrochemical performance.

4. Engineered Interfaces Based on 3D Carbon Nanostructures

3D carbon nanostructures enable the design of more complex functional interfaces due to the involvement of additional processes, mechanisms and effects as shown in Figure 2. Well-developed surfaces of the 3D nanostructures allow for a larger interfacial surface area, which causes stronger interactions between various materials and material systems.^[127–129] Moreover, complex functional metamaterials can be designed on 3D interfacial systems for different applications, including energy,^[130,131] plasmonics,^[132,133] water treatment,^[134,135] photonics,^[136,137] and many others.^[138,139] According to our concept of 3D interface, all the below considered examples illustrate the idea of 3D interface. Titanium carbide (TiC) nanoflake composites arranged in a described manner (i.e., as nano-onions) create a complex 3D structure able to store large electric charges. A multidoped porous carbon was also presented as an example of the use of the material as a matrix to create a metal–organic-framework. The effect of freestanding N-doped porous carbon nanofibers with the embedded Se can be considered as a superposition of effects caused by the spatial shape (physical patterning) and chemical patterning, thus creating a 3D interface.

4.1. Interfaces Based on 3D Carbons for Photonics Applications

Photonics-based applications could utilize many benefits of 3D developed interfaces, since many light-induced processes could be enhanced in the strongly coupled interfacial systems.^[140,141] As a characteristic example, we can mention the prominent role played by Ψ functions in determining key properties of metamaterials through the associated morphological parameters.^[136,137]

Hierarchical carbon-based metamaterials have been recently demonstrated to generate white light via photoluminescence from a single structure, without the use of red–green–blue emitters.^[142] The former were created by applying an advanced technology resulting from a simple yet effective combination of oxygen plasma with a high-temperature treatment; when

used individually or in combination, these technologies have previously been demonstrated to be promising technology for the synthesis and modification of nanomaterials and their systems.^[143,144] The depositions have been carried out using a radio-frequency (RF) inductively-coupled plasma enhanced chemical vapor deposition (ICP-PECVD) reactor^[145,146] shown in Figure 10a. Photoluminescence investigations performed using a Yb-KGW laser crystal suggest that the presence of sharp nanocones in the studied composites yield photoluminescent properties distinct from those of standard composites of the same material. Indeed, the use of several well-known techniques such as 2D-FFT spectra analysis, Hough distribution evaluations, and application of standard Minkowsky functionals, suggest that the photoluminescent response of the treated material is governed by the resulting Minkowsky boundary functional and the associated surface material ordering and connectivity.^[147] It is found that the optical properties of such carbon–nanocone composites cover a wide range of the visible spectrum making them excellent white light emitters, as substantiated by International Commission on Illumination color space coordinates (Figure 10b–d). Furthermore, we can correlate such novel optical properties with the morphological parameters defining the surface structure of these metamaterials, consistent with their overlap with the Ψ functions mentioned above.

A very interesting and extremely important application of a carbon-based interfacial system has been recently reported by Park et al. Carbon nitride-based photonic retina-inspired synapses were designed for selective detection of UV light.^[148] Such organic photonic synapses (OPS) are capable of integrating both sensing and processing functions realized within a single small device, so that they are considered to be promising tools for emulating a biological retina characteristic of human visual perception.^[149,150] Up until now, photonic synapses with a variable wavelength, have not been practically realized, yet they are an essential characteristic of visual perception in humans. In their article, for the first time ever, the authors have reported the fabrication of OPS for the detection of UV rays and the processing of a number of optical stimuli. Such OPS use carbon nitride (C_3N_4) within a floating-gate sheath in a transistor composition as the UV-responsive element. Since C_3N_4 nanodots mostly absorb UV light, they are chosen as the basic components responsible for providing UV selectivity in OPS. Importantly, this device requires just ≈ 18 fJ per synaptic event, comparable to that of biological synapses. Moreover, the modulation of in situ exposure to UV-light was reported by building the devices together with UV transmittance modulators. Cross-sectional schematics of the human eye illustrating the multilayer structure of the retina is shown in Figure 11a, while the scheme of the device and the photoresponses of OPS, for various durations of UV light C_3N_4 -treated layers, are shown in Figure 11b,c. This relatively simple yet effective system may be applicable to advanced electronic skin devices to detect and block UV, since it is able to automatically adapt itself to an ever changing UV-light environment. It can also promote the development of next generation windows that can control transmittance of UV light in a selective way, providing a more environmentally friendly mechanism for light and heat management in cars and buildings. In a similar manner, the system can enable the development

3D CARBON-BASED INTERFACES FOR PHOTONICS APPLICATIONS

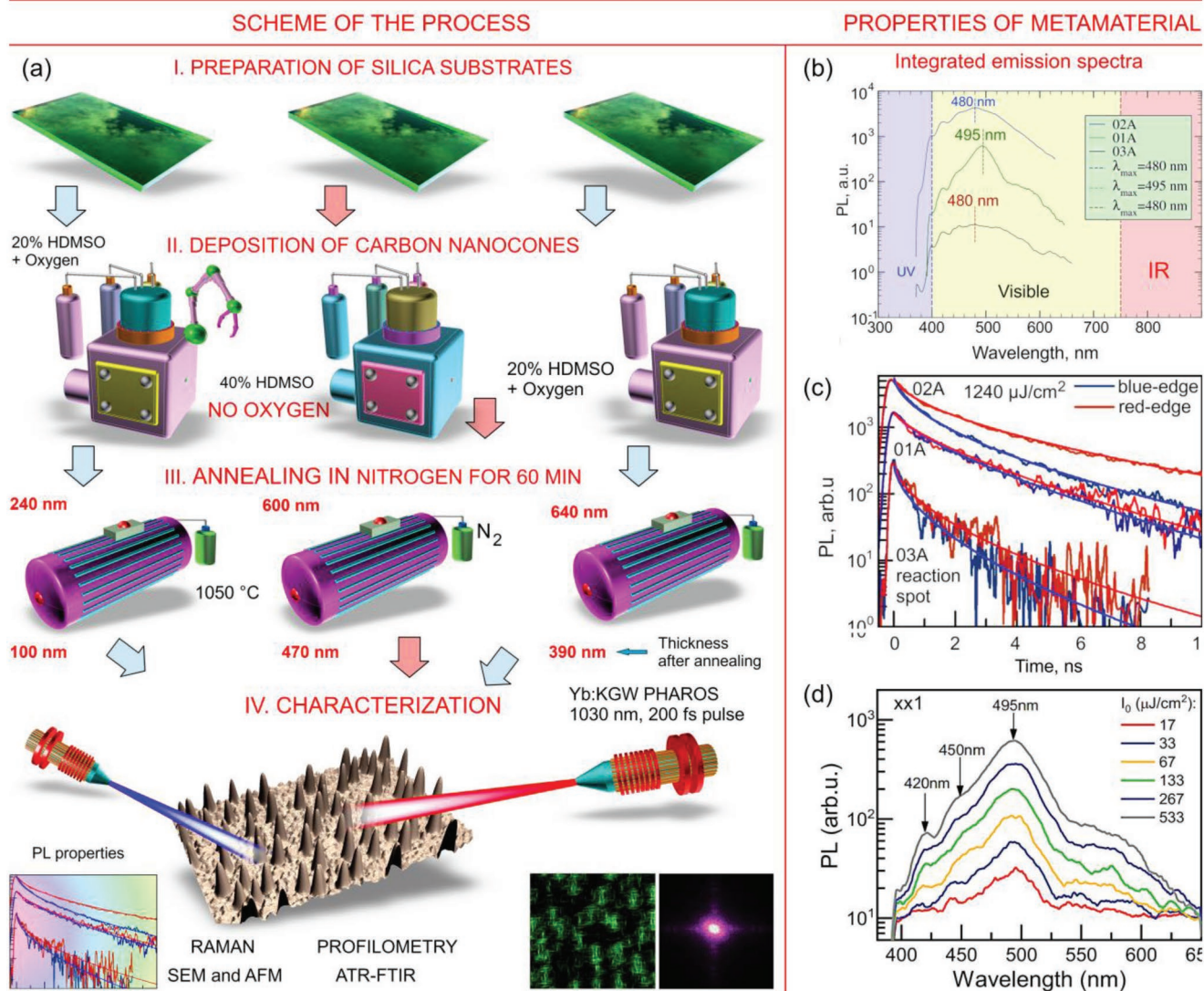


Figure 10. Hierarchical carbon nanocone-silica metamaterial for the white light photoluminescence. a) Schematical representation of the experimental protocol. Preparation of raw silica samples is followed by their mounting in the reactor, where they are treated using an inductively-coupled RF plasma. Different environmental processes can be selected. Finally, the carbon nanocone composite is annealed in a nitrogen atmosphere. b) Total emission spectra for a few selected samples (see inset) as a function of light-emission wavelength. In all cases, a 350 nm wavelength excitation of constant fluence was used. The maxima of the spectra are marked on the graph and listed in the inset. c) Photoluminescence decay rates for various samples. The sample group with the sharpest cones also features the shortest time of decay. d) Photoluminescence spectra measured on the annealed sample for different fluences I_0 , demonstrating the linear dependence from I_0 . Reproduced with permission.^[142] Copyright 2022, ACS.

of smart glasses capable of filtering excessive UV rays; as well as being used in novel sensors, in artificial retinas for advanced human-like robots, and in neural prostheses aimed to be compatible with optic nerves.

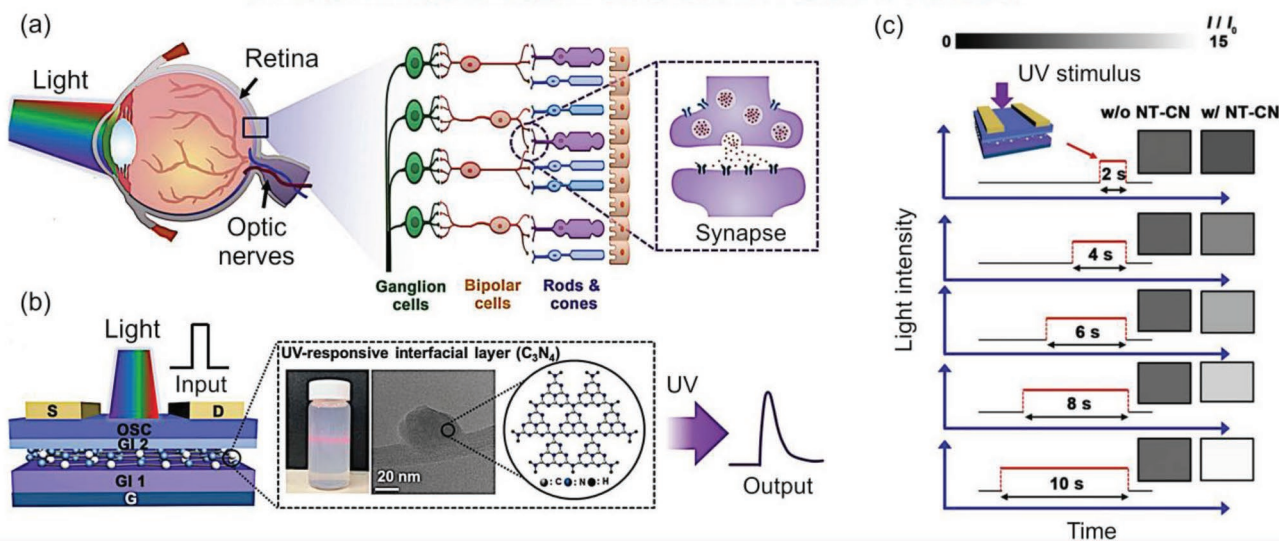
We should stress here that the developing efficient artificial retinas for miniaturized robots and particularly for humans is the problem of exceptional importance. On the other hand, retinas feature essentially interfacial systems, where several functional levels convert the light signals and transmit the electric signals. Moreover, the layers should be very thin, to ensure the transmission of light, and absorbing enough to convert light energy into electric signals. These contradicting

requirements could be satisfied by designing artificial interfacial systems.^[148]

Magneto-responsive optical fibers with a fluorinated graphene oxide core is one more highly important, quite recent result that is promising for many high-tech applications (Figure 11d).^[151] For years, optical fibers, both silica and polymer in their nature, have been used extensively in communications, being a particularly critical enabling platform for long-distance communication. Despite significant progress in the development of optical fibers, there remains an issue of irreversible changes these fibers may undergo when used to transmit high power signals. Up until now, these

3D CARBON-BASED INTERFACES FOR PHOTONICS APPLICATIONS

CARBON NITRIDE-BASED PHOTONIC SYNAPSES FOR UV LIGHT



MAGNETORESPONSIVE OPTICAL FIBER WITH FLUORINATED GRAPHENE OXIDE CORE

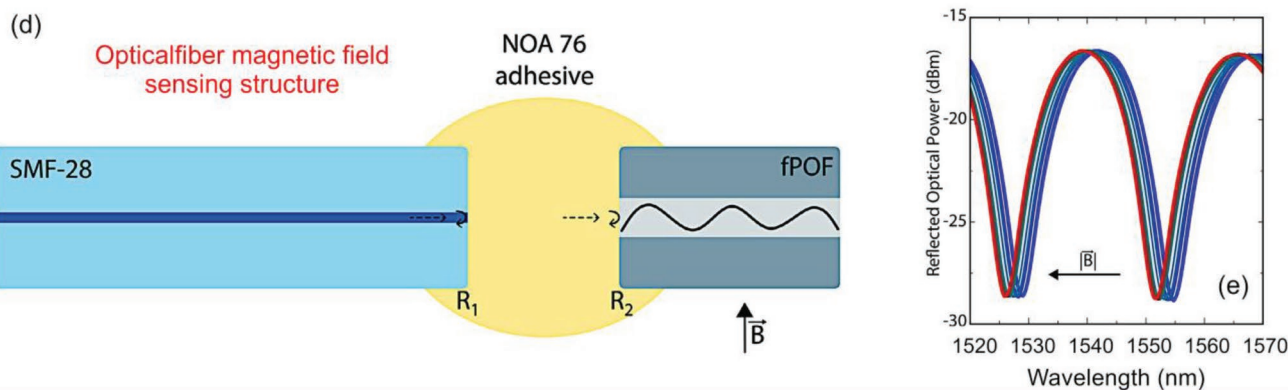


Figure 11. Carbon nitride-based photonic retina-inspired synapses for selective detection of UV light. a) Schematic illustration of a cross-sectional area of a human eye, together with the typical multilayer structure of a retina. b) Scheme of a device structure of carbon nitride-based photonic retina-inspired synapses (left box): Source (S), drain (D), organic semiconductor (OSC), the first gate insulator (GI 1), the second gate insulator (GI 2), and gate (G). (Right box) A photo of a homogenous colloidal DMF suspension of NT-CN displaying the Tyndall effect. A TEM image, and a chemical composition of nitric acid-treated C_3N_4 . c) Photoreponse of the devices, for different C_3N_4 layers treatments of various lengths of UV light exposure. Here, I/I_0 represents the ratio of photocurrent I to the dark current I_0 . Reproduced with permission.^[148] Copyright 2020, Wiley-VCH. Magnetoresponse optical fiber with a fluorinated graphene oxide core. d) Schematics of the magnetic field sensing structure based on the optical fiber. Here, R_1 and R_2 denote the reflective mirrors of Fabry–Pérot interferometer. The incident and reflected light are indicated with the dashed and curved arrows, respectively. e) Reflection spectra evolution with increasing applied magnetic field intensity. Reproduced under the terms of the CC-BY license.^[151] Copyright 2022, The Authors, published by Wiley-VCH.

structural changes remained not fully understood due to the challenges of studying the process of material fusing under these conditions. To address this knowledge gap, Paixão et al. have conducted an extensive study of how fibers fuse, and what materials form in the fiber core, and in the process of doing so have demonstrated such high power signal-induced fusing to be a simple yet effective means of producing novel fiber materials with a fluorinated graphene oxide. Additionally, similarly to other fluorographenes, the formation of fluorinated graphene oxides has significantly increased the magnetic susceptibility of the fiber, by nearly an order of magnitude.

At the conclusion of these efforts, thus-fabricated fused polymer optical fibers were used to design a sensor capable of detecting magnetic field with a maximum sensitivity of 4.66 pm Oe^{-1} , thus placing the device at the top end among those known in literature. These results pave the way for the design and fabrication of future sensing and actuation devices, thus opening the door to a variety of applications across biomedical, telecommunications, and aerospace engineering.

Thus, new metamaterials produced recently by plasma-enhanced chemical vapor deposition technique display remarkable photoluminescence properties. Importantly, they are based on hierarchical carbon nanostructures, where the efficient

interfacial systems are formed via connected 3D network of nanocones that ensure excellent optical properties due to its collective response properties covering essentially the whole visible range, making them suitable as white light emitters, often performing much better than the traditional devices.

Another interesting application is the development of above discussed organic photonic devices based on carbon interfacial modules, which are able to mimic the behavior of human retina synapses.^[148] This discovery opens the door to the design of future single miniaturized devices to be used for detection of UV rays and for the processing of a variety of optical stimuli. Many applications are envisaged, including smart UV glasses, novel sensors for advanced human-like robots, neural prostheses compatible with human optic nerves.

Moreover, fluorinated graphene oxide thin-film interfaces employed in new magneto-responsive optical fibers represent a promising area of research with many potential applications.^[151] The newly developed fibers display remarkable long-lived performance, superior to the present technology used for long-distance communication as they are more resilient to the transmission of high-power signals, in addition to show an enhanced magnetic susceptibility, by about one order of magnitude, with respect to their standard counterparts. These properties are to a large extent a result of the prominent modifications in the chemical structure of the material.

- ✓ Above discussed examples of nanoengineered interfacial carbon-based systems demonstrate their ability to perform the most complex functions such as single-device white light emitters, artificial retinas and magneto-responsive graphene-based optics. This proves their great potential for designing cutting edge technologies, and thus justifies the further research and design effort in this field.

4.2. Interfaces Based on 3D Carbon Nanostructures for Energy: Batteries

The exceptional abilities of carbon-based interfaces for the photonics applications bring a promise that the energy-oriented technologies also could greatly benefit from these systems. Indeed, various materials and systems were studied and excellent results found.^[152,153] In this subsection we will outline several very recent, important examples of carbon-based interfaces that improved key performance characteristics of electric batteries.

A novel material system based on freestanding N-doped porous carbon nanofibers with the embedded small-molecule Se were successfully used to enhance the flexible potassium-selenium batteries.^[154] In fact, due to the relatively large natural potassium reservoirs on Earth, the latter batteries are considered a valid alternative to other solutions for energy storage. Yet, the microscopic mechanism for energy storage remains to be understood. By means of computational methods, supported by experiments, the authors discuss a possible origin for K-ion confinement within a Se cathode. To this end, a flexible K-Se battery was implemented by exploiting the small size of Se molecule and embedding it in N-doped thin film (Se@NPCFs) made of porous carbon nanofibers, the latter constituting the cathode (Figure 12a). It turns out that short-chains molecular

Se gets encapsulated within a microporous cavity, thus transforming the chain into K_2Se undergoing a two-step reaction through a purely solid state treatment taking place within the carbonate electrolyte solid, envisaging a possible reaction mechanism. In such scenario, polyselenides are to a large extent electrochemically suppressed due to the dominating role of Se_2 molecules, leading to a notable enhancement in the use of Se for the effective realization of a K-Se battery. Characteristics (the rate performance and prolonged cyclability) of this newly developed system are shown in Figure 12b. Figure 12c illustrates the optimized structures for the intermediates. This figure shows that, because of their lower free energy, adsorption of single Se_2 composites onto the N-doped porous carbon nanofibers is promoted during the infiltration. These results suggest that by a suitable engineering and handling of selenium chemistry, the actual generation of selective species promote a way to optimize the performance of a K-Se battery, in addition to revealing the internal reaction mechanism in the carbonate electrolyte.

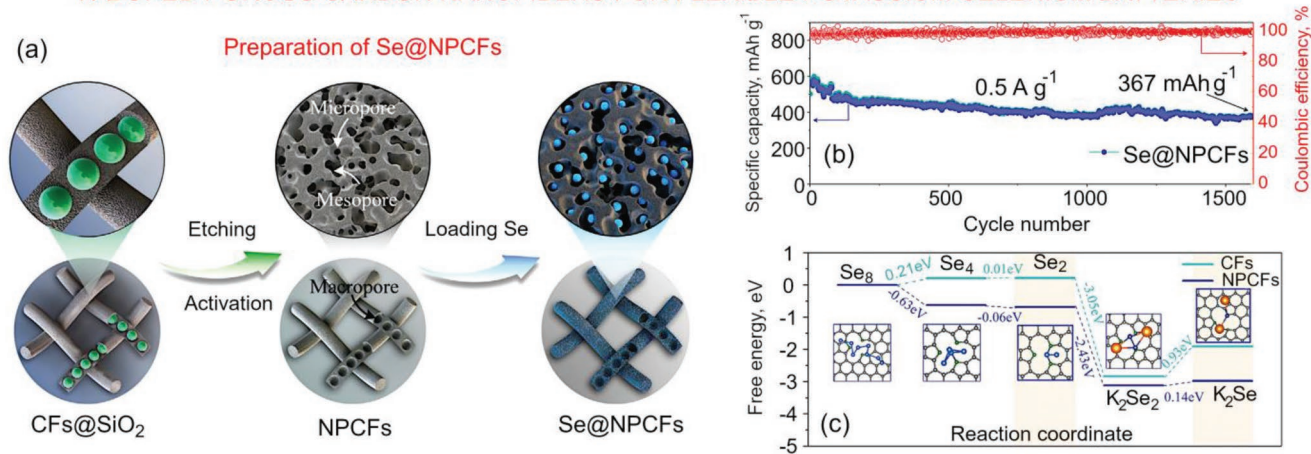
This important result stresses the potential of the use of interfacial systems in devices that utilize the synergistic effects. In this case, synergy was established using the pore confinement and doping. Apparently, synergistic effects could be expected in many other interfacial systems with strong interaction between layers, thus enabling designing various advanced systems.

A somewhat similar system comprising N-doped carbon nanotubes and the embedded NiFe nanoparticles (Figure 12d) was used to enhance the performance of wearable solid-state Zn-air batteries.^[155] As a result of their prominent characteristics, Zn-air batteries are expected to make a major advance in the development of flexible electronics and power sources.^[156] For now, actual implementation of Zn-air batteries is limited by their unsatisfactory low power capacity and a small number of possible recharging cycles. The latter arises from the slow kinetics typical of oxygen reduction and evolution reactions (ORR and OER) on a cathode in air. The authors designed a nanotube/nanoparticle interfacial system to produce high-power, wearable Zn-air batteries characterized by excellent electrochemical performances, which are developed on a base of a new bifunctional nanocomposite electrocatalyst composed of NiFe nanoparticles embedded in N-doped carbon nanotubes (NiFe/N-CNTs) (Figure 12e,f). This novel material can efficiently enhance O_2 adsorption in ORR and OH adsorption in OER, thus enabling a manifestly superior electrocatalytic activity with respect to both ORR and OER. The resulting wearable batteries, together with the novel nanocomposite electrocatalyst as air cathode, yield an ultrahigh open-circuit potential of ≈ 1.4 V and a high peak power density of ≈ 105 mW cm^{-2} . Moreover, the battery demonstrated a small gap with respect to the charging—of ≈ 0.6 V, and a remarkable durability of 800 min, thus suggesting new strategies for the design of high-performance nanoengineered metal-air batteries.

Figure 13a illustrates one more example of successfully designed carbon-based interfacial material for the Zn-air batteries. This flexible solid-state Zn-air battery was made utilizing interface based on sandwiched leaf-like carbon nanotubes.^[157] A two-functional oxygen electrocatalyst, interwoven with carbon nanotubes, built upon $Co/ZnCo_2O_4$ nanoparticles stocked in

3D CARBON-BASED INTERFACES FOR ENERGY: BATTERIES

N-DOPED POROUS CARBON NANOFIBERS FOR FLEXIBLE POTASSIUM-SELENIUM BATTERIES



NiFe NANOPARTICLES EMBEDDED N-DOPED CARBON NANOTUBES CATALYST FOR FLEXIBLE BATTERIES

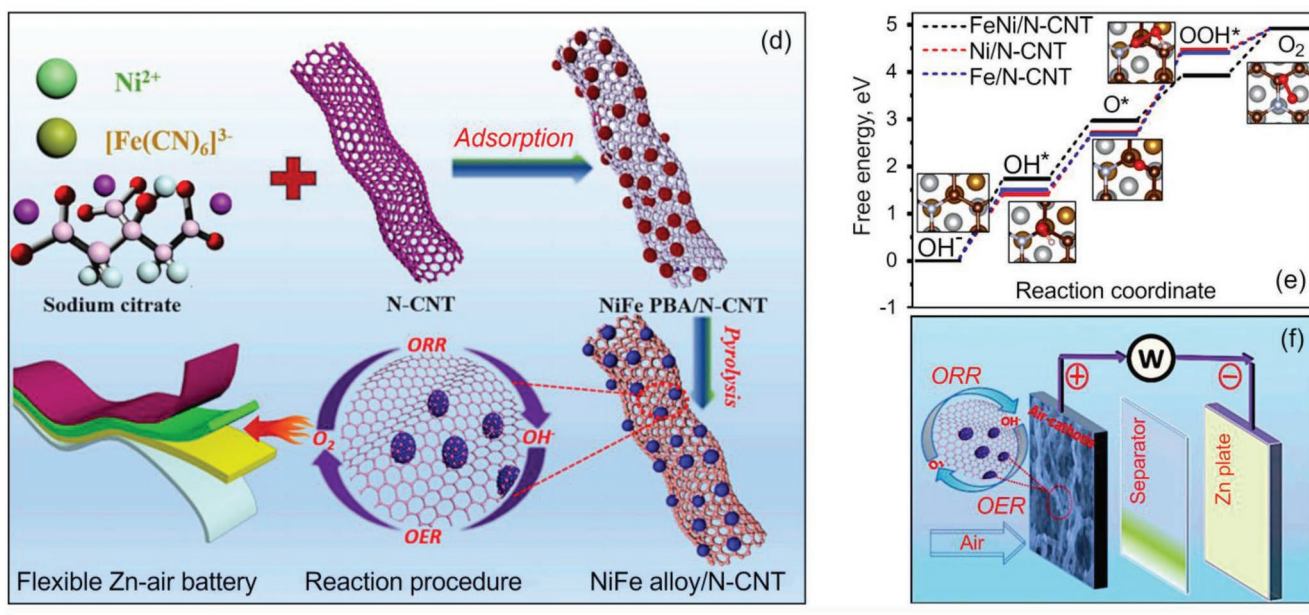


Figure 12. N-doped porous carbon nanofibers for potassium–selenium batteries. a) Preparation of small-molecule Se embedded in freestanding N-doped porous carbon nanofibers (Se@NPCFs) material. (Rate performance and persistent cyclability for 0.5 A g^{-1} . c) Plots of free energy for deposited Se chains, K_2Se_2 and K_2Se on pure graphene and N-5 doped graphene. The optimized structures for the different intermediates are shown in the insets. The lower free energy promotes the deposition of Se_2 molecules on the NPCFs substrate during the infiltration. Reproduced with permission.^[154] Copyright 2020, Wiley-VCH. NiFe nanoparticles embedded N-doped carbon nanotubes for the flexible Zn–air batteries. d) Scheme of the synthesis of NiFe nanoparticles embedded in an N-doped CNT catalyst and the associated flexible Zn–air batteries that utilize this catalyst. e) The theoretical diagram of free energy of catalyst representatives. The increased adsorption capacity for oxygen and OH^- in NiFe/N-CNT electrocatalyst. f) Schematic of the liquid Zn–air battery. Reproduced with permission.^[155] Copyright 2020, Elsevier.

leaf-like nitrogen-doped carbon microplates ($\text{ZnCo}_2\text{O}_4@\text{NCNTs}$). Due to the large concentration of metal– N_x and Co^{3+} active nodes, as well as the closely intertwined carbon nanotubes on the microplates, this novel catalyst yields outstanding oxygen reduction and evolution reaction performance displaying: a small potential gap accompanied with the power density of 305 mW cm^2 and almost constant rechargeability at 103 h working

hours with the Zn–air battery. So far, such novel catalyst flexible Zn–air battery is found to display satisfactory peak power density of $\approx 150 \text{ mW cm}^2$, potent flexibility and integrability. Figure 13b shows the discharge and power density curves of two batteries, connected in series, and of a single battery. Figure 13c presents the voltage–current density and power density–current density dependencies for various catalysts, demonstrating the excellent

3D CARBON-BASED INTERFACES FOR ENERGY: BATTERIES

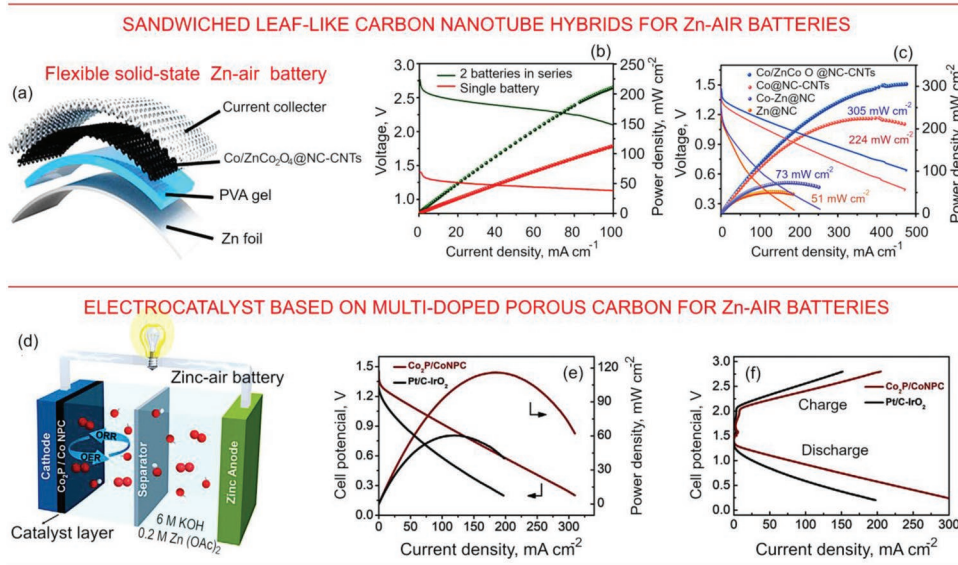


Figure 13. Sandwicheed leaf-like carbon nanotube hybrids for high-power-density Zn-air batteries. a) Scheme of flexible solid-state Zn-air battery utilizing interface based on sandwicheed leaf-like carbon nanotubes. b) Graph of the discharge and power density curves for two flexible solid batteries connected in series connection, and for a single battery. c) Voltage-current density and power density-current density for various catalysts. Reproduced with permission.^[157] Copyright 2021, Elsevier. Electrocatalyst based on multidoped porous carbon for Zn-air batteries. d) Scheme of Zn-air battery utilizing electrocatalyst based on multidoped porous carbon and Co_2P nanoparticles. e) Cell potential and power density curves for the Zn-air battery. f) Charge/discharge polarization curves for the Zn-air battery. Reproduced with permission.^[160] Copyright 2020, Wiley-VCH.

characteristics of the novel catalyst based on sandwicheed leaf-like carbon nanotubes and nitrogen-doped carbon microplates. Application of carbon-based interfacial material systems ensures significant enhancement in the performance characteristics of the flexible solid-state Zn-air batteries.

Multidoped porous carbon was used as a base to enhance the Zn-air batteries by designing the nanocomposite material system with metal-organic-framework-derived Co_2P nanoparticles. This strategy to improve the properties of the batteries is to utilize the carbonous substrate and then to anchor the nanoparticles of transition metal phosphides to construct a hybrid structure. The metal-organic framework which features the tunable pore structure is a promising precursor for designing such a hybrid structure.^[158] The interaction between Co_2P and the doped carbon samples leads to formation of composites with electrocatalytic properties for oxygen and hydrogen evolution reactions and oxygen reduction reaction, at least comparable to those of commercial RuO_2 or Pt/C catalysts. This technology was adopted not only for batteries, but also for water-splitting, and obtained results confirmed its effectiveness. Figure 13d shows the scheme of Zn-air battery utilizing electrocatalyst based on multidoped porous carbon and Co_2P nanoparticles. Figure 13e shows the cell potential and power density curves for the Zn-air battery, and Figure 13f demonstrates the charge/discharge polarization curves for the Zn-air battery assembled using the nanocomposite material system with metal-organic-framework-derived Co_2P nanoparticles. The reported facile MOF-based technology demonstrates outstanding application for the Zn-air batteries.

Thus, electric batteries constitute another promising and useful application of carbon-based interfacial systems for

energy storage. A number of above discussed interface-based applications have demonstrated a great potential of such systems for the durable, powerful batteries, which are urgently required for various advanced application, such as, e.g., miniaturized propulsion systems for small satellites.^[159]

Among many important results, we can stress here that the small-molecule Se, embedded in N-doped porous carbon nanofibers, significantly enhance the performance of potassium-selenium batteries.^[154] This application is greatly favored by the relatively large natural potassium reservoirs on Earth, making such batteries a valid alternative to other more standard solutions for energy storage. Recent investigations suggest that specific manipulations of selenium chemistry can lead to the generation of selective species to optimize the K-Se battery performance, in addition to revealing actual reaction mechanisms taking place in the carbonate electrolyte. Similarly, a system based on N-doped carbon nanotubes with NiFe nanoparticles is at the basis of highly performance wearable solid-state Zn-air batteries, the use of which was so far limited by unsatisfactory low power capacity and a small number of recharging cycles.^[155] Further improvements on Zn-air batteries were achieved by employing multidoped porous carbon containing Co_2P nanoparticles. Such metal-organic frameworks constitute a promising precursor for designing novel hybrid structures, as reported by the use of facile MOF-based technology demonstrating the outstanding versatility of Zn-air batteries.

✓ The above examined examples suggest that the nanoengineered interfacial carbon-based systems are able to significantly boost the performance characteristics of advanced batteries, ensuring very high numbers for the specific

capacitances and power density. Importantly, their application in flexible and wearable batteries is very promising. Further research and design efforts in the nanoengineered interfacial materials will contribute to the advancement of novel batteries, required for wearable and advanced transportation systems, wearable sensors, and health monitoring systems.

4.3. Interfaces Based on 3D Carbons for Energy: Supercapacitors

Very efficient application of multilayered fullerene-based interfacial materials for supercapacitors has been recently demonstrated. The discovery of carbon nano-onions with their well-developed surface area (due to the high level of defects present in the sp^2 carbon shells of multilayered fullerenes) and very high electrical conductivity (similar to that for carbon black), provided us with a new family of nanomaterials for future energy applications. Unfortunately, the poor efficiency of the synthesis of carbon nano-onions at the level required for industrial production (i.e., in gram quantities) has prevented their use in many potential applications. Recently, Lei et al. have demonstrated the synthesis of activated carbon (P@PC-AC) material for supercapacitors derived from pitch-coated petroleum coke,^[161] both petroleum pitch and coke being carbon-rich products of petroleum refining. Carbon nano-onions of sizes between ≈ 5 and 30 nm in diameter, possessing abundant micropores, have been produced. **Figure 14a–c** illustrates the synthesis technology, growth mechanism of the hollow carbon nano-onions by template technology, and characteristics of the supercapacitor assembled using the pitch-coated petroleum coke derived activated carbon material. It delivered large specific capacitance of 312 F g^{-1} at 1 A g^{-1} , keeping a residual one of $\approx 251 \text{ F g}^{-1}$ at 20 A g^{-1} . Importantly, ordered graphitic structures could reach a fast charge transfer characteristics conditioned by their sp^2 -hybridized structure, thus positively contributing to the enhancement of their supercapacitor properties under high current density conditions. Furthermore, to gain further insight the authors proposed an associated mechanism for the growth of nano-onions from carbon precursors that are by-products of petrochemical refinement.

Interestingly, the synthesis method where the bubbles were used as templates for growing curved carbonous flakes is essentially interface-driven process, accruing at the bubble surface–carbon contact areas. In fact, in the above discussed fullerene-based materials for supercapacitors the interfacial processes play significant role at the stage of material formation and in the as-ready supercapacitors. These results illustrate the great potential of multilayered fullerene-based interfacial systems for a large-scale production of very efficient supercapacitors.

Novel results on the application of graphene nanocomposites and vanadium oxides (VO_x) for assembling electrodes for supercapacitors are illustrated in **Figure 14d,e**. A straightforward fabrication of multivalent VO_x /graphene nanocomposite electrodes for efficient symmetric supercapacitors with high density of energy has been recently reported by Huang et al.^[162] Hybrid electrodes, resulting from the combination of transition metal oxides and carbon composites, are selected as strong candidates to further improve the performance of supercapacitors. The authors demonstrated a practical design of gra-

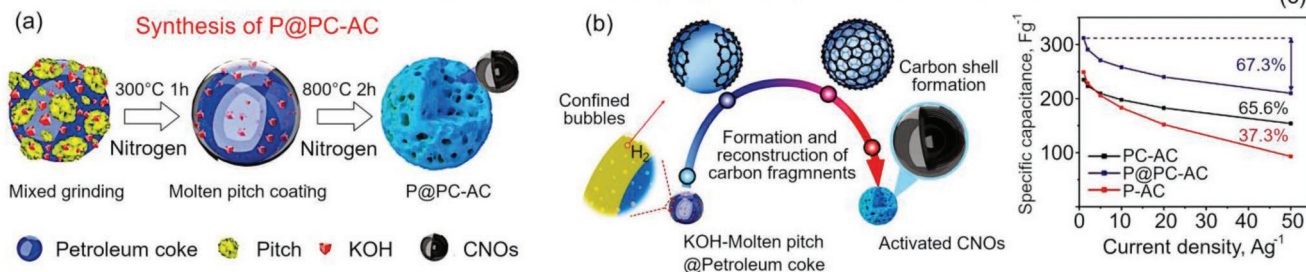
phene/ VO_x electrodes, which includes both vanadium oxides and a highly conductive graphene shell with multiple-oxidation states, which were obtained via a standard laser-scribing method (**Figure 14d**). It is found that such graphene/ VO_x three-electrodes display large potential ranges, having a high specific capacitance of 1110 F g^{-1} . The associated aqueous graphene/ VO_x supercapacitors allow one to obtain the energy densities as high as 54 Wh kg^{-1} , resulting in almost no capacitance loss after 20 000 cycles. In addition, the flexible (quasi-solid-state) graphene/ VO_x SSCs can account for very large densities of about 72 Wh kg^{-1} , or 77 mWh cm^{-3} (**Figure 14e**), exceeding the performance of many presently available industrial devices. These gel graphene/ VO_x SSCs, having Coulombic efficiencies close to 100%, exhibit over 92% of their initial capacitance after 20 000 cycles. The suggested technique allows one the possibility of a straightforward manufacturing of redox-active electrodes, which can be combined with almost any other substrate, including the more common silicon wafers and also flexible substrates, opening the way for new flexible and wearable electronic devices.

Another promising nanocomposite for the advanced supercapacitors is TiC. Interestingly, this material was prepared using biotemplates.^[163] As we have mentioned above, transition metal oxides are promising for the supercapacitors; transition metal carbides also hold a strong promise for the fabrication of electrodes. By using a cotton towel as a carbon source, and a suitable template, TiC nanosheet structures have been successfully prepared by a reliable and cost-effective biotemplate method (**Figure 14f**). It is found that the properties of thus-formed nanostructures are highly affected by the sintering time at elevated temperatures. Electrodes made of TiC nanosheets display a very high specific capacitance of $\approx 276.1 \text{ F g}^{-1}$ at 5 mVs^{-1} , and a consistent capacitance of 94% over 1000 cycles at a current density of 10 A g^{-1} . Moreover, symmetric supercapacitors with outstanding electrochemical properties conditioned by the utilization of TiC-nanosheets (276.1 F g^{-1}) have been successfully manufactured (**Figure 14g**). They have shown a maximum specific capacitance of $\approx 194.5 \text{ F g}^{-1}$ and a capacitance retention of 80.5% after 20 000 cycles. This appears to be one of the highest capacitances ever reported for such a system. When connected in series, the capacitors demonstrate high densities of energy (reaching 41 Wh kg^{-1}) and power ($\approx 2.3 \text{ kW kg}^{-1}$), and excellent cycling stability. Interestingly, the device was able to operate as a white light-emitting diode indicator for over 10 min. All the parameters make the nanostructure quite useful for energy storage applications. **Figure 14h** shows the charge–discharge dependencies for current densities in the range from 5 to 40 A g^{-1} .

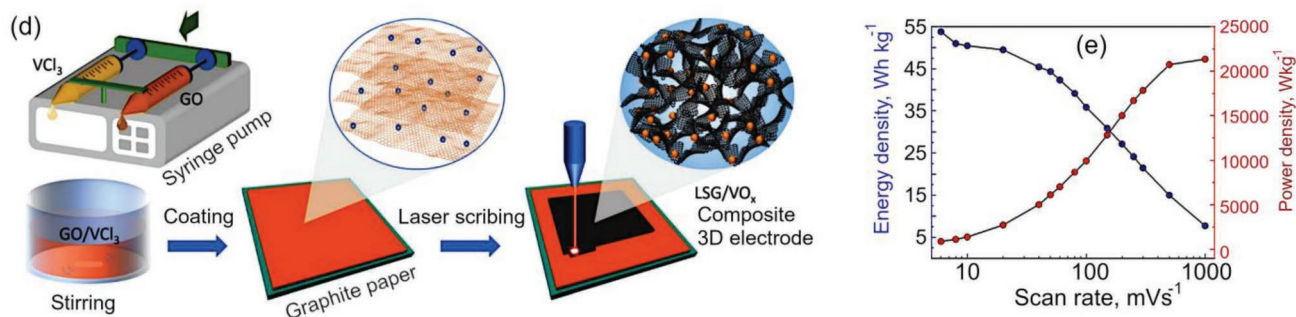
A novel complex interfacial carbon/ MoS_2 material has been recently demonstrated for an important and interesting application—a photoresponsive supercapacitor. In general, the construction of highly integrated and self-powered machines can be facilitated by using the stimuli-responsive supercapacitors as building blocks.^[164,165] The increasing demand for highly cyclic stability, however, places stringent requirements on the electrode material, and in particular its stability under dynamic conditions or when subjected to a stimulus. Tang et al. addressed this problem by working out a novel design of a MoS_2 @carbon core–shell structure, having ultrathin MoS_2

3D GRAPHENE-BASED INTERFACES FOR ENERGY: SUPERCAPACITORS

PITCH COATED ACTIVATED CARBON (P@PC-AC) FOR SUPERCAPACITORS



GRAPHENE NANOCOMPOSITE-BASED ELECTRODES FOR HIGH-ENERGY-DENSITY SUPERCAPACITORS



MULTILAYERED TiC NANOFLEAKS FOR HIGH PERFORMANCE SYMMETRIC SUPERCAPACITORS

Synthesis of layered TiC nanoflakes for supercapacitor

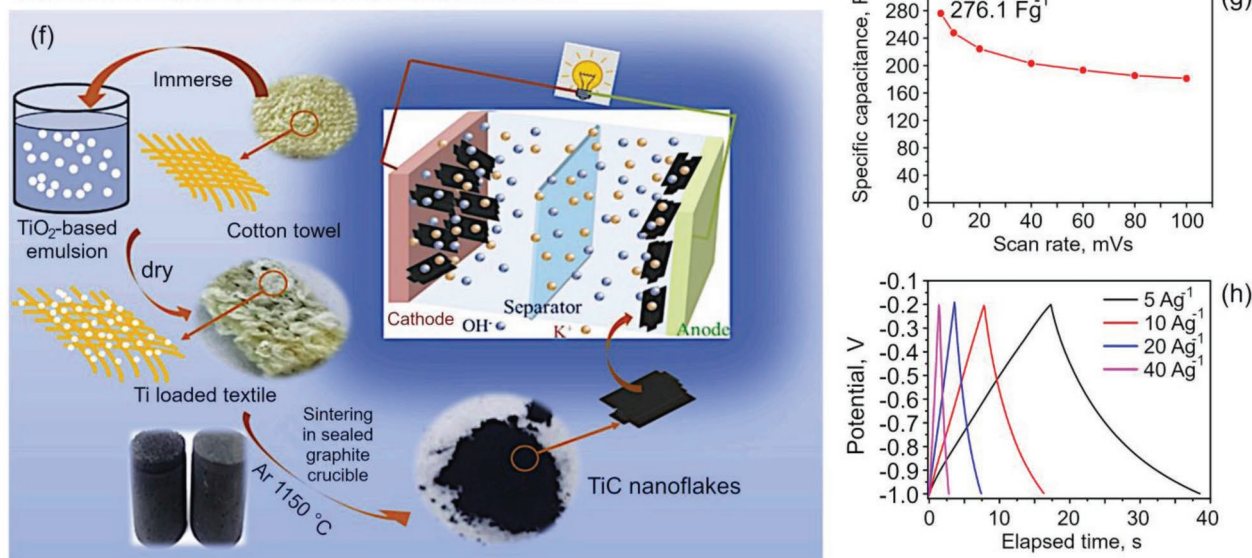


Figure 14. Carbon nano-onion-based material for supercapacitors. a) Synthesis of pitch coated petroleum coke derived activated carbon (P@PC-AC) material from heavy oil for supercapacitors. Complex interfacial structures are formed. b) Growth of hollow carbon nano-onions by bubble template technology. c) Specific capacitance versus current densities. The ordered graphitic structures are able to facilitate rapid charge transfer characteristics originated from the sp^2 -hybridized structure. This increases also the supercapacitor-like behavior at high current densities. Reproduced with permission.^[161] Copyright 2021, Wiley-VCH. Graphene nanocomposite-based electrodes for high-energy-density supercapacitors. d) Schematics of the electrode fabrication technology. e) Gravimetric energy and power densities of an aqueous laser-scribed graphene/ VO_x symmetric supercapacitor at various scan rates. Reproduced with permission.^[162] Copyright 2021, Wiley-VCH. Multilayered TiC nanoflake composites for high performance symmetric supercapacitors. f) Scheme of the manufacturing of TiC nanosheets (by use of the biotemplate method) aimed at producing the electrode materials to be used as symmetric supercapacitors. g) Plot of the specific capacitance for various scan rates in the range 5 to 100 mVs^{-1} . h) The galvanostatic charge and discharge curves for current densities within the range 5 to 40 A g^{-1} . Reproduced with permission.^[163] Copyright 2020 Elsevier.

3D CARBON-BASED INTERFACES FOR ENERGY: SUPERCAPACITORS

ULTRATHIN MoS₂ NANOSHEETS IN CARBON MATRIX FOR PHOTO-RESPONSIVE SUPERCAPACITORS

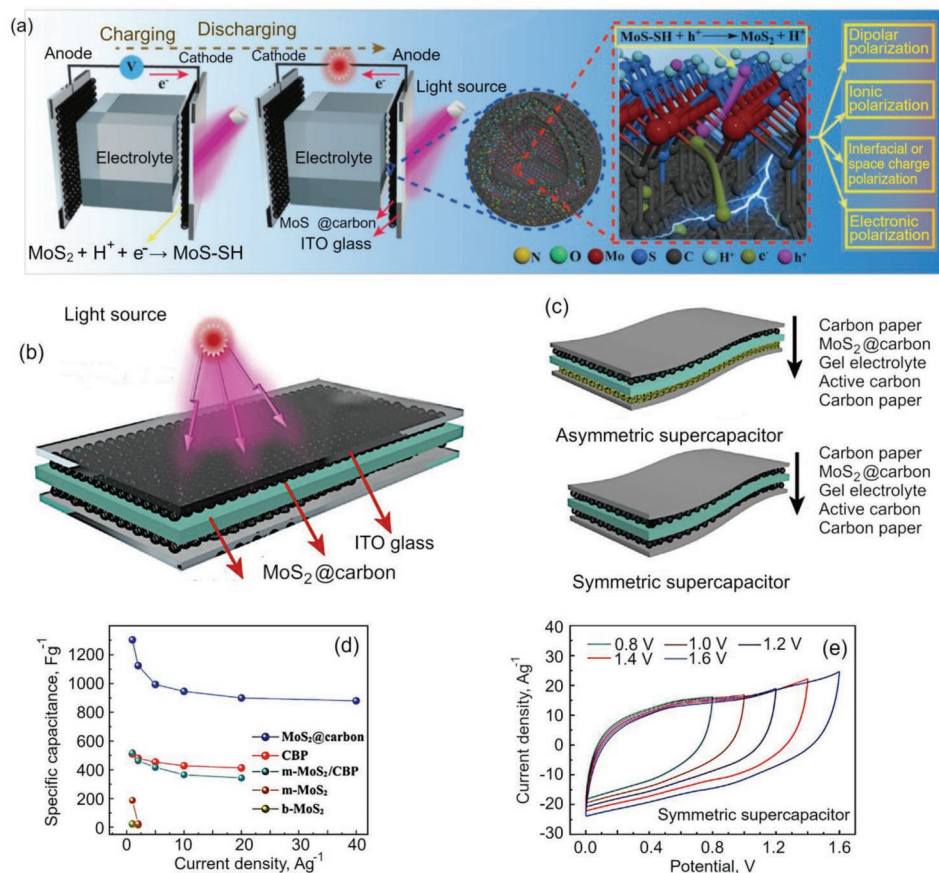


Figure 15. Ultrathin MoS₂ nanosheets in carbon matrix for photoresponsive supercapacitors. a) Scheme of the photoresponse of MoS₂@carbon core-shell structure. b) Schematics of a photoresponsive symmetric supercapacitor assembled on the base of a gel electrolyte film and MoS₂@carbon structures. c) Schematics of the asymmetric and symmetric supercapacitors based on carbon paper and MoS₂@carbon. d) Specific capacitances for MoS₂@carbon, carbon particles (CBP), and other nanocomposites. e) CV curves for symmetric supercapacitors in various potentials. Reproduced under the terms of the CC-BY license.^[166] Copyright 2022, The Authors, published by Wiley-VCH.

nanosheets combined with a carbon matrix (Figure 15a).^[166] In the case of a three-electrode system, such a composition is able to provide a specific capacitance of $\approx 1302 \text{ F g}^{-1}$ at a current densities near 1.0 A g^{-1} , showing a 90% consistent capacitance after $\approx 10\,000$ cycles. At the power density of 900 W kg^{-1} , the MoS₂@carbon-based asymmetric supercapacitor displays an energy density of $\approx 75.1 \text{ Wh kg}^{-1}$. The manufactured photoresponsive supercapacitor can respond to ultraviolet-visible-near infrared light with an increase in capacitance that is explained by the effective diffusion of the photoelectrons from MoS₂ 2D-structures to the carbon matrix. In particular, under the action of UV light at 365 nm wavelength and 0.08 W cm^{-2} of power density, the rise in the capacitance of $\approx 4.50\%$ ($\approx 13.9 \text{ F g}^{-1}$) is observed after each cycle of charge and discharge. The results report a summary of the designing steps required for getting multifunctional supercapacitors being useful as both energy suppliers and photodetectors.

The authors have stacked the gel-based H₂SO₄-PVA electrolyte between the structures produced by applying MoS₂@carbon onto ITO glass, and thus have produced a promising

supercapacitor with photoresponsive properties (Figure 15b,c). The specific capacitances for MoS₂@carbon, carbon particles, and other nanocomposites are shown in Figure 15d, and the CV curves for symmetric supercapacitors in various potentials are shown in Figure 15e.

This is one more example that justifies the gear potential of interfacial systems for designing elements for the most sophisticated devices. Indeed, the photoresponsive and in the general case, stimuli-responsive elements such as supercapacitors are the key elements for autonomous robots, health monitoring systems, and many other applications of critical importance. In the above discussed case, the well-developed interfaces which ensure diffusion of photoelectrons between various structures of the device were the key elements to design the system capable to respond to ultraviolet-visible-near infrared light.

The holey graphene/cellulose nanofiber-based film composite was used to boost the capacitance of the all-solid-state flexible supercapacitors.^[167] A novel method for the preparation of holey graphene/cellulose nanofiber-based films, presenting high specific surface area and multiple graphene nanosheets

channels, have been developed. In this method, the GO nanosheets were treated by use of the pyrolysis gas obtained from a cellulose nanofiber (CNF) in order to introduce holes into their structure. CNF acts as a spacer and activating tool at the same time. The CNF was uniformly distributed in the volume of the hybrid films, and neatly arranged between CNF structures.

It is found that the mesoporosity and nanopore perforation of the activated reduced GO/CNF (A-RGO/CNF) film become more pronounced as the CNF concentration increases. The resulting A-RGO/CNF composite reveals the best specific capacitance of $\approx 323 \text{ F g}^{-1}$ at 1 A g^{-1} . An outstanding electrochemical characteristic of $\approx 208 \text{ F g}^{-1}$ at 60 A g^{-1} is observed for the A-RGO₅/CNF₅ film a ratio of CNF to GO of 1:1, while in an all-solid-state flexible symmetric supercapacitor, the A-RGO₅/CNF₅ electrode ensures the performance of 250 F g^{-1} at 1 A g^{-1} . The investigation suggests a novel method for the actual realization of perforated graphene-based nanostructures for supercapacitor applications. The preparation and structure of this material system are shown in Figure 16a,b.

Electrospinning technology was used to synthesize the highly graphitized carbon nanofibers with metal oxide nanoparticles to enhance the flexible hybrid supercapacitors.^[168] Electrospun carbonaceous fibers are becoming a strong candidate for electrodes for energy storage. The expected application is however hindered by both their low conductivity and capacitive performance (essentially due to the unavoidable presence of amorphous carbon structures). The authors reported a pyrolytic method of treatment of MOF-embedded electrospun nanofibers for assembly of the composite structure that includes the carbon nanofibers with a high degree of graphitization and nanoparticles of metal oxides (Fe₂O₃, NiO, etc.). The embedded nanofibers are highly graphitized and display a large mesopore volume with high concentration of Faradic metal oxide nanoparticles. Large specific capacitances are conditioned by the remarkable mechanical flexibility and excellent electrical conductivity provided by the fast ion transfer channels of the fibers. To conclude, asymmetric flexible hybrid supercapacitors, obtained by manufacturing Fe₂O₃/NiO-embedded highly graphitized carbon nanofibers (FOCNF and NOCNF, respectively), exhibit both high energy densities reaching about 43.1 Wh kg^{-1} , at a power density of 412.5 W kg^{-1} , and perfect flexibility. Figure 16c–e illustrates the preparation technology for graphitized carbon nanofibers and NiO-embedded highly graphitized carbon nanofibers, and the structure of the flexible hybrid supercapacitor.

The described examples illustrate a number of pathways by which 3D interfaces could complement or augment the opportunities presented by 2D interfaces in various applications. Pronounced spatial anisotropy allows implementing them not only as gel or sol compounds, but also as clearly outlined elements of some structure that defines the performance of a device. A striking example of this is their use in photonics applications, where the use of 3D structures provides an avenue to exploit not only chemical but also physicochemical phenomena that take place across multiple length scales. Indeed, the fixed pattern of carbon–nanocone composites powered with the properties of a separate structure developed by Carra et al. create a powerful tool to combine the photoluminescence of a structure

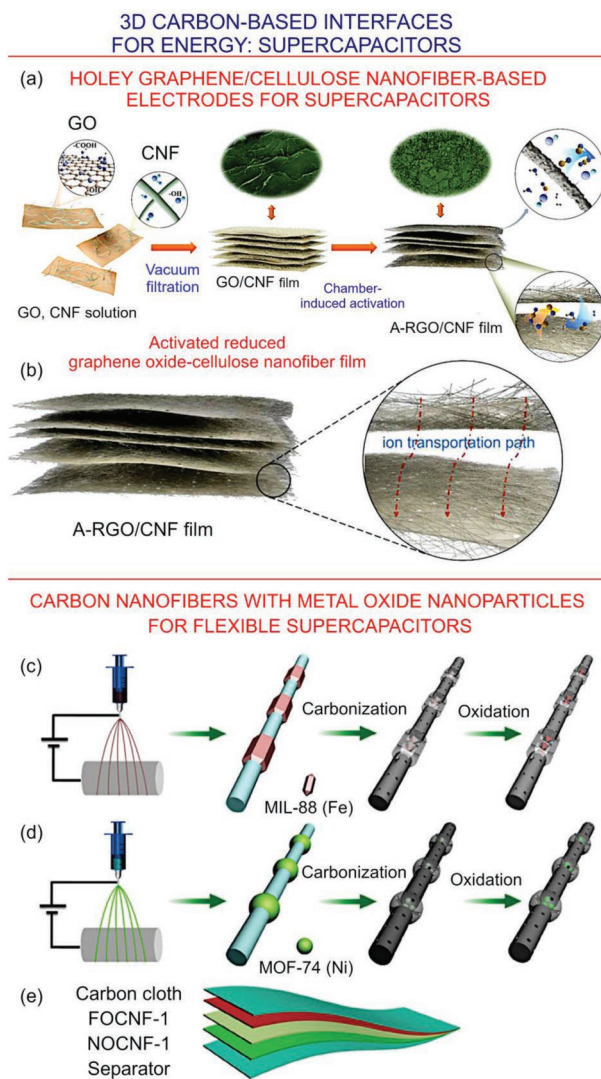


Figure 16. Holey graphene/cellulose nanofiber-based electrodes for supercapacitors. a) Preparation of activated reduced graphene oxide/cellulose nanofiber electrodes. b) Scheme illustrating the diffusion of electrolyte ions through the graphene nanosheet interfaces. Reproduced under the terms of the CC-BY license.^[167] Copyright 2022, The Authors, published by Wiley-VCH. Highly graphitized carbon nanofibers with metal oxide nanoparticles for flexible hybrid supercapacitors. Preparation technology for c) graphitized carbon nanofibers (FOCNF) and d) NiO-embedded highly graphitized carbon nanofibers (NOCNF). e) Structure of the flexible hybrid supercapacitor. Reproduced with permission.^[168] Copyright 2022, Wiley-VCH.

with the diffraction properties of the whole array. Moreover, by changing chemical or biochemical properties of a single 1D structure, it may be possible to enhance the properties and performance of such 1D–2D composites as was demonstrated by Park et al. Moreover, even the simplest alteration of such structures can result in huge (by an order of magnitude) changes of certain properties, as was shown by Paixão et al.

While the arrays of 0D and 1D nanostructures formed on surfaces of 2D carbon nanostructures proved their effectiveness in photonics, freestanding 2D nanofibers expand the possibilities of 2D interfaces in application for batteries applications. Potential opportunities of N-doped porous carbon nanofibers

combined with the possibility of using the readily available materials like potassium look really impressive according to the reports by Xu et al. with respect to the energy storage, yet there is still a lot of theoretical and experimental research to be done on the way to the successful application of such complex structures. Generally, for this application, nitrogen doping promises to be the most powerful tool to control the performance of a device, since it is applied not only for carbon nanofibers but also for carbon nanotubes with NiFe nanoparticles embedded in their structure (Lei et al.) or leaf-like carbon microplates with Co/ZnCo₂O₄ nanoparticles stocked in them (Yan et al.). The decoration of the N-doped carbon nanostructures by the nanoparticles is also additional control tool, as was demonstrated by Joo et al. and Liu et al., since it not only creates the new nucleation sites thus promoting the development of the structure, but results in the acquisition of the necessary electrocatalytic properties (with respect to oxygen and hydrogen reactions, for example) by the structure as well.

Supercapacitor applications also adopted even the simplest 3D carbon nanostructures such as carbon nano-onions due to the unique combination of electrical conductivity and large surface area. However, they are not the only structures suitable for the purpose. Graphene nanocomposites combined with vanadium oxides, as well as titanium carbide exhibited both excellent performance and flexibility of manufacturing due to implementation of various physical methods of their treatment like laser-scribing (Huang et al.) or biotemplate method (Chen et al.), which is also considered as reliable and cost-effective. However, the list of perspective materials is far from being finalized, as was demonstrated in the experiments with MoS₂ 2D-structures combined with a carbon matrix (Tang et al.), the implementation of which allowed to greatly enhance the dynamic stability of the electrode material. At the same time, more complex methods like preparation of the holey graphene/cellulose nanofiber composites or introduction electrospinning technology allow boosting the capacitance and reaching the really outstanding electrochemical performance as was proved by Wu et al. and Li et al.

5. Outlook and Perspectives

Sections 3 and 4 outlined the widest spectrum of carbon types and interfacing materials for highly efficient energy and photonics applications, recently successfully demonstrated and discussed in the literature. In **Table 1** we have listed all discussed examples of carbon-based interfacial material systems for energy and photonics, to better stress the flourishing variety of approaches, techniques and materials that could be involved in the carbon-based interfacial material systems, and thus to further motivate the researchers to engage in the ongoing development of these promising systems.

It should be noted that when considering a problem of engineering of new functional materials to manage the fluxes of material, energy, and information in a specified way,^[169,170] the flat and 3D-shaped interfaces are the key elements yet their roles are quite different. Detailed overview and discussion of various processes at (conditionally) flat and 3D, i.e., curved, surfaces is presented in Section 2 and Figure 2. Here, we would

like to emphasize that at present, the fundamental processes such as adsorption, decomposition, diffusion, implantation, nucleation, and many others, which occur on the flat interfaces, are the main subject of the management. Unfortunately, the current demands of modern industry do not allow obtaining the necessary surface structure in a beneficial way with respect to their size, production time, energy consumption, and environmental issues.^[171,172] Thus, additional tools that expand greatly the possibilities of the existing technologies should be developed, and 3D-shaped interfaces appear to be the appropriate response to the challenge.^[173,174]

Generally, the 3D-shaped interfaces should be considered as surface structures that can be either static or dynamic while performing one of the two tasks: i) expanding the functionality of a flat interface with the application of the new material in a device, or ii) determining the maps of processing fluxes during the manufacturing of the material.^[175] Focusing of fluxes of particles, generation of specified maps of electric and magnetic fields, or gradients of temperature and particle concentration, change of the particle interaction energies are just a small part of the arsenal of capabilities that should be associated with the 3D-shaped interfaces for their prosperous implementation.^[176]

The processes occurring in 3D-shaped interfaces themselves are specified by a set of necessary functional properties (conductivity, wettability, etc.) that should be demonstrated during the exploitation of the new material, while a set of necessary treatment parameters specifies the processes that should occur in the material during its synthesis. Hence, both of the sets (functional properties and treatment parameters) can be considered as “controls” with respect to the architecture of the 3D-shaped interfaces, the main purpose of which, in turn, is the expansion of the potential of the flat interfaces.

Thus, to continue the parallel with a Kroemer’s transistor where the heterojunction became what defined the device, with respect to the application and manufacturing of a new material, the generalized set “controls” means a specification (list and values) of the parameters that should be obtained on/in these 3D interfaces to manage the “power circuit” that includes the flows of material, energy, and information during the application of a new material, or a specification of the treatment parameters that should be obtained to manage the “power circuit” during the synthesis of a new material.

The potential presence of a large number of parameters in the controls urges to conclude that a small variation in them, which may lead to even in the smallest change in the 3D interface, can result in drastic changes of material properties with respect to the manufacturing and application. The analyzed interaction between the “controls” and “power circuit” induces an analogy, where the set “controls” is an analog of a box that controls a current in a base-emitter circuit base of a bipolar transistor to control a much larger current in a collector–emitter circuit in a common emitter amplifier schematic with a typical current gain of a few hundreds. As it is known, such schematics simulate a principle, where a small control force allows controlling much higher forces necessary to make a process. **Figure 17** not only illustrates the described relation between the flat and 3D-shaped interfaces, and their role in effective management of flows of material, energy, and information necessary to successful manufacturing and application of a new functional material, but also

Table 1. List of nanoengineered interfacial systems discussed in detail in this paper. Table illustrates the widest spectrum of carbon types and interfacing materials for highly efficient applications, successfully demonstrated recently (within the two last years). Abbreviations: GO – graphene oxide; RGO – reduced graphene oxide; CVD – chemical vapor deposition.

Type of carbon	Interfacing material	Process	Application	Year	Refs.
Graphene	Graphene	Exfoliation, cut and stack	Superconductivity	2021	[57]
Graphene	Graphene	Exfoliation, stackig	Superconductivity	2022	[58]
RGO	Silver oxide	Hydrothermal synthesis	Photocatalysis	2022	[82]
RGO	Metal oxide nanoparticles (NiFe ₂ O ₄)	Hydrothermal synthesis	Photocatalysis	2022	[83]
Graphene	PbS nanorods	Electrochemical	Photodetection	2021	[85]
RGO	Bismuth oxybromideiodied solid solution	Single-step solar-driven fixation	Photocatalysis	2021	[86]
Carbon	ZnMn ₂ O ₄ , ZnMn ₂ O ₄ -MnO	Drying and calcination	Zn-ion batteries	2021	[96]
N-doped carbon	2D molybdenum dichalcogenide	Hard-template/CVD	Potassium-ion batteries	2020	[97]
Graphene	Topologically insulating SnSb ₂ Te ₄ nanodots	Ball milling and unzipping with graphite	Li-Ion batteries	2020	[98]
Hard carbon	Fe/Mn-based layered oxide	Electrospinning, heat treatment	Sodium-ion	2020	[102]
Graphene	CoS _x @Cu ₂ MoS ₄ core@shell structures	Modified Hummer method, CVD	Zn-air battery	2020	[103]
Graphite	FeN ₄ edge sites	Polymerization, pyrolysis	Zn-air batteries	2020	[104]
Graphene	Metal oxides (MnO ₂ /WO ₃ structures)	Plasma-enabled	Supercapacitors	2020	[116]
RGO	NiO and NiFe ₂ O ₄ nanoparticles	Hydrothermal technique	Supercapacitors	2022	[83]
Graphene	MnO ₂ /WO ₃ composites	Stamping	Supercapacitors	2020	[117]
Graphene	Metal-organic frameworks	Solvothermal synthesis	Supercapacitors	2021	[124]
Graphene	Amino acid	Sonication, heat treatment, centrifugation	Supercapacitors	2021	[125]
RGO	N-doped Graphene	GO-ethanol dispersion filtration	Supercapacitors	2020	[126]
Carbon nanocones	Silicon	ICP-PECVD	White light photoluminescence	2022	[142]
Carbon nitride (C ₃ N ₄)	Nitric acid-treated C ₃ N ₄	Solution processes	Retina-inspired synapses	2020	[148]
Fluorinated graphene oxide	Polymer	Polymer optical fiber fuse	Magnetoresponse optics	2022	[151]
Porous carbon	Small-molecule Se (Se@NPCF)	Electrospinning	Flexible K-Se batteries	2020	[154]
Carbon nanotubes	NiFe nanoparticles	Hydrothermal and pyrolysis	Wearable Zn-air batteries	2020	[155]
Carbon nanotubes	Co/ZnCo ₂ O ₄ nanoparticles	Pyrolysis	Flexible Zn-air batteries	2021	[157]
Porous carbon	Co ₂ P nanoparticles	Chemical, thermal activation	Zn-air batteries	2021	[160]
Carbon nano-onions	Pitch	Thermal	Supercapacitors	2021	[161]
Graphene	Vanadium oxides (VO _x)	Facile laser-scribing	Supercapacitors	2021	[162]
TiC nanoflakes	Titanium carbide	Biotemplate method	Supercapacitors	2020	[163]
Carbon	MoS Nanosheets	Pyrolysis-assisted in situ growth	Stimuli-responsive supercapacitors	2022	[166]
RGO	Cellulose	Pyrolysis	Supercapacitors	2022	[167]
Carbon nanofibers	Metal oxide nanoparticles	Electrospinning	Flexible supercapacitors	2022	[168]

emphasizes the accuracy of the process of designing the interfaces, thus outlining the future challenges for large communities of scientists and engineers.

In the light of above discussed challenges and problems, we formulate here several points that, in the authors' opinion, are of particular importance to the ongoing development of advanced interfacial material systems.

✓ Further development of cost-effective, highly productive, flexible, and eco-friendly methods for the formation of interfaces with different dimensionality and controlled transitions between them.^[177–180] The spectrum of application for such systems is ultimately wide, ranging from extremely important

ecological systems, e.g., nanomaterial-based marine antifouling materials that require sophisticated control of processes at the material–ecosystem interfaces,^[181,182] novel aquaponic systems that require advanced functional materials and interfacial systems,^[183,184] nanomaterials for waste management via green, efficient synthesis of valuable materials from low-cost natural products,^[46,185] nanocomposites for supercapacitors and energy storage,^[87,186] to space technology application where complex material systems could be used for, e.g., solid propellant supply in space thrusters^[187] and building the human habitats.^[188,189]

✓ Better approaches for modeling the nonstationary 3D processes of a surface formation and the effects of the surface

PARALLEL WITH A CONCEPT OF A TRANSISTOR:
ENGINEERED INTERFACES CAN TRANSFORM THE PROCESS TO CREATE
NEW FUNCTIONAL MATERIAL OUTPUT FROM RELATIVELY SIMPLE INPUTS

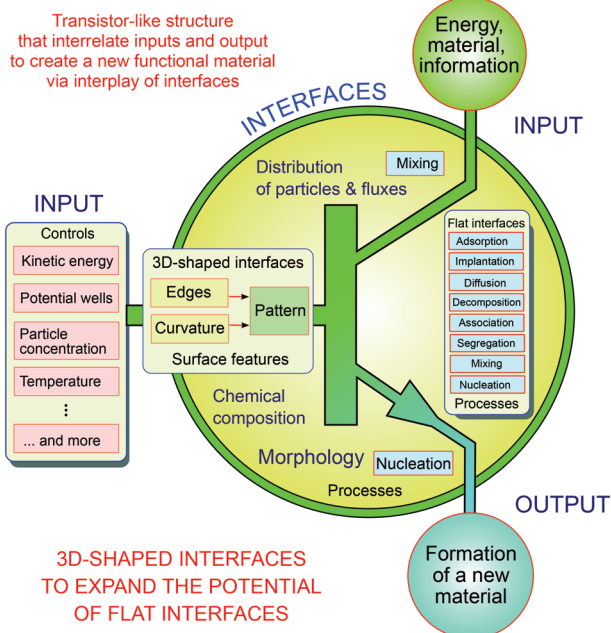


Figure 17. Drawing a parallel with a concept of a transistor, an engineered interface can amplify or transform the process to create new (often more sophisticated) functional material outputs from relatively simple inputs. To produce and apply a new material with a specified set of useful properties, an effective beneficial management (or “control”) should be provided at the stage of manufacturing, as well as at the stage of application of the material in a device. To manage the processes, 3D-shaped interfaces are applied, which allow guiding, focusing, and arranging the “power flows” (i.e., the flows of the material, energy, and information necessary to perform the task of synthesis of a new material), thus expanding greatly the possibilities of the flat interfaces, where the basic processes like adsorption, diffusion and nucleation take place. Thus, the flat interfaces are considered as a “foundation”, which can be modified or upgraded to (or by) 3D interfaces. The required functional properties specify the processes in the interfaces during the material exploitation, while the treatment parameters specify the processes during its synthesis. The functional and treatment parameters are designated as “controls” and determine the architecture of the interfaces, which is responsible for the management of the processes, in addition to the process specification. The transistor-like structure that connects controls with the “power circuit” where the “power flows” with the formation of a new material are included, reflects the sensitivity of the process output with respect to the control parameters and architectures.

interaction with flows of energy and material to establish the mechanisms of nucleation, growth, change of physical and chemical properties, generation of fields and gradients, including the self-sustained. Further development of artificial intelligence-based techniques for designing novel interfacial systems. Application of multiscale modeling technologies for deeper understanding the processes during formation of complex interfacial material systems.^[190,191]

- ✓ Development of predictive models based on data mining for establishing the relations between the variety of material properties and measured descriptors for interfaces with a purpose of selecting essential descriptors and their arrangement by contribution to the desired properties. Application of

novel descriptors and fractality-based method and approaches for designing complex interfacial systems.^[3,192]

6. Conclusions

A limited number of examples presented in this review highlight both the potential of complex, sophisticated carbon-based interfacial material systems for energy and photonics applications, as well as the breadth and the fast rate with which advancements are made in this field. There is little doubt that as our understanding of complex interfaces grows, and our ability to study, develop, and fabricate these intricate structures evolves, their impact on all facets of our life, from medicine and energy to environment and space exploration, will become even more significant.

Acknowledgements

I.L. acknowledges the support from the Nanyang Technological University, Plasma Sources and Applications Centre. K.B. acknowledges the support from the Australian National University and Australian Research Council (DP180101254 and FT190100819). U.C. acknowledges the support of Slovenian Research Agency program P1-0417 and Grant No. N2-0107 as well as EU Graphene Flagship project VEGA. O.B. acknowledges the support from the National Research Foundation of Ukraine under Grant Agreement No. 2020.02/0119, and the NATO Science for Peace and Security Programme under Grant No. G5814 project NOOSE. E.I. acknowledges the support from the ARC Industrial Transformation Training Centre in Surface Engineering for Advanced Materials (SEAM) under Grant No. IC1180100005.

Conflict of Interest

The authors declare no conflict of interest.

Keywords

carbon, functional nanomaterials, graphene, interfaces, reduced graphene oxide

Received: August 5, 2022
Revised: October 6, 2022
Published online: November 23, 2022

- [1] H. Kroemer, *Rev. Mod. Phys.* **2001**, 73, 783.
- [2] I. Levchenko, K. Bazaka, M. Keidar, S. Xu, J. Fang, *Adv. Mater.* **2018**, 30, 1702226.
- [3] C. Piferi, K. Bazaka, D. L. D’Aversa, R. Di Girolamo, C. De Rosa, H. E. Roman, C. Riccardi, I. Levchenko, *Adv. Mater. Interfaces* **2021**, 8, 2100724.
- [4] P. Wang, H. Zhang, H. Wang, D. Li, J. Xuan, L. Zhang, *Adv. Mater. Technol.* **2020**, 5, 1901030.
- [5] R. Granberry, J. Barry, B. Holschuh, J. Abel, *Adv. Mater. Technol.* **2021**, 6, 2000825.
- [6] F. J. Martin-Martinez, K. Jin, D. López Barreiro, M. J. Buehler, *ACS Nano* **2018**, 12, 7425.
- [7] M. Matsunaga, J. Hirotani, S. Kishimoto, Y. Ohno, *Nano Energy* **2020**, 67, 104297.

- [8] C. Zhang, Z. Peng, C. Huang, B. Zhang, C. Xing, H. Chen, H. Cheng, J. Wang, S. Tang, *Nano Energy* **2021**, *81*, 105609.
- [9] L. Shi, H. Jin, S. Dong, S. Huang, H. Kuang, H. Xu, J. Chen, W. Xuan, S. Zhang, S. Li, X. Wang, J. Luo, *Nano Energy* **2021**, *80*, 105599.
- [10] K. Li, Y. de Rancourt de Mimérand, X. Jin, J. Yi, J. Guo, *ACS Appl. Nano Mater.* **2020**, *3*, 2830.
- [11] Q. Xiang, X. Ma, D. Zhang, H. Zhou, Y. Liao, H. Zhang, S. Xu, I. Levchenko, K. Bazaka, *J. Colloid Interface Sci.* **2019**, *556*, 376.
- [12] V. Sadykov, S. Pavlova, J. Fedorova, A. Bobin, V. Fedorova, M. Simonov, A. Ishchenko, T. Krieger, M. Melgunov, T. Glazneva, T. Larina, V. Kaichev, A.-C. Roger, *Catal. Today* **2021**, *379*, 166.
- [13] N. Kosinov, E. M. Hensen, *Adv. Mater.* **2020**, *32*, 2002565.
- [14] B. Han, Y.-Y. Gao, L. Zhu, Z.-C. Ma, X.-L. Zhang, H. Ding, Y.-L. Zhang, *Adv. Mater. Technol.* **2020**, *5*, 1900963.
- [15] X.-K. Wan, H. B. Wu, B. Y. Guan, D. Luan, X. W. D. Lou, *Adv. Mater.* **2020**, *32*, 1901349.
- [16] Y. Xu, M. Fan, W. Yang, Y. Xiao, L. Zeng, X. Wu, Q. Xu, C. Su, Q. He, *Adv. Mater.* **2021**, *33*, 2101455.
- [17] I. Gouzman, E. Grossman, R. Verker, N. Atar, A. Bolker, N. Eliaz, *Adv. Mater.* **2019**, *31*, 1807738.
- [18] E. C. Welch, J. M. Powell, T. B. Clevinger, A. E. Fairman, A. Shukla, *Adv. Funct. Mater.* **2021**, *31*, 2104126.
- [19] H. P. Zhou, X. Ye, W. Huang, M. Q. Wu, L. N. Mao, B. Yu, S. Xu, I. Levchenko, K. Bazaka, *ACS Appl. Mater. Interfaces* **2019**, *11*, 15122.
- [20] J. D. Miller, D. Cabarkapa, M. J. Hermes, A. C. Fry, C. J. Berkland, *Adv. Mater. Technol.* **2021**, *7*, 2100784.
- [21] R. Abdel-Karim, Y. Reda, A. Abdel-Fattah, *J. Electrochem. Soc.* **2020**, *167*, 037554.
- [22] M. Kaur, T.-H. Kim, W. S. Kim, *Adv. Mater.* **2021**, *33*, 2002534.
- [23] Z. Chen, S. Zhang, I. Levchenko, I. I. Beilis, M. Keidar, *Sci. Rep.* **2017**, *7*, 12163.
- [24] G. Maduraiveeran, M. Sasidharan, V. Ganesan, *Biosens. Bioelectron.* **2018**, *103*, 113.
- [25] K. Ganguly, D. K. Patel, S. D. Dutta, W. C. Shin, K. T. Lim, *Int. J. Biol. Macromol.* **2020**, *155*, 456.
- [26] P. Liu, G. Wang, Q. Ruan, K. Tang, P. K. Chu, *Bioact. Mater.* **2021**, *6*, 2134.
- [27] X. Zhang, Y. Liu, *Environ. Sci.: Nano* **2020**, *7*, 1008.
- [28] N. Natter, N. Kostoglou, C. Koczwarra, C. Tampaxis, T. Steriotis, R. Gupta, O. Paris, C. Rebholz, C. Mitterer, *J. Hydrocarbons, Mines Environ. Res.* **2019**, *5*, 16.
- [29] P. Yan, Y. Hu, E. Shoko, T. T. Isimjan, J. Tian, X. Yang, *Adv. Mater. Interfaces* **2021**, *8*, 2100065.
- [30] H. Yu, Y. Wang, C. Zhu, Y. Jing, Q. Song, C. Guan, C.-F. Du, *Adv. Mater. Interfaces* **2021**, *8*, 2001310.
- [31] W. Yang, S. Cai, Y. Chen, W. Liang, Y. Lai, H. Yu, Y. Wang, L. Liu, *Adv. Mater. Technol.* **2020**, *5*, 1900847.
- [32] K. Fu, H. Wu, Z. Su, *Biotechnol. Adv.* **2021**, *49*, 107752.
- [33] R. Zeng, C. Lv, C. Wang, G. Zhao, *Biotechnol. Adv.* **2021**, *52*, 107835.
- [34] L. Ma, L. Diao, Z. Peng, Y. Jia, H. Xie, B. Li, J. Ma, M. Zhang, L. Cheng, D. Ding, X. Zhang, H. Chen, F. Mo, H. Jiang, G. Xu, F. Meng, Z. Zhong, M. Liu, *Adv. Mater.* **2021**, *33*, 2104849.
- [35] S. Moon, Q. Zhang, D. Huang, S. Senapati, H.-C. Chang, E. Lee, T. Luo, *Adv. Mater. Interfaces* **2020**, *7*, 2000597.
- [36] I. Levchenko, K. Bazaka, T. Belmonte, M. Keidar, S. Xu, *Adv. Mater.* **2018**, *30*, 1802201.
- [37] I. Levchenko, M. Keidar, J. Cantrell, Y.-L. Wu, H. Kuninaka, K. Bazaka, S. Xu, *Nature* **2018**, *562*, 185.
- [38] N. Singhal, I. Levchenko, S. Huang, L. Xu, G.-C. Potrivitu, O. Cherkun, J. Fang, K. Bazaka, S. Xu, *Adv. Eng. Mater.* **2019**, *21*, 1900401.
- [39] I. Levchenko, S. Xu, G. Teel, D. Mariotti, M. L. R. Walker, M. Keidar, *Nat. Commun.* **2018**, *9*, 879.
- [40] M. Hołyńska, A. Tighe, C. Semprimoschnig, *Adv. Mater. Interfaces* **2018**, *5*, 1701644.
- [41] I. Levchenko, I. I. Beilis, M. Keidar, *Adv. Mater. Technol.* **2016**, *1*, 1600008.
- [42] H. Röhm, T. Leonhard, A. D. Schulz, S. Wagner, M. J. Hoffmann, A. Colsmann, *Adv. Mater.* **2019**, *31*, 1806661.
- [43] C. Xu, A. R. Puente-Santiago, D. Rodríguez-Padrón, M. J. Muñoz-Batista, M. A. Ahsan, J. C. Noveron, R. Luque, *Chem. Soc. Rev.* **2021**, *50*, 4856.
- [44] B. Graves, S. Engelke, C. Jo, H. G. Baldovi, J. de la Verpilliere, M. De Volder, A. Boies, *Nanoscale* **2020**, *12*, 5196.
- [45] S. W. Leung, B. Williams, K. De Jesus, J. C. K. Lai, *IOP Conf. Ser.: Earth Environ. Sci.* **2017**, *68*, 012019.
- [46] I. Levchenko, M. Mandhakini, K. Prasad, O. Bazaka, E. P. Ivanova, M. V. Jacob, O. Baranov, C. Riccardi, H. E. Roman, S. Xu, K. Bazaka, *Adv. Mater. Technol.* **2022**, *7*, 2101471.
- [47] M. R. Abukhadra, M. Shaban, *Int. J. Environ. Sci. Technol.* **2019**, *16*, 7573.
- [48] X. Liu, S. Zhang, X. Wen, X. Chen, Y. Wen, X. Shi, E. Mijowska, *Sci. Rep.* **2020**, *10*, 3518.
- [49] R. Abolghasemi, M. Haghghi, M. Solgi, A. Mobinikhaledi, *Int. J. Environ. Sci. Technol.* **2019**, *16*, 6985.
- [50] J. Y. Zhu, U. P. Agarwal, P. N. Ciesielski, M. E. Himmel, R. Gao, Y. Deng, M. Morits, M. Österberg, *Biotechnol. Biofuels* **2021**, *14*, 114.
- [51] R. Ajdary, B. L. Tardy, B. D. Mattos, L. Bai, O. J. Rojas, *Adv. Mater.* **2021**, *33*, 2001085.
- [52] G. S. Lekshmi, R. Tamilselvi, K. Prasad, O. Bazaka, I. Levchenko, K. Bazaka, M. Mohandas, *Carbon Lett.* **2021**, *31*, 763.
- [53] J. Ramirez, B. McCabe, P. D. Jensen, R. Speight, M. Harrison, L. van den Berg, I. O'Hara, *Anim. Prod. Sci.* **2021**, *61*, 541.
- [54] G. Xu, H. Jiang, M. Stapelberg, J. Zhou, M. Liu, Q.-J. Li, Y. Cao, R. Gao, M. Cai, J. Qiao, M. S. Galanek, W. Fan, W. Xue, B. Marelli, M. Zhu, J. Li, *Environ. Sci. Technol.* **2021**, *55*, 6239.
- [55] S. M. Abdelbasir, K. M. McCourt, C. M. Lee, D. C. Vanegas, *Front. Chem.* **2020**, *8*, 782.
- [56] X. Lu, P. Stepanov, W. Yang, M. Xie, M. A. Aamir, I. Das, C. Urgell, K. Watanabe, T. Taniguchi, G. Zhang, A. Bachtold, A. H. MacDonald, D. K. Efetov, *Nature* **2019**, *574*, 653.
- [57] J. M. Park, Y. Cao, K. Watanabe, T. Taniguchi, P. Jarillo-Herrero, *Nature* **2021**, *590*, 249.
- [58] G. W. Burg, E. Khalaf, Y. Wang, K. Watanabe, T. Taniguchi, E. Tutuc, *Nat. Mater.* **2022**, *21*, 884.
- [59] M. Yankowitz, S. Chen, H. Polshyn, Y. Zhang, K. Watanabe, T. Taniguchi, D. Graf, A. F. Young, C. R. Dean, *Science* **2019**, *363*, 1059.
- [60] Z. Hao, A. M. Zimmerman, P. Ledwith, E. Khalaf, D. H. Najafabadi, K. Watanabe, T. Taniguchi, A. Vishwanath, P. Kim, *Science* **2021**, *371*, 1133.
- [61] J. M. Park, Y. Cao, L.-Q. Xia, S. Sun, K. Watanabe, T. Taniguchi, P. Jarillo-Herrero, *Nat. Mater.* **2022**, *21*, 877.
- [62] A. L. Sharpe, *Nat. Mater.* **2022**, *21*, 842.
- [63] I. Levchenko, K. Ostrikov, D. Mariotti, V. Svrcek, *Carbon* **2009**, *47*, 2379.
- [64] I. Levchenko, O. Baranov, *Vacuum* **2004**, *72*, 205.
- [65] K. Ostrikov, I. Levchenko, S. Xu, S. Y. Huang, Q. J. Cheng, J. D. Long, M. Xu, *Thin Solid Films* **2008**, *516*, 6609.
- [66] I. Levchenko, A. E. Rider, K. Ostrikov, *Appl. Phys. Lett.* **2007**, *90*, 193110.
- [67] I. Levchenko, U. Cvelbar, M. Modic, G. Filipič, X. X. Zhong, M. Mozetič, K. Ostrikov, *J. Phys. Chem. Lett.* **2013**, *4*, 681.
- [68] D. H. K. Nguyen, O. Bazaka, K. Bazaka, R. J. Crawford, E. P. Ivanova, *Trends Biotechnol.* **2020**, *38*, 558.
- [69] S. Shao, M. A. Loi, *Adv. Mater. Interfaces* **2020**, *7*, 1901469.
- [70] L. Chen, J. Huang, R. Zeng, Y. Xiong, J. Wei, K. Yuan, Y. Chen, *Adv. Mater. Interfaces* **2020**, *7*, 1901729.

- [71] J. Li, F. Li, J. Liao, H. Li, D. Dang, Q. Liu, H.-J. Peng, *Adv. Mater. Interfaces* **2020**, *7*, 2000667.
- [72] T. Dong, J. Simões, Z. Yang, *Adv. Mater. Interfaces* **2020**, *7*, 1901657.
- [73] S. K. Jain, M. X. Low, P. Vashishtha, S. Nirantar, L. Zhu, C. Ton-That, T. Ahmed, S. Sriram, S. Walia, G. Gupta, M. Bhaskaran, *Adv. Mater. Interfaces* **2021**, *8*, 2100593.
- [74] F. Davitt, H. G. Manning, F. Robinson, S. L. Hawken, S. Biswas, N. Petkov, M. V. Druenen, J. J. Boland, G. Reid, J. D. Holmes, *Adv. Mater. Interfaces* **2020**, *7*, 2000474.
- [75] Y. Miao, X. Zhang, J. Zhan, Y. Sui, J. Qi, F. Wei, Q. Meng, Y. He, Y. Ren, Z. Zhan, Z. Sun, *Adv. Mater. Interfaces* **2020**, *7*, 1901618.
- [76] Q. Jiang, J. Xu, Z. Li, C. Zhou, X. Chen, H. Meng, Y. Han, X. Shi, C. Zhan, Y. Zhang, Q. Zhang, X. Jia, R. Zhang, *Adv. Mater. Interfaces* **2021**, *8*, 2002034.
- [77] D. Xu, H. Feng, Y. Dong, Q. Wang, G. Zhang, L. Lv, Z. Ren, P. Wang, *Adv. Mater. Interfaces* **2020**, *7*, 2000548.
- [78] K. Luo, Q. Zhang, H. Yuan, Y. Liu, X. Wang, J. Zhang, W. Hu, M. Xu, S. Xu, I. Levchenko, K. Bazaka, *Ceram. Int.* **2021**, *47*, 48.
- [79] N. M. Santhosh, V. Shvalya, M. Modic, N. Hojnik, J. Zavašnik, J. Olenik, M. Košiček, G. Filipič, I. Abdulhalim, U. Cvelbar, *Small* **2021**, *17*, 2103677.
- [80] Y. Liu, Q. Zhang, H. Yuan, K. Luo, J. Li, W. Hu, Z. Pan, M. Xu, S. Xu, I. Levchenko, K. Bazaka, *J. Alloys Compd.* **2021**, *868*, 158723.
- [81] K. Bazaka, M. V. Jacob, K. Ostrikov, *Chem. Rev.* **2016**, *116*, 163.
- [82] G. S. Lekshmi, R. Tamilselvi, R. Geethalakshmi, S. D. Kirupha, O. Bazaka, I. Levchenko, K. Bazaka, M. Mandhakini, *J. Colloid Interface Sci.* **2022**, *608*, 294.
- [83] R. Tamilselvi, G. S. Lekshmi, N. Padmanathan, V. Selvaraj, O. Bazaka, I. Levchenko, K. Bazaka, M. Mandhakini, *Renewable Energy* **2022**, *181*, 1386.
- [84] Q. Wang, Z. Liu, D. Liu, G. Liu, M. Yang, F. Cui, W. Wang, *Appl. Catal., B* **2018**, *236*, 222.
- [85] C. Yang, S. Feng, L. Tang, J. Shen, X. Wei, H. Shi, *Adv. Mater. Interfaces* **2021**, *8*, 2001464.
- [86] A. M. Alansi, T. F. Qahtan, T. A. Saleh, *Adv. Mater. Interfaces* **2021**, *8*, 2001463.
- [87] X. Zhang, Q. Wang, *Micro Nano Lett.* **2020**, *15*, 992.
- [88] T. Guo, M. Fu, D. Zhou, L. Pang, J. Su, H. Lin, X. Yao, A. S. B. Sombra, *Small Struct.* **2021**, *2*, 2100015.
- [89] L. Shi, H. Jin, S. Dong, S. Huang, H. Kuang, H. Xu, J. Chen, W. Xuan, S. Zhang, S. Li, X. Wang, J. Luo, *Nano Energy* **2021**, *80*, 105599.
- [90] N. M. Santhosh, N. Shaji, P. Stražar, G. Filipič, J. Zavašnik, C. W. Ho, M. Nanthagopal, C. W. Lee, U. Cvelbar, *J. Energy Chem.* **2022**, *67*, 8.
- [91] N. M. Santhosh, K. K. Upadhyay, P. Stražar, G. Filipič, J. Zavašnik, A. M. de Ferro, R. P. Silva, E. Tatarova, M. Montemor, U. Cvelbar, *ACS Appl. Mater. Interfaces* **2021**, *13*, 20559.
- [92] B. Yu, A. Huang, D. Chen, K. Srinivas, X. Zhang, X. Wang, B. Wang, F. Ma, C. Liu, W. Zhang, J. He, Z. Wang, Y. Chen, *Small* **2021**, *17*, 2100460.
- [93] Y. Pan, X. Cheng, M. Gao, Y. Fu, J. Feng, L. Gong, H. Ahmed, H. Zhang, V. S. Battaglia, *ACS Appl. Mater. Interfaces* **2020**, *12*, 33621.
- [94] Q. Wu, L. Yang, X. Wang, Z. Hu, *Adv. Mater.* **2020**, *32*, 1904177.
- [95] Y. Liu, J. Wang, J. Wu, Z. Ding, P. Yao, S. Zhang, Y. Chen, *Adv. Energy Mater.* **2020**, *10*, 1903139.
- [96] S. Islam, M. H. Alfaruqi, D. Y. Putro, S. Park, S. Kim, S. Lee, M. S. Ahmed, V. Mathew, Y.-K. Sun, J.-Y. Hwang, J. Kim, *Adv. Sci.* **2021**, *8*, 2002636.
- [97] M. Ma, S. Zhang, Y. Yao, H. Wang, H. Huang, R. Xu, J. Wang, X. Zhou, W. Yang, Z. Peng, X. Wu, Y. Hou, Y. Yu, *Adv. Mater.* **2020**, *32*, 2000958.
- [98] Z. Wu, G. Liang, W. K. Pang, T. Zhou, Z. Cheng, W. Zhang, Y. Liu, B. Johannessen, Z. Guo, *Adv. Mater.* **2020**, *32*, 1905632.
- [99] J.-Y. Hwang, S.-T. Myung, Y.-K. Sun, *Chem. Soc. Rev.* **2017**, *46*, 3529.
- [100] Y. Liu, W. Li, Y. Ma, D. Fan, *Adv. Mater. Interfaces* **2020**, *7*, 2000777.
- [101] X. Wang, Y. Jia, X. Mao, D. Liu, W. He, J. Li, J. Liu, X. Yan, J. Chen, L. Song, A. Du, X. Yao, *Adv. Mater.* **2020**, *32*, 2000966.
- [102] Q. Shen, X. Zhao, Y. Liu, Y. Li, J. Zhang, N. Zhang, C. Yang, J. Chen, *Adv. Sci.* **2020**, *7*, 2002199.
- [103] D. C. Nguyen, D. T. Tran, T. L. L. Doan, D. H. Kim, N. H. Kim, J. H. Lee, *Adv. Energy Mater.* **2020**, *10*, 1903289.
- [104] M. Xiao, Z. Xing, Z. Jin, C. Liu, J. Ge, J. Zhu, Y. Wang, X. Zhao, Z. Chen, *Adv. Mater.* **2020**, *32*, 2004900.
- [105] Y.-P. Deng, Y. Jiang, R. Liang, S.-J. Zhang, D. Luo, Y. Hu, X. Wang, J.-T. Li, A. Yu, Z. Chen, *Nat. Commun.* **2020**, *11*, 1952.
- [106] J. Zhu, M. Xiao, G. Li, S. Li, J. Zhang, G. Liu, L. Ma, T. Wu, J. Lu, A. Yu, D. Su, H. Jin, S. Wang, Z. Chen, *Adv. Energy Mater.* **2020**, *10*, 1903003.
- [107] S. Deshmukh, P. Jakobczyk, M. Ficek, J. Ryl, D. Geng, R. Bogdanowicz, *Adv. Funct. Mater.* **2022**, *32*, 2206097.
- [108] L. W. Le Fevre, J. Cao, I. A. Kinloch, A. Forsyth, R. A. W. Dryfe, *ChemistryOpen* **2019**, *8*, 418.
- [109] M. Askari, P. Salarizadeh, A. Beheshti-Marnani, A. Bartolomeo, *Adv. Mater. Interfaces* **2021**, *8*, 2100149.
- [110] A. Dias, N. Bundaleska, E. Felizardo, D. Tsyganov, A. Almeida, A. M. Ferraria, A. M. B. Rego, M. Abrashev, Th. Strunskus, N. M. Santhosh, U. Cvelbar, M. F. Montemor, M. M. Almeida, P. A. Carvalho, J. Kissovski, L. L. Alves, E. Tatarova, *Chem. Eng. J.* **2022**, *430*, 133153.
- [111] A. G.-M. Ferrari, J. L. Pimlott, M. P. Down, S. J. Rowley-Neale, *Adv. Energy Mater.* **2021**, *11*, 2100433.
- [112] M. Reina, A. Scalia, G. Auxilia, M. Fontana, F. Bella, S. Ferrero, A. Lamberti, *Adv. Sustainable Syst.* **2022**, *6*, 2100228.
- [113] J. Han, G.-H. Jang, D. K. Kim, J. Y. Kim, J. W. Shin, C.-S. Hwang, Y. Piao, T.-D. Kim, *Int. J. Energy Res.* **2022**, *46*, 10822.
- [114] X. Hou, P. Ren, Z. Dai, Z. Guo, Z. Zhang, A. Sun, W. He, F. Ren, Y. Jin, *Energy Technol.* **2021**, *9*, 2100743.
- [115] X. Wang, P. Fan, S. Wang, H. Liu, L. Liao, *ChemistrySelect* **2022**, *7*, 202104402.
- [116] S.-Y. Huang, P.-A. Le, P.-J. Yen, Y.-C. Lu, S. K. Sahoo, H.-W. Cheng, P.-W. Chiu, T.-Y. Tseng, K.-H. Wei, *Electrochim. Acta* **2020**, *342*, 136043.
- [117] F. Li, J. Qu, Y. Li, J. Wang, M. Zhu, L. Liu, J. Ge, S. Duan, T. Li, V. K. Bandari, M. Huang, F. Zhu, O. G. Schmidt, *Adv. Sci.* **2020**, *7*, 2001561.
- [118] X. Li, J. Xie, Z. Du, R. Yu, J. Jia, Z. Chen, K. Zhu, *Chem. Commun.* **2022**, *58*, 5829.
- [119] X. Yao, K. E. Cordova, Y.-B. Zhang, *Small Struct.* **2022**, *3*, 2100209.
- [120] P. I. Scheurle, A. Biewald, A. Mähringer, A. Hartschuh, D. D. Medina, T. Bein, *Small Struct.* **2022**, *3*, 2100195.
- [121] M. Woellner, S. Hausdorf, N. Klein, P. Mueller, M. W. Smith, S. Kaskel, *Adv. Mater.* **2018**, *30*, 1704679.
- [122] L. Deng, C. Zhou, Z. Ma, G. Fan, *J. Colloid Interface Sci.* **2020**, *561*, 416.
- [123] D. M. El-Gendy, N. A. A. Ghany, E. E. F. El Sherbini, N. K. Allam, *Sci. Rep.* **2017**, *7*, 43104.
- [124] K. Jayaramulu, M. Horn, A. Schneemann, H. Saini, A. Bakandritsos, V. Ranc, M. Petr, V. Stavila, C. Narayana, B. Scheibe, Š. Kment, M. Otyepka, N. Motta, D. Dubal, R. Zbořil, R. A. Fischer, *Adv. Mater.* **2021**, *33*, 2004560.
- [125] E. C. Vermisoglou, P. Jakubec, A. Bakandritsos, V. Kupka, M. Pykal, V. Šedajová, J. Vlček, O. Tomanec, M. Scheibe, R. Zbořil, M. Otyepka, *ChemSusChem* **2021**, *14*, 3904.
- [126] H. Zhang, A. Li, Y. Yuan, Y. Wei, D. Zheng, Z. Geng, H. Zhang, G. Li, F. Zhang, *Carbon Energy* **2020**, *2*, 656.
- [127] Y. Segawa, T. Watanabe, K. Yamanoue, M. Kuwayama, K. Watanabe, J. Pirillo, Y. Hijikata, K. Itami, *Anti-Cancer Drugs: Nat., Synth. Cell* **2022**, *1*, 535.
- [128] I. Calaresu, J. Hernandez, R. Rauti, B. L. Rodilla, A. Arché-Núñez, L. Perez, J. Camarero, R. Miranda, M. T. González, I. Rodríguez, D. Scaini, L. Ballerini, *Adv. Mater. Interfaces* **2021**, *8*, 2002121.
- [129] N. Li, K. Zhang, K. Xie, W. Wei, Y. Gao, M. Bai, Y. Gao, Q. Hou, C. Shen, Z. Xia, B. Wei, *Adv. Mater.* **2020**, *32*, 1907079.

- [130] Y. Shi, Y. Duan, L. Huang, H. Pang, X. Ma, X. Liu, Z. Li, *Adv. Opt. Mater.* **2022**, *10*, 2200951.
- [131] H. Meddeb, M. Götz-Köhler, N. Neugebohrn, U. Banik, N. Osterthun, O. Sergeev, D. Berends, C. Lattyak, K. Gehrke, M. Vehse, *Adv. Energy Mater.* **2022**, *12*, 2200713.
- [132] J. Huang, X. Wang, D. Li, T. Jin, P. Lu, D. Zhang, P.-T. Lin, H.-T. Chen, J. Narayan, X. Zhang, H. Wang, *Adv. Mater. Interfaces* **2020**, *7*, 2000493.
- [133] Y. Chen, H. Yin, D. Sikdar, H. Liu, Q. Zhu, G. Yao, H. Qi, N. Gu, *Adv. Mater. Interfaces* **2020**, *7*, 2000248.
- [134] K. H. Choi, D. Y. Hwang, J. E. Park, D. H. Suh, *Adv. Mater. Interfaces* **2021**, *8*, 2100184.
- [135] I. Dobryden, Z. Yang, P. M. Claesson, M. P. Pileni, *Adv. Mater. Interfaces* **2020**, *8*, 2001687.
- [136] J. N. Acharyya, A. K. Mishra, D. N. Rao, A. Kumar, G. V. Prakash, *Adv. Mater. Interfaces* **2021**, *8*, 2100757.
- [137] G. He, J. Yan, D. Zhu, J. Xie, *Adv. Mater. Interfaces* **2021**, *9*, 2101232.
- [138] J. E. Lee, C. K. Lim, H. J. Park, H. Song, S.-Y. Choi, D.-S. Lee, *ACS Appl. Mater. Interfaces* **2020**, *12*, 35688.
- [139] W. Liu, Y. Zheng, Z. Wang, Z. Wang, J. Yang, M. Chen, M. Qi, S. U. Rehman, P. P. Shum, L. Zhu, L. Wei, *Adv. Mater. Interfaces* **2021**, *8*, 2001978.
- [140] Y. Ding, L. Huang, T. Barakat, B.-L. Su, *Adv. Mater. Interfaces* **2021**, *8*, 2001879.
- [141] S. Lin, R. Mandavkar, R. Kulkarni, S. Pandit, S. Burse, M. A. Habib, S. Kunwar, J. Lee, *Adv. Mater. Interfaces* **2021**, *8*, 2101084.
- [142] C. Carra, A. Medvids, D. Litvinas, P. Ščaje, T. Malinauskas, A. Selskis, H. E. Roman, K. Bazaka, I. Levchenko, C. Riccardi, *ACS Appl. Nano Mater.* **2022**, *5*, 4787.
- [143] B. Guo, M. Košiček, J. Fu, Y. Qu, G. Lin, O. Baranov, J. Zavašnik, Q. Cheng, K. Ostrikov, U. Cvelbar, *Nanomaterials* **2019**, *9*, 1405.
- [144] K. Bazaka, O. Baranov, U. Cvelbar, B. Podgornik, Y. Wang, S. Huang, L. Xu, J. W. M. Lim, I. Levchenko, S. Xu, *Nanoscale* **2018**, *10*, 17494.
- [145] E. C. Dell'Orto, S. Caldirola, A. Sassella, V. Morandi, C. Riccardi, *Appl. Surf. Sci.* **2017**, *425*, 407.
- [146] C. Carra, E. Carra, V. Morandi, C. Riccardi, *Coatings* **2020**, *10*, 788.
- [147] B. B. Wang, X. L. Qu, M. K. Zhu, I. Levchenko, O. Baranov, X. X. Zhong, S. Xu, K. Ostrikov, *Appl. Surf. Sci.* **2018**, *442*, 682.
- [148] H.-L. Park, H. Kim, D. Lim, H. Zhou, Y.-H. Kim, Y. Lee, S. Park, T.-W. Lee, *Adv. Mater.* **2020**, *32*, 1906899.
- [149] Y. Sun, L. Qian, D. Xie, Y. Lin, M. Sun, W. Li, L. Ding, T. Ren, T. Palacios, *Adv. Funct. Mater.* **2019**, *29*, 1902538.
- [150] H. L. Park, Y. Lee, N. Kim, D. G. Seo, G. T. Go, T. W. Lee, *Adv. Mater.* **2020**, *32*, 1903558.
- [151] T. Paixão, J. H. Belo, A. F. Carvalho, V. S. Amaral, J. P. Araújo, H. Lee, K. Nakamura, Y. Mizuno, P. André, P. Antunes, *Adv. Photonics Res.* **2022**, *3*, 2100209.
- [152] S. Alancherry, K. Bazaka, I. Levchenko, A. Al-Jumaili, B. Kandel, A. Alex, F. C. R. Hernandez, O. K. Varghese, M. V. Jacob, *ACS Appl. Mater. Interfaces* **2020**, *12*, 29594.
- [153] A. Huang, M. F. El-Kady, X. Chang, M. Anderson, C.-W. Lin, C. L. Turner, R. B. Kaner, *Adv. Energy Mater.* **2021**, *11*, 2100768.
- [154] R. Xu, Y. Yao, H. Wang, Y. Yuan, J. Wang, H. Yang, Y. Jiang, P. Shi, X. Wu, Z. Peng, Z.-S. Wu, J. Lu, Y. Yu, *Adv. Mater.* **2020**, *32*, 2003879.
- [155] H. Lei, Z. Wang, F. Yang, X. Huang, J. Liu, Y. Liang, J. Xie, M. S. Javed, X. Lu, S. Tan, W. Mai, *Nano Energy* **2020**, *68*, 104293.
- [156] D. Kundu, B. D. Adams, V. Duffort, S. H. Vajargah, L. F. Nazar, *Nat. Energy* **2016**, *1*, 16119.
- [157] L. Yan, Z. Xu, W. Hu, J. Ning, Y. Zhong, Y. Hu, *Nano Energy* **2021**, *82*, 105710.
- [158] S.-H. Joo, J. W. Bae, W.-Y. Park, Y. Shimada, T. Wada, H. S. Kim, A. Takeuchi, T. J. Konno, H. Kato, I. V. Okulov, *Adv. Mater.* **2020**, *32*, 1906160.
- [159] I. Levchenko, D. M. Goebel, K. Bazaka, *Phys. Today* **2022**, *75*, 38.
- [160] H. Liu, J. Guan, S. Yang, Y. Yu, R. Shao, Z. Zhang, M. Dou, F. Wang, Q. Xu, *Adv. Mater.* **2020**, *32*, 2003649.
- [161] J. Lei, J. Liu, N. Tang, H. Han, Z. Li, K. Li, T. Zhai, H. Chen, H. Xia, *Adv. Mater. Interfaces* **2021**, *8*, 2101208.
- [162] A. Huang, M. F. El-Kady, X. Chang, M. Anderson, C.-W. Lin, C. L. Turner, R. B. Kaner, *Adv. Energy Mater.* **2021**, *11*, 2100768.
- [163] T. Chen, M. Li, S. Song, P. Kim, J. Bae, *Nano Energy* **2020**, *71*, 104549.
- [164] H. Park, J. W. Kim, S. Y. Hong, G. Lee, H. Lee, C. Song, K. Keum, Y. R. Jeong, S. W. Jin, D. S. Kim, J. S. Ha, *ACS Nano* **2019**, *13*, 10469.
- [165] F. Mo, Y. Huang, Q. Li, Z. Wang, R. Jiang, W. Gai, C. Zhi, *Adv. Funct. Mater.* **2021**, *31*, 2010830.
- [166] Z. Tang, J. Dai, W. Wei, Z. Gao, Z. Liang, C. Wu, B. Zeng, Y. Xu, G. Chen, W. Luo, C. Yuan, L. Dai, *Adv. Sci.* **2022**, *9*, 2201685.
- [167] H. Wu, W. Yuan, X. Yuan, L. Cheng, *Carbon Energy* **2022**, <https://doi.org/10.1002/cey2.229>.
- [168] Y. Li, G. Zhu, X. Xu, L. Chen, T. Lu, J. P. Hill, L. Pan, Y. Yamauchi, *Small Struct.* **2022**, *3*, 2200015.
- [169] G. Filipic, O. Baranov, M. Mozetic, K. Ostrikov, U. Cvelbar, *Phys. Plasmas* **2014**, *21*, 113506.
- [170] O. Baranov, S. Xu, K. Ostrikov, B. B. Wang, U. Cvelbar, K. Bazaka, I. Levchenko, *Rev. Mod. Plasma Phys.* **2018**, *2*, 4.
- [171] O. Baranov, I. Levchenko, J. Bell, M. Lim, S. Huang, L. Xu, B. Wang, D. U. B. Aussems, S. Xu, K. Bazaka, *Mater. Horiz.* **2018**, *5*, 765.
- [172] S. Alancherry, M. V. Jacob, K. Prasad, J. Joseph, O. Bazaka, R. Neupane, O. K. Varghese, O. Baranov, S. Xu, I. Levchenko, K. Bazaka, *Carbon* **2020**, *159*, 668.
- [173] O. Baranov, I. Levchenko, S. Xu, J. W. M. Lim, U. Cvelbar, K. Bazaka, *2D Mater.* **2018**, *5*, 668.
- [174] N. M. Santhosh, G. Filipic, E. Tatarova, O. Baranov, H. Kondo, M. Sekine, M. Hori, K. Ostrikov, U. Cvelbar, *Micromachines* **2018**, *9*, 565.
- [175] O. Baranov, M. Košiček, G. Filipič, U. Cvelbar, *Appl. Surf. Sci.* **2021**, *566*, 150619.
- [176] I. Levchenko, K. Bazaka, O. Baranov, O. Cherkun, M. Keidar, S. Xu, *AAPPS Bull.* **2020**, *30*, 37.
- [177] T. Sada, K. Tsuji, A. Ndayishimiye, Z. Fan, Y. Fujioka, C. A. Randall, *Adv. Mater. Interfaces* **2021**, *8*, 2100963.
- [178] M. Baginski, M. Tupikowska, G. González-Rubio, M. Wójcik, W. Lewandowski, *Adv. Mater.* **2020**, *32*, 1904581.
- [179] F. Shahzad, A. Iqbal, H. Kim, C. M. Koo, *Adv. Mater.* **2020**, *32*, 2002159.
- [180] X. Sui, X. Wang, S. Zhang, M. Yan, W. Li, J. Hao, W. Liu, *Adv. Mater. Interfaces* **2020**, *7*, 2000857.
- [181] A. Kumar, A. Aljumaili, O. Bazaka, E. P. Ivanova, I. Levchenko, K. Bazaka, M. Jacob, *Mater. Horiz.* **2021**, *8*, 3201.
- [182] H. H. Hao, P. Liu, P. Su, T. Chen, M. Zhu, Z. B. Jiang, J.-P. Li, D.-Q. Feng, *Int. Biodeterior. Biodegrad.* **2022**, *170*, 105400.
- [183] S. Sasi, K. Prasad, J. Weerasinghe, O. Bazaka, E. P. Ivanova, I. Levchenko, K. Bazaka, *Trends Biotechnol.* **2022** (in press).
- [184] C. E. Finke, H. F. Leandri, E. T. Karumb, D. Zheng, M. R. Hoffmann, N. A. Fromer, *Energy Environ. Sci.* **2021**, *14*, 1517.
- [185] G. V. Sree, P. Rajasekaran, O. Bazaka, I. Levchenko, K. Bazaka, M. Mandhakini, *Tanso Sen'i no Saisentan Gijutsu* **2021**, *5*, 100083.
- [186] K. K. R. Reddygunta, A. Callander, L. Šiller, K. Faulds, L. Berlouis, A. Ivaturi, *Int. J. Energy Res.* **2022**, *46*, 16512.
- [187] I. Levchenko, K. Bazaka, *Nature* **2021**, *599*, 373.
- [188] I. Levchenko, S. Xu, S. Mazouffre, M. Keidar, K. Bazaka, in *Terraforming Mars*, John Wiley & Sons, New York **2021**, Ch. 5, pp. 73–98.
- [189] G. Genta, *Terraforming Mars*, John Wiley & Sons, New York **2021**, Ch. 1.
- [190] G. Filipic, O. Baranov, M. Mozetic, U. Cvelbar, *J. Appl. Phys.* **2015**, *117*, 043304.
- [191] O. Baranov, G. Filipič, U. Cvelbar, *Plasma Sources Sci. Technol.* **2019**, *28*, 084002.
- [192] J. Tan, Q. Li, S. Meng, Y. Li, J. Yang, Y. Ye, Z. Tang, S. Qu, X. Ren, *Adv. Mater.* **2021**, *33*, 2006781.



Oleg Baranov is professor and head of the Department of Theoretical Mechanics, Engineering and Robomechanical Systems, National Aerospace University “Kharkiv Aviation Institute”, Kharkiv, Ukraine. He is also associated with the Department of Gaseous Electronics, Institut “Jožef Stefan”, Ljubljana, Slovenia. His research interests are plasma physics and nanotechnology (graphene and oxide nanostructures), plasma propulsion, PVD coatings, magnetron and vacuum arc deposition, plasma control and diagnostics in deposition setups, mechanical properties of materials and thin films, surface plasma processing. Development of nanomaterials for explosive traces detection is his current activity.



Claudia Riccardi PhD in physics at the University of Milano (Italy). Her scientific interests in the field of plasma physics are also oriented towards applications to materials and nano materials in sectors such as energy, environment and manufacturing. She was involved in the development of plasma sources, diagnostics and processing, which expanded the understanding of plasma-material interaction and plasma applications. She is director of the Plasma Prometeo Center at the University of Milano-Bicocca dedicated to the research and development of plasma applications and to the technological transfer to industry.



H. Eduardo Roman is currently working at the Plasma Research Group of the Department of Physics, of the University of Milano-Bicocca. He has been awarded a visiting professorship at Pohang University of Science and Technology (POSTECH) Division of IT Convergence Engineering, Pohang, Korea. He has been guest scientist at the Max Planck Institute for the Physics of Complex Systems (Dresden). His interests cover different areas of complex systems such as biomolecules, nanomaterials, fractals, and finance. He is co-editor/author of 7 books and of over 200 publications in international journals.



Uroš Cvelbar is a senior researcher, university professor and head of the Department of Gaseous Electronics (F6) at the Jozef Stefan Institute. He is a member of the ECS executive board and a chair of the Division for Dielectric Science and Technology, chair of the Plasma Nanoscience, an Erudite professor in India and visiting professor at Shanghai Jiao Tong University, and a fellow of World Academy of Arts and Sciences. Dr. Cvelbar's bibliography contains over 200 international scientific papers, 100 invited talks, and 20 patents. His research interests cover plasma and material science, including nanotechnology.

Dr. Patrik Ščajev obtained his PhD at Vilnius University in 2013. Now he has a position as a senior researcher at the Institute of Photonics and Nanotechnology in Vilnius University. He is specialized in characterization of semiconductor structures and devices by time-resolved optical techniques in the UV-NIR spectral range. Carrier recombination lifetime, diffusion coefficient, mobility, diffusion length are the main investigation parameters. Materials as nitrides, oxides, carbides, diamonds, tin alloys, and perovskites were investigated by differential absorption, differential reflection, time resolved photoluminescence, time-resolved photoconductivity and light induced transient grating methods.



Tadas Malinauskas PhD in physics at Vilnius University (Lithuania). He is a senior research fellow at Institute of Photonics and Nanotechnology at Vilnius University. His scientific interests are MOCVD growth of III-nitrides, remote epitaxy via graphene, optical and structural characterization of semiconductors, ultrafast carrier dynamics.